Review article

Magnetic nanoparticles for ferroptosis cancer therapy with diagnostic imaging

Min Jun Ko [a,1], Sunhong Min [b,1], Hyunsik Hong [b], Woojung Yoo [c], Jinmyoung Joo [c], Yu Shrike Zhang [d], Heemin Kang [b,e,**], Dong-Hyun Kim [a,f,g,h,*]

[a] Department of Radiology, Feinberg School of Medicine, Northwestern University, Chicago, IL, 60611, USA
[b] Department of Materials Science and Engineering, Korea University, Seoul, 02841, Republic of Korea
[c] Department of Biomedical Engineering, Ulsan National Institute of Science and Technology (UNIST), Ulsan, 44919, Republic of Korea
[d] Division of Engineering in Medicine, Department of Medicine, Brigham and Women's Hospital Harvard Medical School, Cambridge, MA, 02139, USA
[e] College of Medicine, Korea University, Seoul, 02841, Republic of Korea
[f] Department of Biomedical Engineering, University of Illinois, Chicago, IL, 60607, USA
[g] Robert H. Lurie Comprehensive Cancer Center, Northwestern University, Chicago, IL, 60611, USA
[h] Department of Biomedical Engineering, McCormick School of Engineering, Northwestern University, Evanston, IL, 60208, USA

ARTICLE INFO

ABSTRACT

Ferroptosis offers a novel method for overcoming therapeutic resistance of cancers to conventional cancer treatment regimens. Its effective use as a cancer therapy requires a precisely targeted approach, which can be facilitated by using nanoparticles and nanomedicine, and their use to enhance ferroptosis is indeed a growing area of research. While a few review papers have been published on iron-dependent mechanism and inducers of ferroptosis cancer therapy that partly covers ferroptosis nanoparticles, there is a need for a comprehensive review focusing on the design of magnetic nanoparticles that can typically supply iron ions to promote ferroptosis and simultaneously enable targeted ferroptosis cancer nanomedicine. Furthermore, magnetic nanoparticles can locally induce ferroptosis and combinational ferroptosis with diagnostic magnetic resonance imaging (MRI). The use of remotely controllable magnetic nanocarriers can offer highly effective localized image-guided ferroptosis cancer nanomedicine. Here, recent developments in magnetically manipulable nanocarriers for ferroptosis cancer nanomedicine with medical imaging are summarized. This review also highlights the advantages of current state-of-the-art image-guided ferroptosis cancer nanomedicine. Finally, image guided combinational ferroptosis cancer therapy with conventional apoptosis-based therapy that enables synergistic tumor therapy is discussed for clinical translations.

1. Introduction

Cancer is the 2nd most common cause of death that is rising each year (1.95 million new cases are projected in 2023) [1]. Most of conventional major cancer therapies have utilized the caspase-dependent apoptotic cancer cell death. However, the apoptosis associated therapeutic resistance of cancer cells significantly attributed to the continuous increase of mortality in cancer patients [2–7]. Established apoptosis-based therapeutic approaches could be reconsidered with other alternative pathways regulating cancer cell death to make a transformative breakthrough in cancer treatment [8]. Ferroptosis-based cancer therapeutics provide a new strategy for preventing resistance to conventional cancer therapies. Ferroptosis is a recently discovered type of programmed cell death that is genetically and biochemically distinct from caspase-based apoptosis, pyroptosis, or necrosis. Increases in iron-dependent lipid peroxidation (LPO) and hydroxyl radicals are the major processes for ferroptosis through the Fenton reaction, which is mediated by excess iron ions and intracellular hydrogen peroxide (H_2O_2). Ferroptosis is characterized by the accumulation of iron-dependent cellular reactive oxygen species (ROS) leading to the

failure of cell redox homeostasis that results in oxidative damage to cells. Recently, exploiting ferroptosis as a new effective approach has been considered to overcome the limitations of conventional apoptotic cell death-based cancer therapies. In preclinical studies, the ferroptosis process has shown potential for treating therapeutically resistant cancer cells with outstanding treatment outcomes compared to conventional chemotherapy, which frequently results in therapeutic resistance and tumor regrowth. X_c^- transporter system (system X_c^-) inhibitors (e.g., erastin and its analogs, sulfasalazine, and sorafenib), glutathione peroxidase 4 (GPX4) inhibitors (e.g., RSL3, FIN 56, and FINO2), and ROS producers (e.g., artesunate and ruscogenin) are ferroptosis-associated antitumor agents [9–13]. The multifaceted impact of ferroptosis on tumor treatment and development extends beyond its direct cellular effects. It is intricately influenced not only by oncogenes and tumor suppressors but also by the complex TME. As a result, targeting ferroptotic pathways is implicated in augmenting chemotherapeutic, immunotherapeutic, and radiotherapeutic outcomes.

However, there is not yet any clinical evidence of ferroptosis-augmenting agents showing substantial tumor therapeutic outcomes. Currently, various approaches for efficient ferroptosis induction and its combination with conventional cancer therapies are being continually studied. Despite this, currently available ferroptosis inducers have been found to not only treat cancer but also promote cancer and other diseases. Thus, treating cancers based on ferroptosis requires further consideration. Various routes toward pathological cell death and the cause of many diseases are related to ferroptosis. Degenerative pathological changes can also occur due to the reduced ability to repair the damage caused by LPO [14,15]. The specificity and optimal dose of ferroptosis inducers should be further explored to reduce their side effects and damage to normal cells. In addition, the heterogeneity and plasticity of tumor cells affect their sensitivity to ferroptosis inducers differently, while the subsequent specific functionality of signals released from cancer cells in the TME has not yet been determined [16]. Furthermore, translational ferroptosis inducing agents have shown poor bioavailability and low tumor specificity. Thus, exploiting the ferroptosis mechanism and the tumor-specific induction of ferroptosis is currently under investigation.

A promising approach for image-guided ferroptosis-induction and combinational ferroptosis-induction cancer therapies is using magnetically manipulable nanoparticles (MNPs) (Fig. 1). Specifically, the localized delivery and catalytic effect of MNPs for conventional and combinational cancer therapy have been demonstrated and established in the field of translational medicine [17–25]. These MNPs could become a next-generation tool for treating cancer. Their use could help to achieve targeted ferroptosis induction with additional imaging in emerging ferroptosis-induction cancer therapeutics. Representatively, iron oxide NPs, ROS-generating polymeric and inorganic NPs, and multifunctional nano-cargoes combining an imaging component and ferroptosis induction have shown high efficacy in treating tumors [26]. The imaging component is essential for targeting the tumor and localizing the ferroptosis therapy. Image guidance in ferroptosis or ferroptosis-based combinational therapies allows the safe and effective use of ferroptosis for the treatment of therapeutically resistant cancers. Herein, the latest developmental trends of image-guided ferroptosis-induction cancer nanomedicine using MNPs as a future form of cancer medicine are summarized and their advantages and limitations are discussed.

2. Ferroptosis in cancer cells

Metabolic dysfunction related to LPO is the main cause of ferroptosis induction in cancer cells. Therefore, the increases in free ROS radicals, fatty acid supply, and enzymatic LPO are the main effectors of ferroptosis. Although the link between ferroptosis and human disease is still under investigation, validation of the therapeutic efficacy of ferroptosis inhibitors in various disease animal models has contributed to our understanding of the involvement of ferroptosis in cancer and degenerative diseases (Fig. 2). Specifically, the outcomes of recent studies have revealed that iron, lipids, ROS, and cell metabolism play a critical role in ferroptosis induction in cells. Ferroptosis inducers can kill highly metabolic cancer cells. Various strategies to unbalance key regulators of iron, antioxidant, mitochondrial, and lipid metabolism have been developed for ferroptosis-based cancer therapy. Here, the ferroptosis mechanism and key regulators for potential cancer therapy applications are briefly summarized. Since the promise of ferroptosis in cancer research has been recognized, extensive review papers on the ferroptosis mechanism and perspectives on this new cancer therapy opportunity have been published [27–29].

2.1. Iron metabolism

Iron is a key component in regulating metabolism and proliferation of cancer cells. In general, enhancing the antioxidant level upregulates the DNA repair of cancer cells, while the high ROS tolerance of cancer
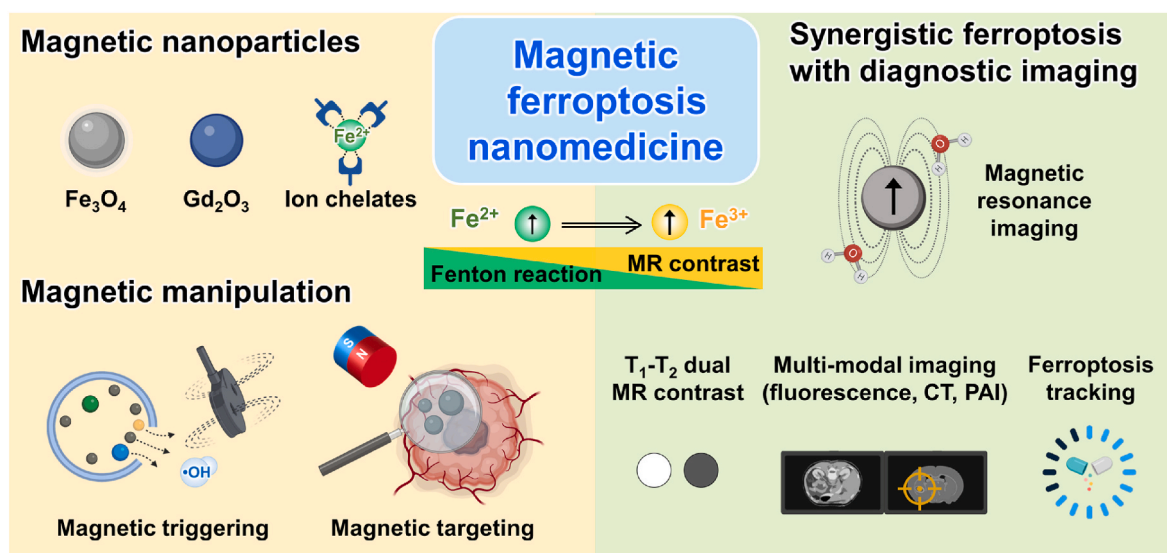

Fig. 1. Schematic illustrations of various magnetic nanoparticles and their multifunction including iron metabolism mediated ferroptosis induction, magnetic manipulation, magnetic energy transduction, and magnetic resonance imaging for synergistic ferroptosis cancer nanomedicine.
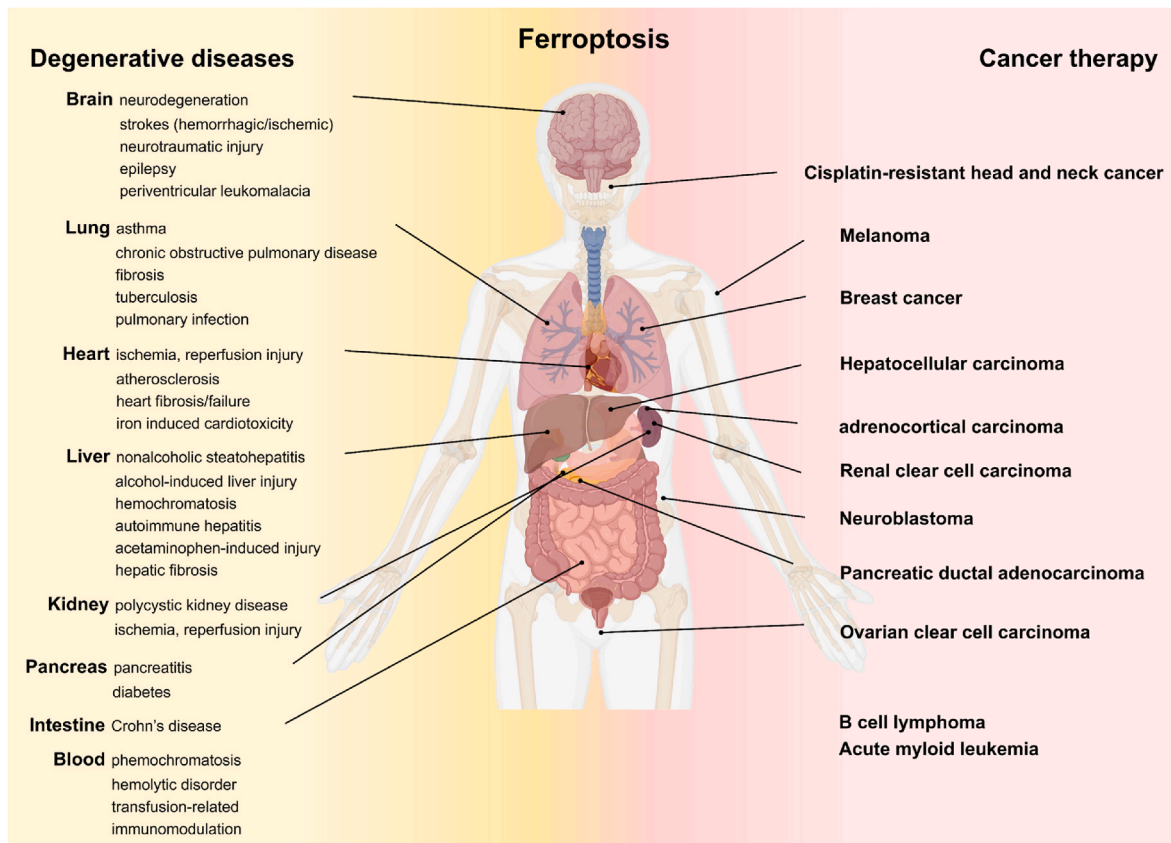
Fig. 2. Ferroptosis related human diseases demonstrating the impact of ferroptosis for treating various tumors and diseases. Reproduced with permission [30]. Copyright 2021, Elsevier B.V.
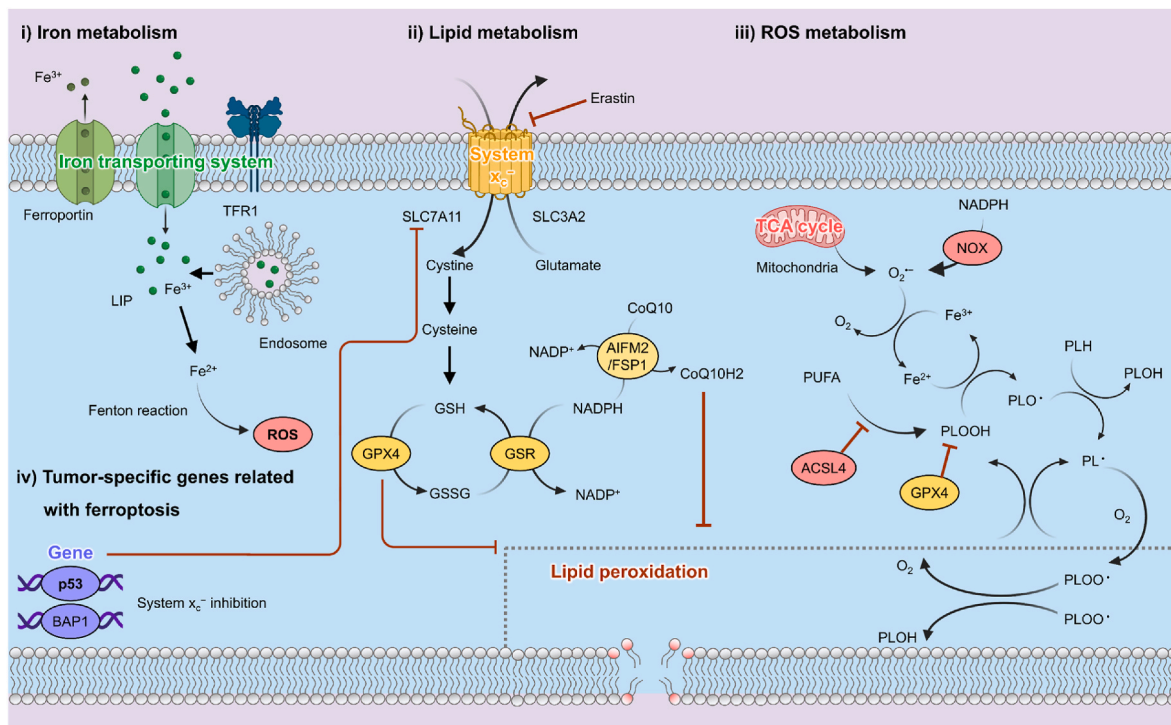

Fig. 3. Ferroptosis mechanism associated with iron metabolism, lipid metabolism and ROS metabolism in cancer cells.

cells makes them more sensitive to iron-induced stress. Thus, various types of cancer cells can finely regulate the more intracellular iron level via tumor-specific iron transportation systems such as ferroportin (FPN), transferrin receptor (TFR), transferrin (TF), ferritin, and ceruloplasmin (Fig. 3). In the iron homeostasis pathway, Fe^{2+} is captured by C-reactive protein and oxidized to Fe^{3+}, which binds to TF and TFRs in the blood circulatory system. Meanwhile, excess iron in cells is exported via the FPN cellular efflux channel, thereby balancing the intracellular iron level. Recently, it has been reported that the iron homeostasis pathway contributes to cancer development, therapeutic resistance, and metastasis [31]. Interference in iron metabolism pathways can induce the LPO-mediated ferroptosis of cancer cells. Various molecules targeting iron-transportation components for the treatment of cancer cells have been studied [32–35].

2.2. Lipids metabolism - antioxidants

Glutathione (GSH), which is generated from glutamate, cysteine, and glycine, is the predominant intracellular antioxidant in most living cells. GSH production is a two-step process involving adenosine triphosphate (ATP)-dependent cytosolic enzymes glutamate-cysteine ligase (GCL) and glutathione synthetase (GSS). Therefore, GSH synthesis is strongly dependent on the availability of cystine and cysteine. Ferroptosis is triggered by depleting or inhibiting GSH synthesis (Fig. 3) [36]. The redox status of the extracellular compartment modulates cystine-cystathionine exchange activity across the cellular membrane. The alanine-serine-cysteine system induces the influx of cysteine under certain redox conditions. The cellular balance of cystine-cystathionine is controlled by the system X_c^- comprising cystine-glutamate antiporters SLC3A2 and SLC7A11. Cystine and glutamic acid influx into cells through system X_c^- in the cell membranes. Subsequently, the synthesis of GSH as the substrate for GPX4 occurs through γ-glutamyl cysteine ligase and GSH synthase [37]. GPX4 converts GSH into oxidized GSH and reduces lipid peroxides to their corresponding alcohols. In general, membrane lipid metabolism is maintained by both GPX4 and GSH-associated functionality. GPX4, a main reductase in the ferroptosis, is involved in the breakdown of lipid membranes, and inactivating it can trigger cancer cell ferroptosis [38,39]. Another ferroptosis-inducing molecule that is related to lipid metabolism, coenzyme Q (CoQ10), is a representative of a ubiquitously expressed family of coenzymes that are regulated by apoptosis-inducing factor mitochondria-associated 2 (AIFM2) recently renamed as ferroptosis suppressor protein 1 (FSP1). Apoptosis and ferroptosis can be inhibited according to the location of CoQ10. The translocation of AIFM2 from the mitochondria to the plasma membrane by enzymatically reducing non-mitochondrial CoQ10 changes its pro-apoptotic activity into anti-ferroptotic activity. The AIFM2-regulated CoQ10 reduction process runs in parallel with the GPX4 pathway for reducing lipid peroxides. Targeting these antioxidant pathways can induce an imbalance in lipid metabolism leading to the ferroptosis of cancer cells.

2.3. ROS metabolism

ROS include peroxides, superoxide, singlet oxygen, and free radicals containing unpaired electrons. Excess as the by-product of oxidative phosphorylation can damage the mitochondria, proteins, DNA, and lipids [40–42]. Ferroptosis is frequently promoted by ROS derived from mitochondrial respiration, a pathway that can be subverted by inhibitors of mitochondrial electron-transfer complexes such as the NADPH oxidase (NOX) family, including NOX1, CYBB/NOX2, and NOX4 (Fig. 3). Besides mitochondrial ROS, ferroptosis-mitigated ROS production can occur from various sources, and the accumulation of oxidative products is considered as a maker of ferroptosis [43]. Polyunsaturated fatty acids (PUFAs), which are highly susceptible to LPO, comprise a key marker for ferroptosis [44,45]. Free PUFAs can be esterified by the activation of acyl-CoA synthetase long-chain family member 4 (ACSL4). Esterified

PUFAs are incorporated into phospholipid membranes via the lyso-phosphatidyl choline acyltransferase 3 (LPCAT3). Thus, upregulating ACSL4 can induce ferroptosis [46,47]. Phosphatidyle-thanolamines (PEs) containing arachidonoyl (AA) or adrenoyl (AdA) are a class of phospholipids that predominantly undergo oxidation during ferroptosis [48]. ROS generation by decomposing lipid peroxides depletes nucleic acids and proteins and induces ferroptosis [49]. Intensive work to investigate the interactions between various ROS and the regulation of ferroptosis is ongoing.

2.4. Tumor suppressor genes

Tumor suppressor genes, including TP53, BRCA1-associated protein 1 (BAP1), alternative reading frame (ARF), and beclin1, suppress system X_c^- activity. TP53 is involved in the cancer development, including cell cycle arrest, senescence, and apoptosis [50]. It has recently been reported that p53 is a key component in modulating cancer cell ferroptosis [51–53]. TP53 transcriptional targets (p533KR (3 KR: K117R + K161R + K162R)) significantly promote ferroptosis via the downregulation of SLC7A11 [54]. At the same time, the loss of an additional acetylation site at K98 (4 KR: K98R + 117R + K161R + K162R) abrogates the ferroptosis activity of p53 [55]. The outcomes from another study infer that interferon-gamma secreted by $CD8^+$ T cells sensitizes tumor cells for ferroptosis by suppressing system X_c^-, suggesting including ferroptosis might be an effective tumor-suppression regimen [56]. BAP1 can induce ferroptosis in a similar process to TP53 by downregulating SLC7A11 [57]. It is frequently deleted or mutated in human cancers such as renal cell carcinoma, uveal melanoma, cholangiocarcinoma, and mesothelioma. It has been reported that the inactivation of BAP1 upregulates SLC7A11 and suppresses ferroptosis, resulting in tumor development. Although the precise mechanism by which BAP1 induces SLC7A11 suppression needs to be further investigated, it could regulate the H2A ubiquitination (H2Aub) level on the SLC7A11 promoter, which suppresses the expression of SLC7A11 [58]. Developing NP-mediated gene editing techniques could make these genes an effective target for ferroptosis-mediated cancer therapy.

3. Ferroptosis inducers for ferroptosis cancer therapy

Since highly metabolic cancer cells could be particularly susceptible to ferroptosis, ferroptosis-induction cancer medicines that can kill therapeutically resistant cancer cells open a new field of cancer therapy research [59]. Extensive research has been conducted to find target signals and molecules that can induce cancer cell ferroptosis. As mentioned earlier, intervention in iron, lipid, and ROS metabolism, as well as upregulating tumor suppressor genes, in cancer cells, can directly induce cancer cell ferroptosis. Various chemotherapeutic agents and nano-materials that are ferroptosis inducers and their potential for the treatment of cancers have been shown (Table 1) [60]. Their action mechanisms and possible applications for cancer therapy are described here.

3.1. General ferroptosis inducers

The synthesis of GSH, the main antioxidant within cells, is dependent on system X_c^--mediated cysteine uptake. Erastin and its derivatives such as piperazine erastin and imidazole ketone erastin have been known to inhibit system X_c^- and induce ferroptosis [61]. Recently, researchers have found that multi-targeted kinase inhibitor sorafenib (SRF) and anti-inflammatory sulfasalazine (SAS) can also block system X_c^- and cause ferroptosis in both hepatocellular carcinoma and glioma cells, respectively [62,63]. GPX4 inhibition is another effective target that can lead directly to the accumulation of LPO. Electrophilic chloroacetamides (RSL3) and nitrile oxide electrophiles (ML210, JKE-1674, and JKE-1716) can initiate ferroptosis by inhibiting selenocysteine activity in the active site of GPX4 [38,64,65]. Iron-based FINO2 can directly

Table 1

Conventional ferroptosis inducers that are available in the clinical trials or the market.

Mechanism of action	Agent	Tumor type	Clinical development phase	Ref.
GSH inhibition	Cisplatin	Ovarian cancer, pancreatic cancer, urothelial cancer)	Marketed	NCT04574960 NCT01561586 NCT03649321
GPX4 inhibition	Altretamine	Lymphoma, sarcoma	Marketed	NCT00002936
	Withaferin A	Breast cancer, osteosarcoma	Phase II	NCT04092647 NCT00689195
Iron activation	Neratinib	Breast cancer, colorectal cancer	Marketed	NCT04366713 NCT03377387 NCT03457896
	Salinomycin	Various solid tumor	Marketed (antibacterial drug) preclinical (anticancer activity)	
	Lapatinib	Breast cancer	Marketed	NCT03085368 NCT00356811 NCT00667251
SLC7A11 inhibition	Erastin analog (PRLX 93936s)	Multiple myeloma	Phase I/II	NCT01695590
	SRF	Acute myeloid leukemia, hepatocellular carcinoma, non-small-cell lung cancer, renal cell carcinoma	Marketed	NCT03247088 NCT02559778 NCT00064350
	Sulfasalazine	Breast cancer, glioblastoma	Marketed (anti-inflammatory agent) phase I (cancer treatment)	
DNA stress induction	Zalcitabine	AIDS-related Kaposi's sarcoma	Marketed (HIV treatment) preclinical (cancer treatment)	NCT00000954
GCL inhibition	Buthionine, sulfoximine	Melanoma, neuroblastoma	Phase I	NCT00002730 NCT00005835 NCT00661336
HMGCR inhibition	Fluvastatin	Breast cancer	Marketed (lipid-lowering agent) phase I (oncology)	NCT00416403
	Pravastatin	Acute myeloid leukemia, hepatocellular carcinoma	Marketed (lipid-lowering agent) phase I (oncology)	
	Lovastatin	Multiple myeloma	Marketed (lipid-lowering agent) phase I (oncology)	
	Simvastatin	Multiple myeloma	Marketed (lipid-lowering agent) phase I (oncology)	

oxidize lipids and indirectly inhibit GPX4 activity resulting in ferroptosis [66]. FIN56, a novel ferroptosis inducer, promotes the breakdown of GPX4, which results in increased intracellular ROS [67]. Various organic peroxide compounds containing one or more oxygen bonds (ROOR) have easily breakable O–O bonds, which can produce RO· radicals leading to ferroptosis induction (Table 1).

3.2. Clinically applicable ferroptosis inducers

Drug-resistant cancer cells commonly present epithelial-to-mesenchymal transition (i.e. upregulation of mesenchymal markers and downregulation of epithelial markers), which makes them more sensitive to ferroptosis [68,69]. Thus, various conventional chemotherapeutic agents against which cancer cells are resistant have been re-evaluated as clinical ferroptosis inducers (Table 1). Representatively,
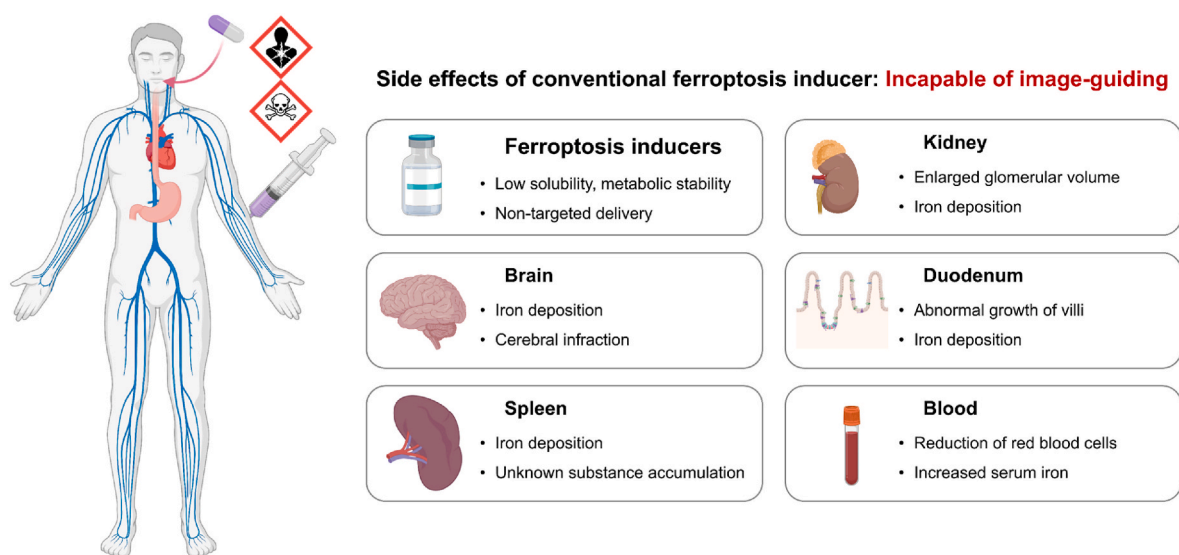

Fig. 4. The potential side effects associated with systemically administered conventional ferroptosis-inducing agents that lack tumor targeting and imaging capabilities.

cisplatin, artemisinins, neratinib, lapatinib, statin, sulfasalazine, SRF, withaferin A, and zalcitabine are being tested in clinical trials for potential repurposing as ferroptosis inducers. At the same time, clinical studies in which several proven ferroptosis inducers are being used in combination with these clinical chemotherapeutic agents to promote ferroptosis of cancer cells are also being conducted.

3.3. The limitation of ferroptosis inducers: their side effects and cancer therapeutic efficacy

The therapeutic efficacy of ferroptosis inducers, as well as other cancer therapeutic agents, is based on the selective targeting and destruction of tumor cells over normal cells, and considering their potential side effects is vital for maximizing their therapeutic benefit (Fig. 4). However, unfortunately, most currently used clinical ferroptosis inducers have poor bioavailability, low solubility, and poor metabolic stability. In a recent preclinical study, it was shown that erastin intraperitoneally injected into healthy mice significantly induced metabolic changes in several tissues [38]. Although erastin increased serum iron and malondialdehyde and decreased GSH and GPX4, it also enhanced iron deposition in the brain, duodenum, kidney, and spleen. The blood index values post-erastin injection also indicate mild cerebral infarction of the brain and enlarged glomerular volume of the kidneys, while pathological analysis showed ferroptosis-mediated growth of the duodenal epithelium. These findings infer that ferroptosis inducers induce pathological changes of healthy tissues in addition to the ferroptosis of cancer cells. Meanwhile, ferroptosis inducers can cause intestinal ischemia/reperfusion, ulcerative colitis and cystic fibrosis, and the enhanced iron level could be involved in abnormal limb development [70–73]. Indeed, erastin and its analogs, system X_c^- inhibitors, and GPX4 inhibitors have also shown side effects in clinical trials (NCT03745716) (Fig. 4) [74]. Thus, targeted ferroptosis-induction cancer medicine is essential for achieving the greatest clinical benefit for cancer patients.

3.4. Nano-ferroptosis inducers

NPs with intrinsic physicochemical properties provide additional options for ferroptosis induction [75]. Iron-based NPs are the representative form of ferroptosis-inducing NPs [76,77]. Approved for clinical use as an iron supplement by the US Food and Drug Administration (FDA), they can induce the Fenton reaction and the ferroptosis of cells. Fe ions from the iron oxide NPs can generate considerable levels of ROS in cells, resulting in LPO, iron accumulation, and GPX4-mediated ferroptosis induction [78,79]. Various iron-doped and iron-based hybrid nanostructures, iron-organic frameworks, and iron-based nanocomposites have been reported. Other lipid-based NPs could promote the PUFA level in the cancer cells, which induces ferroptosis by disrupting the activity of iron receptors/channels on the cell membrane.

3.5. Magnetic nanomedicines for ferroptosis cancer therapy

As previously mentioned, ferroptosis influences several oncogenic pathways, and cancer cells can have a higher susceptibility to ferroptosis than normal cells due to their high metabolic activity. To enhance iron-dependent ferroptosis induction, regulating iron and/or lipid metabolism can effectively modulate the sensitivity of cancer cells toward ferroptosis. At the same time, the composition of the cellular antioxidant system depends on amino acid metabolism and the mevalonate pathway. Moreover, cancer metastasis can be controlled by using ferroptosis-induction cancer medication in combination with immunotherapy. However, as shown by the high failure rate of most small-molecule drugs in clinical trials, it is usually difficult to achieve adequate efficacy in the treatment of cancer using currently available ferroptosis inducers. Non-targeted ferroptosis induction can interfere with iron homeostasis and cause excessive ROS production, which can

affect the immune system and cause neurodegenerative conditions such as Huntington's and Parkinson's disease, heart failure, and leukemia (Fig. 4) [80–86]. Ferroptosis induction in healthy cells can also activate tumorigenesis associated with iron-donating tumor-associated macrophages.

Various MNPs have been considered for the carriers of chemotherapeutic drugs due to their advantages of enhanced bioavailability, minimal side effects, appropriate degradation, and targeted delivery [87–96]. Ferroptosis-induction cancer nanomedicines utilizing MNPs have been produced and tested, a summary of which is provided in Table 2. Emerging nanomedicines that promote LPO or ROS accumulation in cancer cells can control the expression of GPX4 in cancer cells, subsequently resulting in the Fenton reaction and exogenous regulation of peroxidation (Fig. 5) [97,98]. NPs that enhance the intracellular ROS can mediate intracellular chemical reactions and intervene in cancer cellular ferroptosis pathways. Another approach is to increase the uptake of exogenous lipids by cancer cells to boost ferroptosis induction via intracellular lipid peroxide accumulation [45,99,100].

Synergistic ferroptotic nanomedicines with diagnostic imaging are critical for improving their efficacy, and the development of effective MNPs for this has been widely studied in recent years [101–103]. In this review, various MNPs for image-guided ferroptosis induction in cancer cells and innovative possibilities are summarized. Validating the effectiveness of ferroptosis-induction cancer nanomedicines using the MNPs will warrant their successful clinical translation for the treatment of cancer.

4. Magnetic nanoparticles for image-guided ferroptosis cancer nanomedicine

Maximizing the therapeutic efficiency and minimizing the side effects of tumor-specific ferroptosis-induction nanomedicine are challenging issues. The employment of MNPs provides a promising approach for localizing cancer cell ferroptosis [128,129]. MNPs with intrinsic anticancer activity and remote controllable via an external magnetic field have attracted extensive attention [130,131]. Iron-based MNPs have shown effective ferroptosis induction as a result of the Fe^{2+} or Fe^{3+} ions released during the endocytosis process. The subsequent Fenton reaction can produce intracellular ROS, LPO, and macromolecular damage caused by ferroptosis induction. In addition, the unique magnetic properties of iron-based MNPs such as superparamagnetism, high magnetic susceptibility, and magnetization enable them to respond to an externally applied magnetic field [132–134]. Thus, various magnetic targeting and external field triggered behaviors can conduct targeted ferroptosis cancer nanomedicine. The motion of MNPs under an external magnetic field can be converted to mechanical, thermal, or chemical energy. Meanwhile, interaction with the magnetic field enables targeted ferroptosis-induction cancer therapy with T_1 or T_2 magnetic resonance imaging (MRI) contrast capability (Fig. 6) [135]. Indeed, multifunctional MNPs can provide non-invasive localized ferroptosis-inducing nanomedicines for the effective treatment of cancers.

4.1. Magnetic nanoparticles for the fenton reaction

Iron oxide MNPs provide an excellent contrast material for MRI [136, 137]. At the same time, recent studies have proved that iron oxide MNPs can induce ferroptosis of cancer cells through ROS generation via the Fenton reaction [138–140]. Iron oxide MNP-based ferroptosis-induction cancer nanomedicines have become increasingly attractive and investigated extensively [141,142]. Moreover, it was found that iron oxide MNP-induced ferroptosis in cancer cells could eliminate all of the neighboring cancer cells in a fast propagating wave [143]. Cancer cells are highly sensitive to iron concentration, and a slight fluctuation in iron concentration in the process of intracellular iron homeostasis can cause a great impact on the fate of the cancer cells [144–148]. Cancer cells can effectively store and export excess intracellular iron ions released from

Table 2

Summary of nano/micromaterials used to induce ferroptosis, including magnetic nanomedicine, tumor model, ferroptotic cargos, mechanism of action (ferroptosis), and compatible imaging type.

	Magnetic nanoparticles	Tumor model	Ferroptotic cargos	Mechanism of action	Diagnostic imaging	Ref.
Magnetic field targeted ferroptosis	Fe_3O_4@mSiO_2-ANG exosome	Brain cancer	Fe_3O_4 NPs	DHODH disruption GPX4 inhibition	FI	[104]
Magnetic field triggered ferroptosis MRI-guided ferroptosis	PLGA-Fe_3O_4 NPs with AA	Prostate cancer	Fe_3O_4 NPs	Fenton reaction	MRI (T_2)	[105]
	Engineered magnetosomes	Breast cancer	Fe_3O_4 NPs	Fenton reaction	MRI (T_2)	[106]
	Fe^{3+}/Gd^{3+}-chelated polymer	Breast cancer	Fe^{3+} ions	Fenton reaction	MRI (T_1)	[107]
	Cisplatin- Fe_3O_4/Gd_2O_3 hybrid NPs	Brain cancer	Fe_3O_4 NPs	Fenton reaction	MRI (T_1)	[108]
	DOX-tannic acid-Fe^{3+}	Melanoma	Fe^{3+} ions	Fenton reaction	MRI (T_1)	[109]
	DOX-Gd_2O_3–Fe_3O_4 NPs	Breast cancer	Fe_3O_4 NPs	Fenton reaction	MRI (T_1&T_2)	[110]
	Gemcitabine-loaded carbonaceous NPs	Pancreatic cancer	$MnFe_2O_4$	Fenton reaction, GPX4 inhibition	MRI (T_2)	[111]
	Fe_3O_4 NPs-gelatin microsphere	Hepatocellular carcinoma	Fe_3O_4 NPs	Fenton reaction	MRI (T_2)	[112]
	Arginine-rich manganese silicate nanobubbles	Liver cancer	MnO_x	GSH depletion, GPX4 inhibition	MRI (T_1)	[113]
	FePt-MOF	Breast cancer	Fe ions	Fenton reaction	MRI (T_2), CT	[114]
	SRF/Fe_3O_4 NPs-PDA NPs	Rectal cancer	Fe_3O_4 NPs	Fenton reaction, GPX4 inhibition	MRI (T_2)	[115]
	Fe_3O_4–Gd_2O_3 nanopeanuts	Prostate cancer	Fe_3O_4 NPs	Fenton reaction	MRI (T_1)	[116]
Magnetic ferroptosis nanomedicine with immunotherapy	iTGF-β-aPD-1 magnetosomes	Melanoma, breast cancer	Fe_3O_4 NPs	Fenton reaction	MRI (T_2)	[106]
	MnO_x nanospikes	Breast cancer	Mn^{2+} ions	GSH depletion	MRI (T_1), PAI	[117]
	Fe_3O_4-SAS@PLT	Breast cancer	Fe_3O_4 NPs	Fenton reaction	MRI (T_2)	[118]
	FePt/BP nanoplatforms	Breast cancer	FePt NPs	Fenton reaction	MRI (T_2), NIR	[119]
	Ferumoxytol	Prostate cancer	Fe_3O_4 NPs	Fenton reaction	MRI (T_2)	[120]
Magnetic ferroptosis with synergistic diagnostic imaging	Fe_3O_4@$Cu_{1.77}$Se-PEG	Breast cancer	Fe_3O_4 NPs, Cu^{2+}	Fenton reaction, GSH depletion	MRI (T_2), PAI	[121]
	GBP@Fe_3O_4 polypeptide	Prostate cancer	Fe_3O_4 NPs	Fenton reaction, GSH depletion	MRI (T_2), PAI	[122]
	FCSP@DOX MOF@DOX	Breast cancer	DOX, Fe and Cu ions	GSH depletion	MRI (T_2), PAI	[123]
	Cro-Fe@BSA NP	Breast cancer	Fe^{3+} ions	Fenton reaction	MRI (T_1), PAI	[124]
	RGD/Pt-GFNP	Brain cancer	Pt (IV), Fe^{2+}	Fenton reaction, GSH depletion	MRI (T_2)	[125]
	Fe_3O_4-PLGA-Ce6	Breast cancer	Fe_3O_4 NPs	Fenton reaction	MRI (T_2), FI	[126]
	Fe_3O_4@PGL	Colon cancer	Fe_3O_4	Fenton reaction	MRI (T_2), FI	[127]

Fe_3O_4 NPs, IONPs, iron oxide nanoparticles; ANG, angiopep-2 (TFFYGGSRGKRNNFKTEEYC); DHODH, dihydroorotate dehydrogenase; SS, 3′-dithiodipropionic anhydride; GSH, glutathione; GPX4, GSH peroxidase 4; FI, Fluorescence imaging; PLGA, poly(lactic-co-glycolic acid); AA, ascorbic acid; MRI, magnetic resonance imaging; DOX: doxorubicin; MOF, metal organic framework; SRF, sorafenib; PDA, polydopamine; iTGF-β, transforming growth factor-β inhibitor; Fe_3O_4 NCs, iron oxide nanoclusters; aPD-1, programmed death-1 antibody; SAS, sulfasalazine; PLT, platelet; BP, black phosphorous nanosheet; NIR, Near-infrared imaging; GBP. Polypeptide-modified and 1H-perfluoropentane-encapsulated Fe_3O_4 containing nanoformulation; FCSP, PEGylated Fe–Cu MOF; GFNP, Gallic acid/Fe nanomaterial; Cro, croconaine; BSA, bovine serum albumin; PGL, porphyrin grafted lipid.

endocytosed iron oxide MNPs. Moreover, the meso-2, 3-dimercaptosuccinic acid (DMSA)-coated Fe_3O_4 NPs treatment of cancer cells significantly upregulates the transcription of genes responsible for exporting intracellular iron ions [149]. Xiaolian Sun's group utilized ultrasmall single-crystal Fe NPs for targeted ferroptosis-induction cancer therapy [150]. Ultrasmall body-centered-cubic (BCC) Fe NPs comprising 2 nm Fe core and a 0.7 nm iron oxide shell were synthesized via a one-step method (Fig. 7a). The ultrathin shell protects the Fe (0) core from oxidation and escaping from the endosome during cellular uptake. The synthesized bcc-Fe NPs showed high Fenton catalytic activity, thereby inducing oxidative stress and ferroptosis of cancer cells (Fig. 7b). The ultrasmall single-crystal Fe NPs were stable in the physiological environment whereas they were selectively active in the TME because of lysosomal acidic etching of the Fe_3O_4 shell and subsequent exposure of the Fe core. Finally, a low dose of ultrasmall single-crystal Fe NPs efficiently induced tumor cell ferroptosis and immunogenetic cell death. Due to their small size, renal clearance of the NPs was rapid, thereby demonstrating their suitability for potential clinical translation. Furthermore, the cancer cell-targeted delivery of iron enhanced the therapeutic efficacy of the ferroptosis nanomedicine without severe side effects. Thus, the iRGD-labeled ultrasmall single-crystal Fe NPs and the combinational therapy approach provide an effective cancer cell-targeting treatment.

In another report related to iron oxide MNP-based ferroptosis from

Gao et al., the authors deduced that the NP-mediated inhibition of the genes associated with exporting intracellular iron ions, which they named this therapy gene-interference ferroptosis therapy (GIFT), could be effective at inducing cancer cell ferroptosis [151]. DMSA-coated Fe_3O_4 NP (FeNP) was combined with DMP-controlled gene-interference tools (Fig. 8a and b). DNA-mimicking protein (DMP)-controlled CRISPR/Cas13a and microRNA (miRNA) specifically knock down the expression of two iron metabolic genes encoding FPN and lipocalin 2 (LCN 2) in cancer cells. Co-treatment with FeNPs induced significant cancer cell ferroptosis in both hematologic and solid tumors with minimal side effects (Fig. 8a). The growth of different xenografted tumors in mice was significantly inhibited by GIFT therapy (Fig. 8c and d). As iron metabolic genes were successfully knocked down, cancer cells failed to maintain homeostasis by pumping out iron ions, resulting in a significant increase in intracellular ROS levels. This result suggested that intracellular Fe contents could be maximized in target cancer cells by integrating specific gene transfer with Fe source administration, while there is no damage to normal cells.

Next, utilizing iron with conventional chemoagents to become prodrugs for combined apoptosis and ferroptosis-induction cancer therapy is explored. Optimizing the targeting of ferroptosis can be achieved by combining the approach with pH-responsive degradable amorphous calcium carbonate (ACC). Xue et al. reported localized tumor ferroptosis agents that can be combined with apoptosis-based cancer therapy [152].
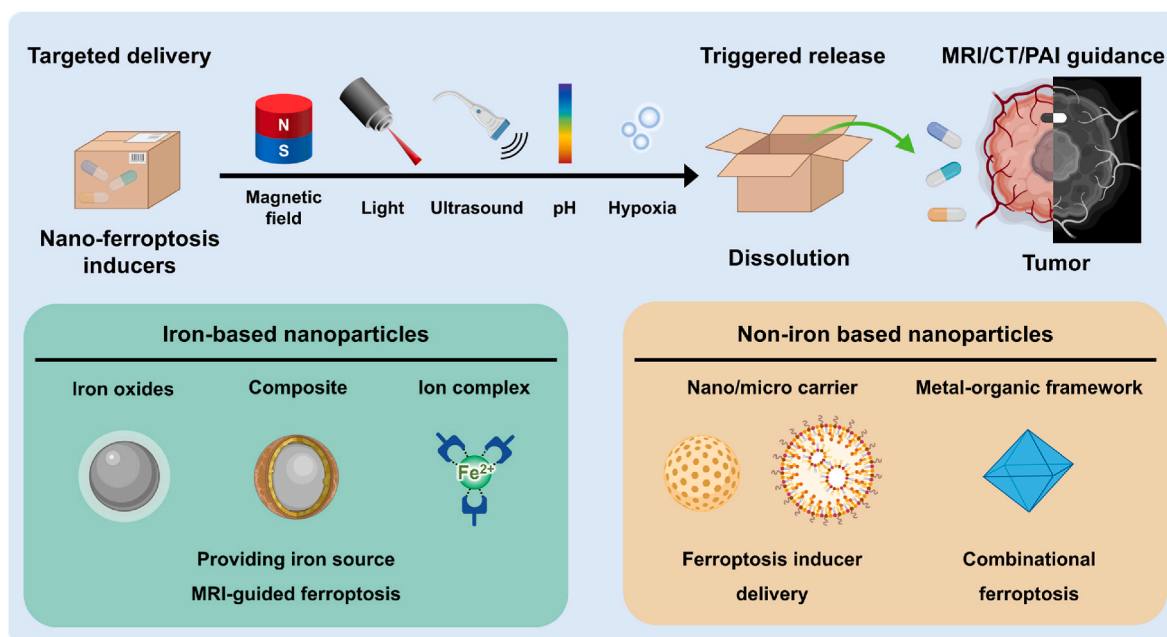
Fig. 5. Various types of nano-ferroptosis inducers categorized by iron based magnetic nanoparticles and non-iron based nanoparticles. Nano-ferroptosis inducers can be utilized for the image guided local ferroptosis induction and triggered ferroptosis induction.
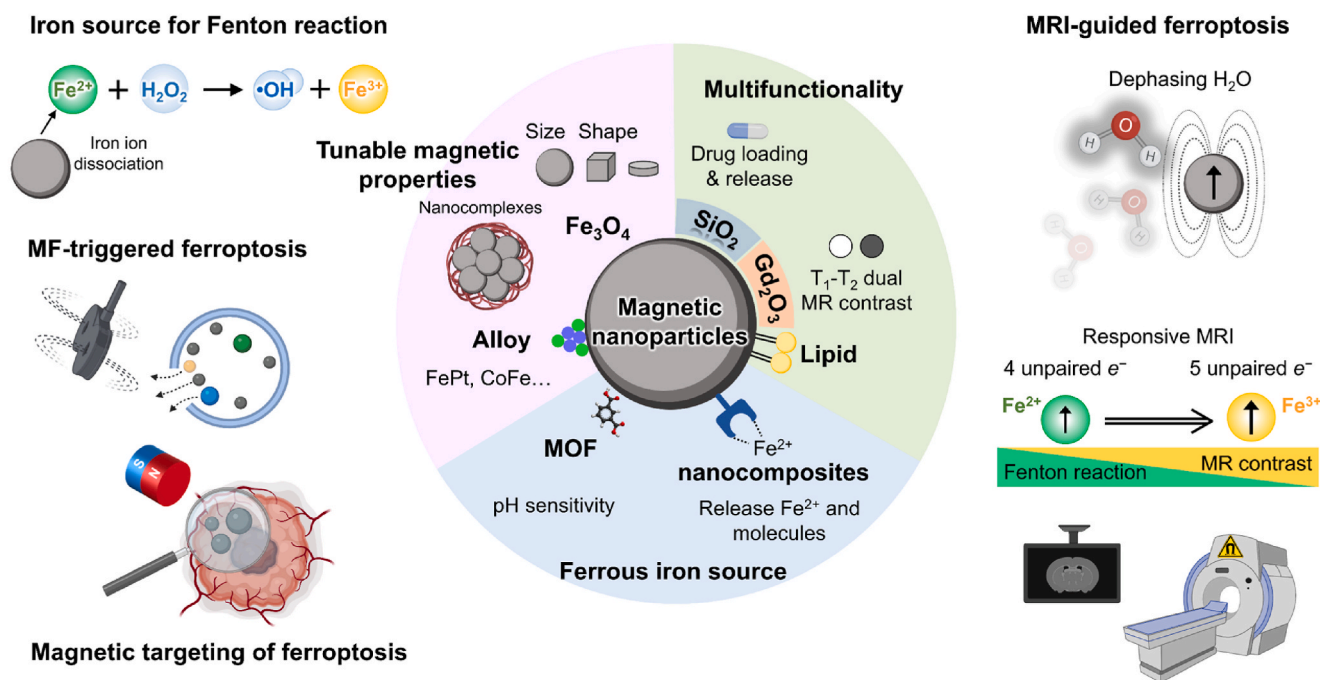

Fig. 6. Multifunctional theranostic magnetic nanoparticles mediated ferroptosis cancer nanomedicines. Nano-engineered magnetic nanoparticles and their nano-composites can be equipped for the image guided ferroptosis cancer nanomedicine.

Doxorubicin (DOX) was chelated with Fe^{2+} ions and co-encapsulated with calcium-silica precursors in a one-step approach (Fig. 9a). The complexation of DOX and Fe^{2+} ions enabled their efficient loading into the nano-assembly and prevented the early release of Fe^{2+} ions in the cancer cells. A thin layer of silica-ACC (CaSi) hybrid was then deposited onto the surface of the nanocomplex. Subsequently, folate-modified and PEGylated polyamidoamine (PAMAM) dendrimers were conjugated to confer the targeting function for the selective treatment of cancer cells. Elevated expression of matrix metalloproteinase-2 (MMP-2) in the extracellular TME targets the cancer cell membranes and TME. MMP-2-cleavable peptides (GPLGVRGDGG) added to the PEG parts of the PAMAM dendrimer provided effective cancer targeting. The prepared nano-formulation could activate selective cancer cell death through combined ferroptosis and apoptosis, while DOX-Fe^{2+} complexation within the nano-formulation protected Fe^{2+} from cellular oxidative stress, which prevented its premature release and enhanced the therapeutic efficacy. In the MMP-2-rich TME, the PEG segments of nano-formulation were shed at the GPLGVRGDGG peptide linker, which
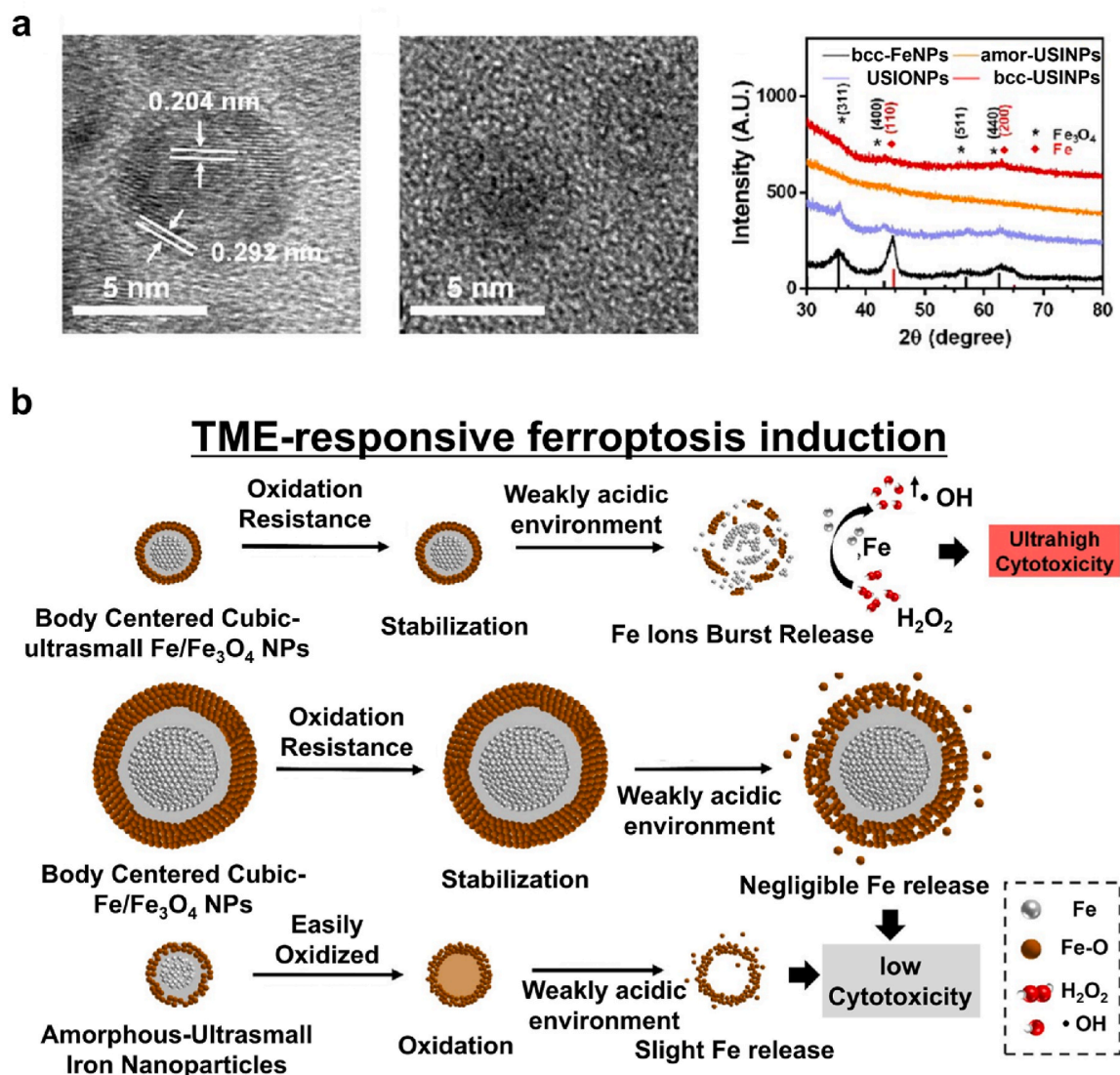
Fig. 7. Rapidly renal clearable ultrasmall iron nanoparticles (USINPs) as a selective ferroptosis inducer. (a) Characterization of the bcc-USINPs. (b) A schematic illustration of the pH-activated Fe release from the bcc-USINPs. Reproduced with permission [150]. Copyright 2021, American Chemical Society.

exposed the tumor-targeting folate moieties and enhanced their uptake by the cancer cells. The proton sponge effect of PAMAM in the nano-formulation subsequently enabled the nano-formulation to release the therapeutic DOX-Fe complex into the cytosolic matrix (Fig. 9b). Finally, ROS generation by DOX-associated NOX activation acted in synergy with the Fe^{2+}-mediated ferroptosis. The ferroptosis-apoptosis combination treatment significantly inhibited tumor growth (Fig. 9c). This strategy offers an effective ferroptosis-induction cancer nano-medicine approach that can overcome the limitations of conventional apoptosis-based anticancer modalities.

Iron-based MNPs are a natural choice for ferroptotic inducers given the role of iron ions in ferroptosis. All iron-based MNPs follow the common principle of the redox reaction to generate Fe^{2+} ions to start the Fenton reaction. Fe_3O_4 NPs can be reduced under acidic conditions which the lysosomes in cells without requiring an external reducing agent. Li et al. showed that Fe^{3+} ions in the Fe_3O_4 NPs were reduced to Fe^{2+} ions in the cells, which then reacted with H_2O_2 to create free radicals via the Fenton reaction that induced ferroptosis [153]. How-ever, the endogenous reduction of iron in the cells might not be suffi-cient to trigger ferroptosis. Hence, novel approaches such as combining ferroptosis with other treatment regimens to boost the Fenton reaction or enhance ferroptosis via multiple pathways including GSH depletion,

and GPX4 inhibition are needed. Further attempts to enhance ferroptosis from the intracellular reduction of iron were reported by Zhou et al. concurrent sonodynamic therapy (SDT) with ferumoxytol-protopor-phyrin IX (PPIX)-loaded nanoliposomes produced enhanced ferroptosis via the Fenton reaction with the ferumoxytol iron oxide core while photosensitization of PPIX via SDT which inhibited ferritin and GPX4 activity [154]. Also, a ferrous ion-croconium dye complex for the controllable delivery of ferrous ions was recently reported to regulate metallomodulation cell death strategies [155].

4.2. Magnetic nanoparticles for targeted ferroptosis cancer nanomedicine

Precise targeting of cells in which to induce ferroptosis is an essential consideration to effectively use ferroptosis for cancer treatment, and magnetically responsive NPs can be used to achieve this [156]. Various magnetic field types can precisely steer the MNPs to the targeted region [157]. Recently, Li et al. reported an approach that can enhance local-ized ferroptosis in glioblastoma multiforme (GBM) cells [104]. In this study, engineered exosome-conjugated MNPs induced ferroptosis by disintegrating dihydroorotate dehydrogenase (DHODH) and GPX4 (Fig. 10a). The platform was composed of two components: magnetic Fe_3O_4 NPs coated with a mesoporous SiO_2 shell containing brequinar
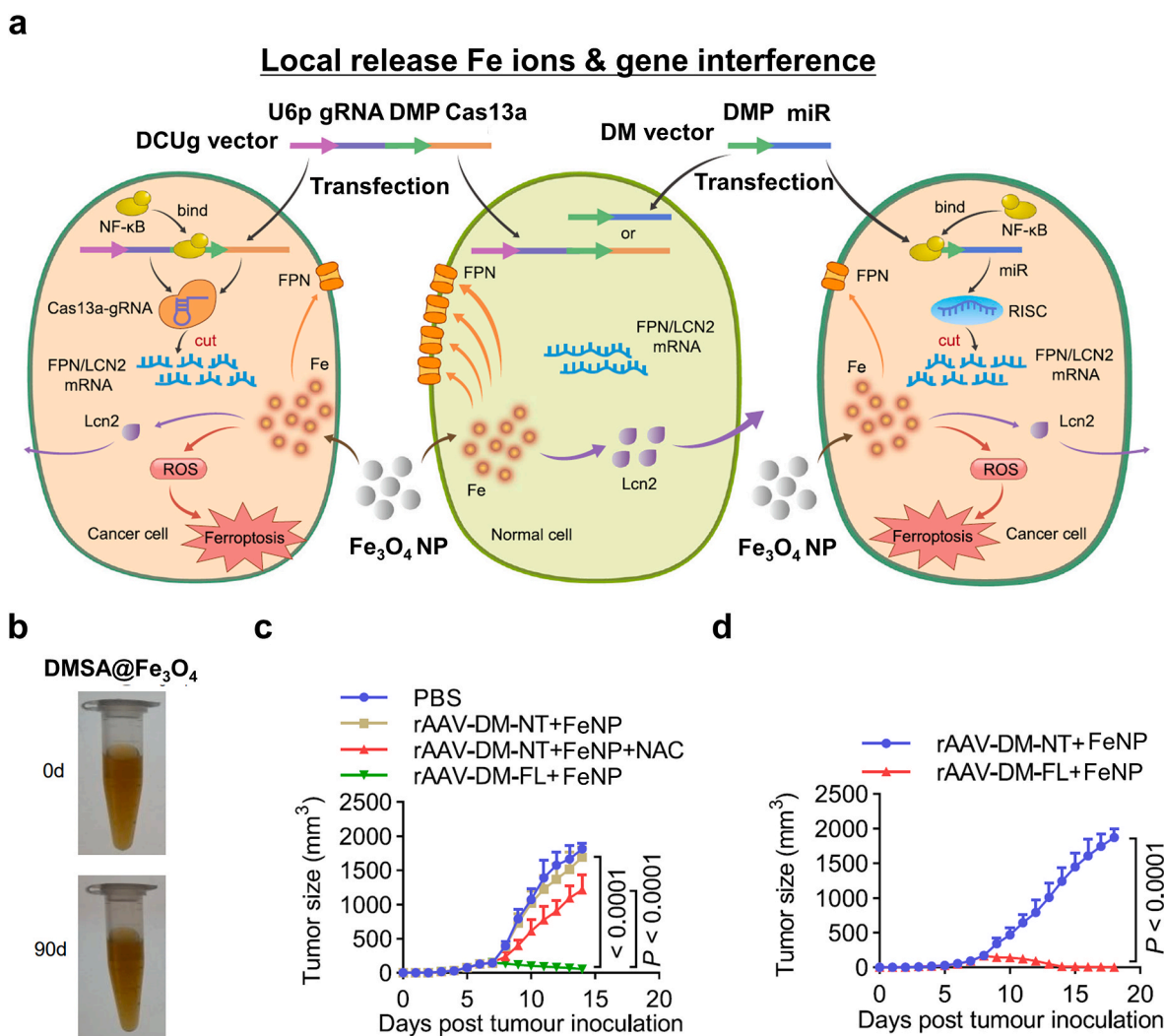
Fig. 8. Gene-interference ferroptosis therapy (GIFT). (a) A schematic diagram of CRISPR/cas13a- and miRNA-based GIFT. (b) Stability of the DMSA-coated Fe_3O_4 nanoparticles over 90 days. (c–d) The *in vivo* antitumor effect of GIFT in (c) WEHI-3-xenografted mice and (d) CT-26-xenografted mice. Data are presented as the mean $\pm$ standard deviation (n = 10 mice). Reproduced with permission [151]. Copyright 2021, Springer Nature.

(BQR; an FDA-approved DHODH inhibitor) and functionalized with CD63 antibodies and human mesenchymal stem cell (hMSC)-derived exosomes with angiopep-2 (ANG) and CD63 embedded in their membranes. In Addition, small interfering RNA of GPX4 (siGPX4) was enveloped in the exosomes via electroporation. The two components were conjugated via antigen-antibody interaction (Fig. 10b). ANG enabled the exosome-conjugated MNPs to cross the blood-brain barrier (BBB) and specifically target GBM cells, while BQR become subsequently localized in the TME (Fig. 10c). Furthermore, the exosome-conjugated MNPs were effectively delivered to the tumor region due to them having 3D-printed magnetic NdFeB helmets (Fig. 10d and e). As a result, the exosome-conjugated MNPs localized within the TME provided a combinational therapeutic effect against GBM cells by distinguishing DHODH, the localized delivery of siGPX4, and the release of Fe^{2+} ions that then induced the Fenton reaction. Thus, magnetic field-targeted ferroptosis induction provides an exciting approach for treating GBM. Furthermore, Wang and co-workers reported that the intratumoral implantation of micromagnet successfully employed 50% more MNPs in a tumor via enhanced permeability and retention (EPR) [158].

4.3. Magnetic nanoparticles for magnetic field-triggered ferroptosis cancer nanomedicine

Among various types of MNPs, Fe_3O_4 NPs comprise a strong candidate for ferroptosis induction owing to their biocompatibility and unique magnetic properties. However, in terms of ROS productivity, Fe_3O_4 may not be a top priority due to its chemical structure comprising two Fe^{3+} and one Fe^{2+} ion. The Fenton-like reaction involving Fe^{3+} ions has a much lower reaction constant than the Fenton reaction involving Fe^{2+} ions, thus Fe_3O_4 is usually combined with a complementary source for reducing Fe^{3+} ions to Fe^{2+} ions to maximize ROS production in catalytic processes (i.e., the photo-Fenton and electro-Fenton processes) [159]. Yu et al. hypothesized that if a reducing agent is released under an external magnetic field, it would be able to utilize reactive Fe^{2+} ions and thereby enhance ferroptosis [105]. They synthesized a hybrid core-shell vesicle (HCSV) composed of ascorbic acid in the core and Fe_3O_4 NPs embedded in a poly(lactic-co-glycolic acid) (PLGA) shell (Fig. 11a). A circularly polarized magnetic field (CPMF) at 2 Hz induced circular back-and-forth vibration of the iron oxide NPs, resulting in the gradual degradation of the PLGA shell and consequential release of ascorbic acid and Fe_3O_4 NPs in the TME (Fig. 11b). Fe^{2+} and Fe^{3+} ions were released from Fe_3O_4 NPs in the acidic TME, and ascorbic acid reduced the Fe^{3+} ions, thereby increasing the Fe^{2+} ions (Fig. 11c). The
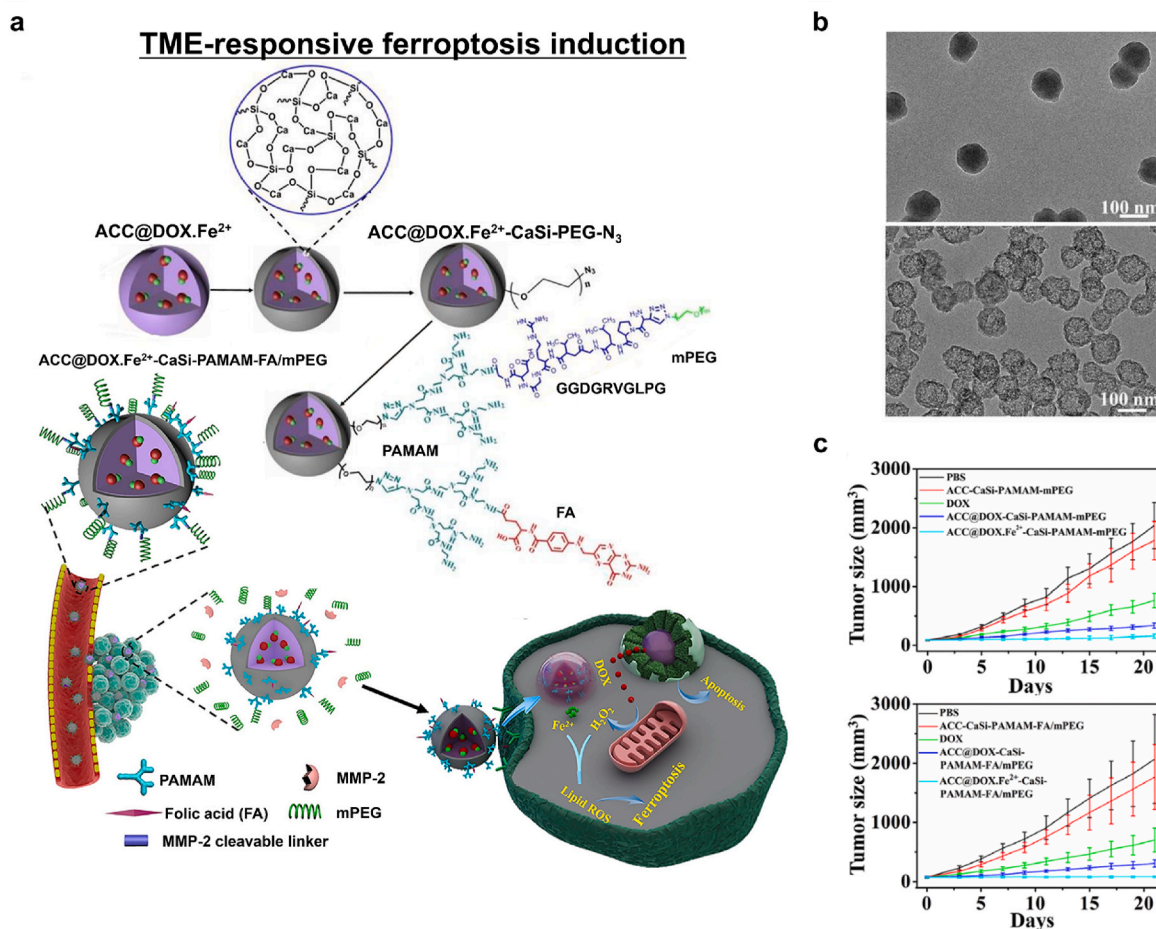
Fig. 9. TME-responsive ferroptosis induction. (a) Schematic diagrams of the synthesis of ACC@DOX.Fe^{2+}-CaSi-PAMAM-folic acid (FA)/mPEG and its mechanism of therapeutic action in the TME. (b) Impact of pH (left, pH 7.4; right, pH 5.5) on the release of DOX-Fe^{2+} from the ACC substrate. (c) The *in vivo* therapeutic efficacy of the nano-formulation using the 4T1 tumor-bearing mice model (n = 6). Reproduced with permission [152]. Copyright 2020, American Association for the Advancement of Science.

Fe^{2+} ions in TME boosted iron metabolism and ROS production, leading to the downregulation of GPX4. Calreticulin (CRT) expression was also upregulated due to the triggered oxidative stress (Fig. 11d). An intra-tumoral injection of HCSVs and CPMF treatment significantly inhibited tumor growth (Fig. 11e). Moreover, the reduction of Fe^{3+} ions made the MRI R2* signal change, which could be used to provide the progress of ferroptosis (Fig. 11f). Thus, an exogenous magnetic field can be used to trigger ferroptosis and combinational immunotherapy applications.

4.4. Magnetic resonance image (MRI)-guided ferroptosis cancer medicine

MRI is the first option for monitoring ferroptosis nano-inducers due to the magnetic moment originating from the iron ions dephasing the dipole moment of adjacent protons via T$_2$ (spin-spin) relaxation [160, 161]. Compared to other imaging modalities such as computed tomography (CT) [162], photoacoustic imaging (PAI) [163], and ultrasound [164–167], MRI has some unique characteristics: non-invasive imaging without radiation, deep tissue penetration, and high resolution for soft tissue. Besides, NP ferroptosis inducers can provide time-dependent MRI contrast changes via the Fenton reaction. Recently, novel strategies for MRI-guided ferroptosis-induction cancer therapy have been reported. Zhang et al. created MRI-guided ferroptosis-induction magnetosomes using magnetic Fe$_3$O$_4$ nanoclusters (NCs) coated with a leukocyte membrane [106]. After injection the magnetosomes intravenously, they could be efficiently localized within the TME by applying an external magnetic field owing to the high magnetism of the NCs. Meanwhile, the

superparamagnetic property of the magnetosomes enabled their non-invasive T$_2$ MRI-guided delivery that consequentially induced ferroptosis and immunomodulation within the TME. Yu and coworkers reported an image-guided ferroptosis inducer comprising hybrid core-shell vesicles that can release ascorbic acid and iron oxide nano-cubes under CPMF [105]. They focused on monitoring the Fe^{3+}: Fe^{2+} ratio via MRI R2* because the two ions exhibited significantly different magnetic relaxation behaviors (Fig. 11f). The progress of the reduction of Fe^{3+} to Fe^{2+} (indicating the progress of Fenton reaction-mediated ferroptosis) was correlated with a decrease in the MRI R2* signal. Therefore, MRI can be utilized to confirm the localization of the nano-medicine as well as track its therapeutic effects. Luo et al. synthesized a theranostic platform composed of Fe^{3+}/Gd^{3+} chelated polyphenol, an amphiphilic polymer skeleton, and cinnamaldehyde as a prodrug [107]. The nanoplatform became depolymerized in the TME due to the high level of GSH, resulting in the activation of the prodrug. Furthermore, increased intracellular H$_2$O$_2$ boosted the Fenton reaction that induced ferroptosis and was subsequently followed by the release of Gd^{3+} ions within the tumor. The T$_1$ MR contrast was significantly enhanced by the free Gd^{3+} ions that accelerated the relaxation of water protons, thereby enabling visualization of the progress of the therapeutic effect and providing the ability to post-operative monitor tumor lesions. Shen et al. fabricated Fenton-reaction-accelerable nanomedicine based on Fe$_3$O$_4$/Gd$_2$O$_3$ hybrid NP [108]. T$_1$-weighted MRI of a brain tumor indicated that the hybrid NPs successfully transported across the BBB. Furthermore, they adopted diffusion-weighted MRI to monitor their
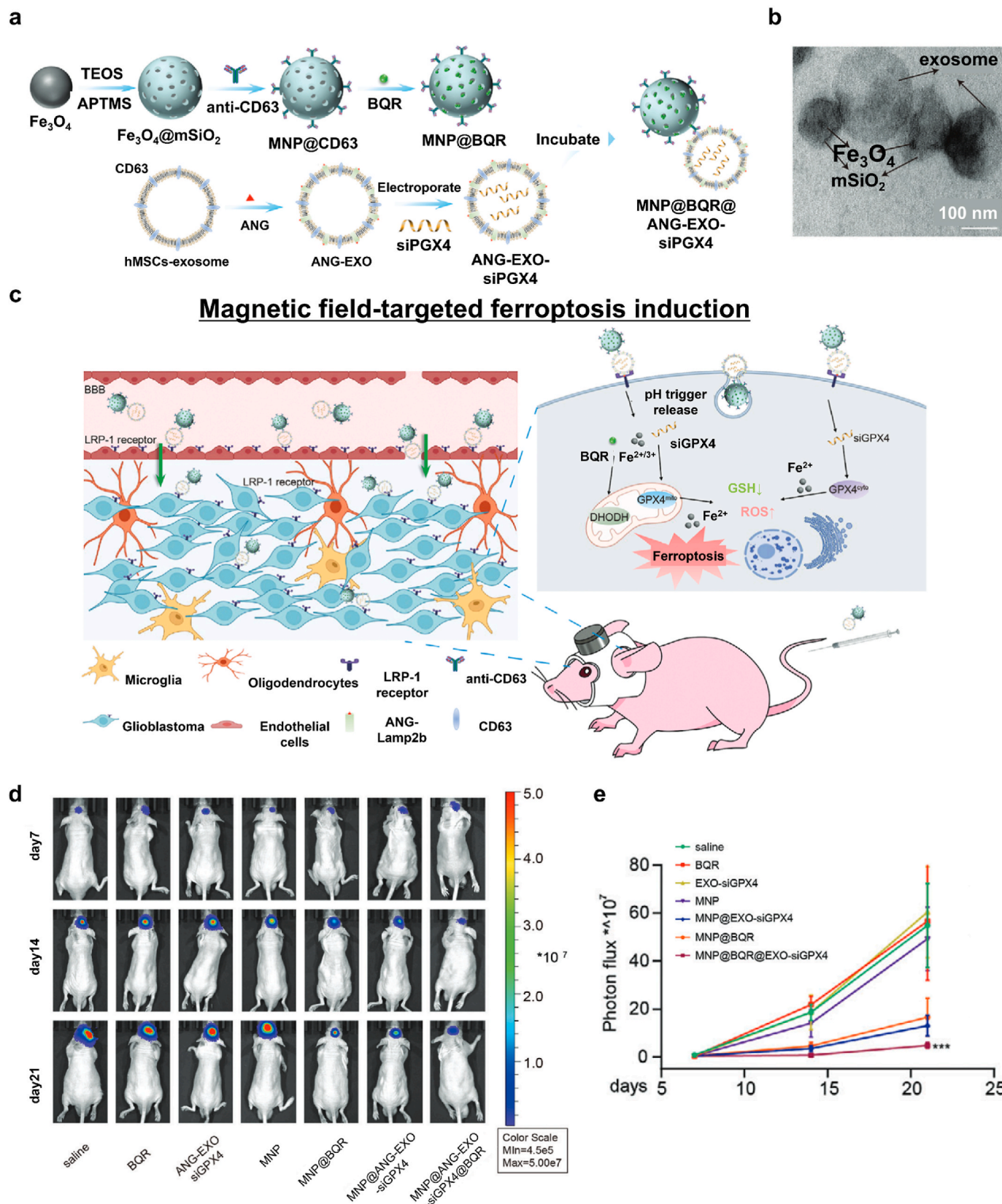
Fig. 10. Ferroptosis-inducing platform using MNPs for magnetic targeting and drug delivery. (a) A schematic illustration of the design and synthesis of MNP@BQR@ANG-EXO-siGPX4. (b) Representative transmission electron microscopy (TEM) images of Fe_3O_4 NPs (top left), MNPs (top right), and the MNP-exosome conjugate (bottom). (c) The mechanism underlying the induction of GBM cell ferroptosis. (d) Luminescence images of orthotopic LN229-Luc + human GBM tumor-bearing nude mice. (e) Quantitative analysis of luminescence images. Reproduced with permission [104]. Copyright 2022, John Wiley & Sons.
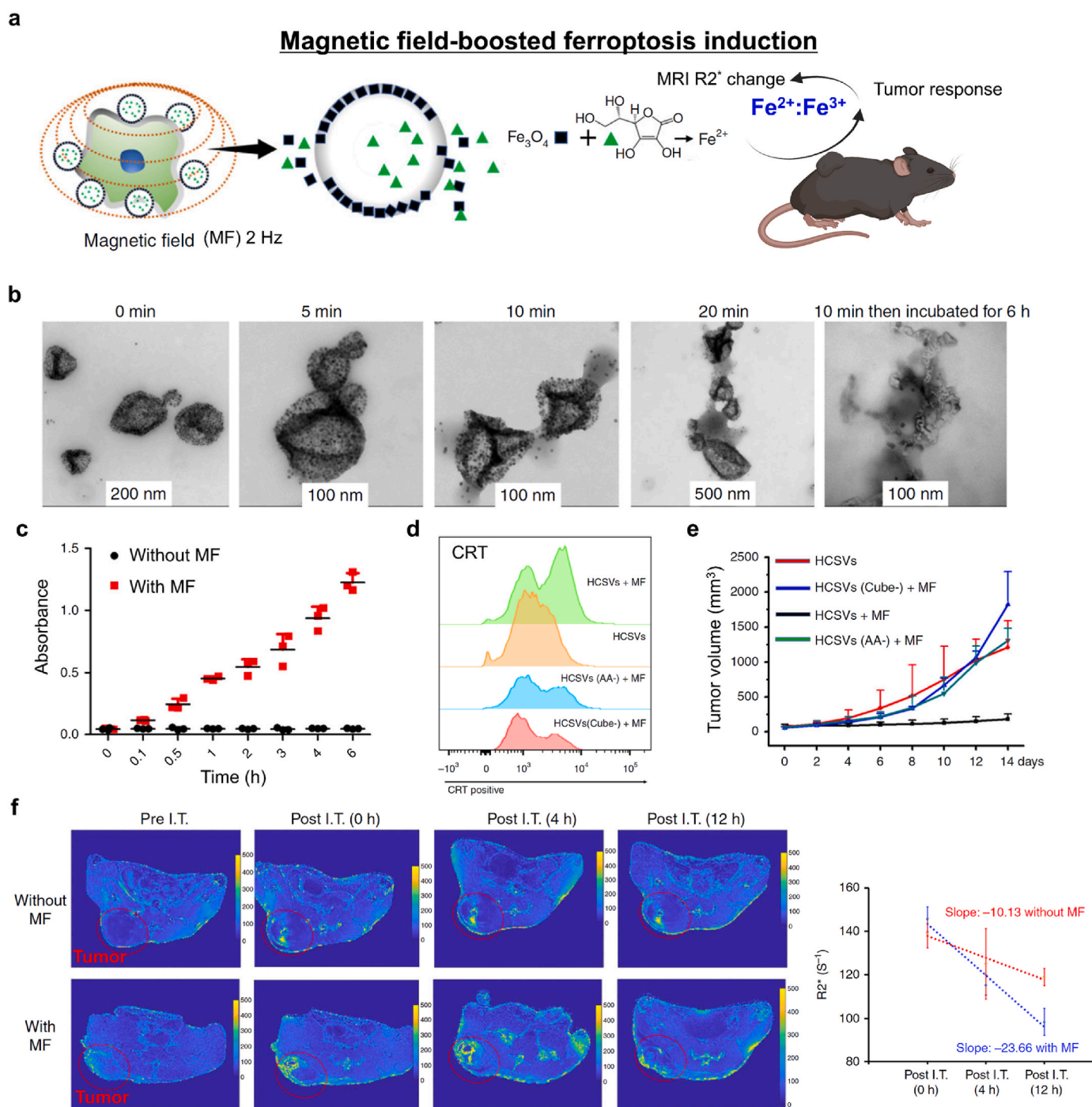
Fig. 11. Magnetic field-mediated ferroptosis induction. (a) A schematic illustration of using an exogenous magnetic field (MF) to boost Fenton reaction. (b) TEM images of HCSVs treated with a circularly polarized MF (2 Hz). (c) The time-dependent relative concentration of Fe^{2+} ions. (d) A flow cytometry histogram of CRT expression on the surfaces of TrampC1 cells after treatment. (e) Tumor response after treatments. (f) R2* mapping and changes after intratumoral injection of HCSVs. The red circle indicates the tumor region. Reproduced with permission [105]. Copyright 2022, Springer Nature.

therapeutic efficacy because it is sensitive to the movement of water protons and so is especially useful for monitoring the progress of ferroptosis via the apparent diffusion coefficient change at the molecular scale. In contrast, T_1-weighted MRI can be used to visualize the therapeutic progress via morphological changes in the tumor at the tissue scale. Xu et al. employed a pH-responsive tannic acid-Fe^{3+} complex as an MRI-guided ferroptosis-induction cancer nanomedicine [109]. Tannic acid releases Fe^{3+} in the acidic TME, thereby increasing the T_1-weighted MR contrast effect originating from the increase in Fe^{2+} ions in the tumor cells as the tannic acid-Fe^{3+} complex dissociates. Koo

et al. suggested Cu–Fe bimetallic peroxide NPs as a TME-sensitive Fenton reaction inducer [168]. Cu–Fe peroxide NPs decompose into free Cu and Fe ions via cyclic redox reactions within the acidic TME. The release of Fe ions caused s 20-fold increase in T_1 relaxivity compared to that at neutral pH. The low r_2/r_1 ratio of the Cu–Fe NPs (1.46) indicates they efficiently improved the T_1 contrast effect and marked the tumor region with a much brighter T_1-weighted MR signal compared to normal tissue. Zhu et al. developed T_1-T_2 dual modal MRI-guided ferroptosis nanomedicine based on incorporating Gd species within iron oxide MNPs [110]. Dual-modal T_1-T_2 MRI offered accurate tumor diagnosis by the

cross-checking because T_2-weighted MR contrast effect from iron oxide MNPs could be affected by material-dependent properties such as calcification, bleeding, or metal deposits. Zhang and colleagues reported a $MnFe_2O_4$ NP-based nanozyme for real-time MR monitoring and ferroptosis-chemotherapy toward pancreatic adenocarcinoma [111]. Manganese-doped iron oxide NPs exhibited enhanced magnetic susceptibility and shortened T_2 relaxivity. Significant T_2-contrast effect of $MnFe_2O_4$ NPs appeared in the tumor region 30 min after intravenous injection and lasted for 4 h. Chen et al. employed superparamagnetic Fe_3O_4 NPs-loaded PLGA particles as an MRI-guided ferroptosis inducer [126]. The acidic TME induced the degradation of PLGA and the release of Fe_3O_4 NPs in the tumor. The Fe_3O_4 NPs exhibited a similar T_2 contrast effect as commercial contrast agents Feridex and Resovist. The authors evaluated the tumor-targeting efficiency and retention in the tumor region of their nanomedicine via T_2-weighted MRI intensity. Additionally, the assembly of γ-Fe_2O_3 nanocrystals could be disassembled under
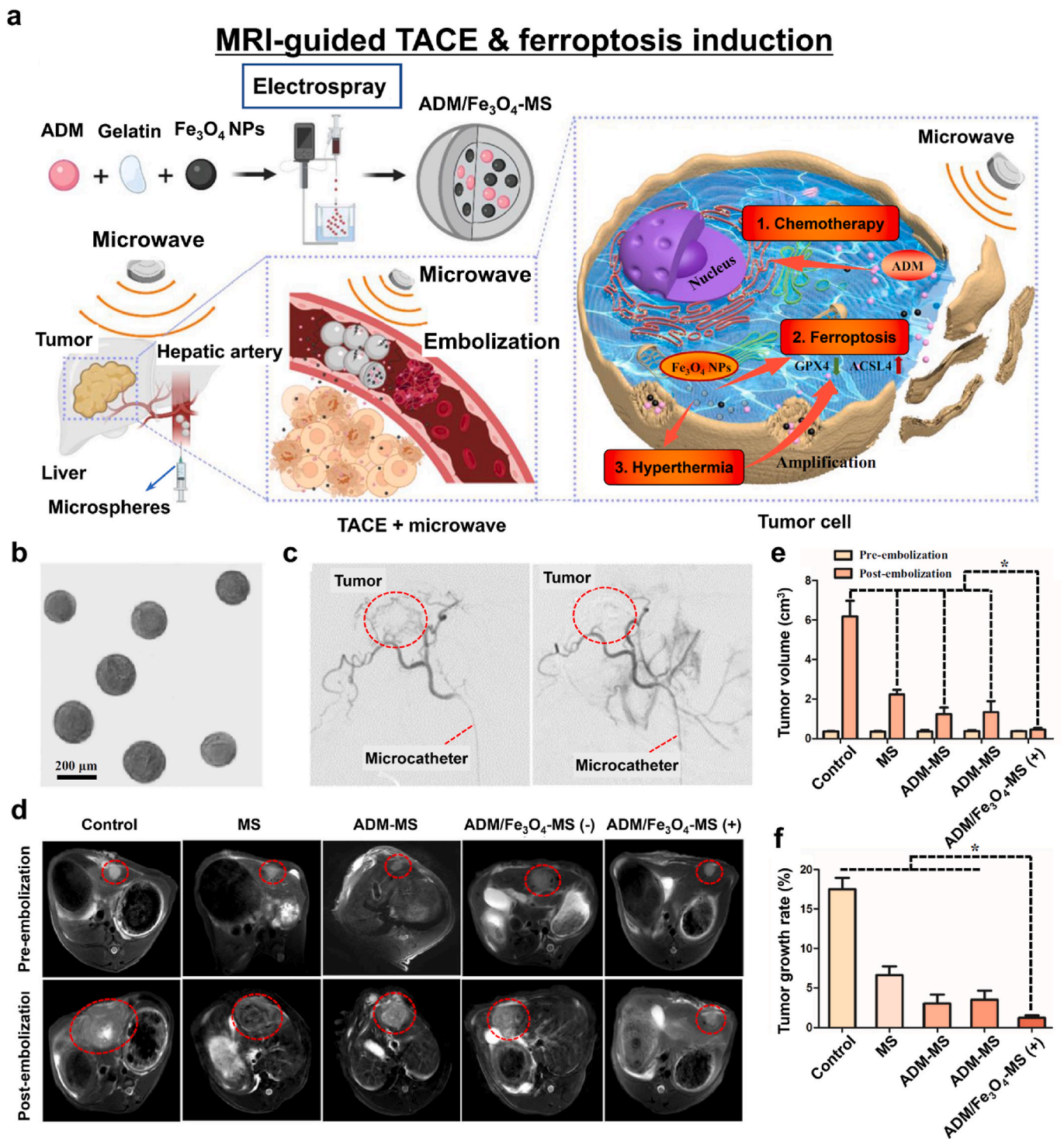
Fig. 12. MRI-guided TACE and ferroptosis induction. (a) A schematic diagram of ADM/Fe_3O_4-MS and TACE treatment. (b) A representative microscopic image of ADM/Fe_3O_4-MS. (c) Digital subtraction angiography before (left) and after (right) embolization. (d) T_2-weighted MR images of tumor-bearing rabbits before and 2 weeks after treatment. (e) Tumor volume and (f) tumor growth rates in each rabbit group. Reproduced with permission [112]. Copyright 2022, Springer Nature.

acidic TME, resulting in the switching from T_2-weighted MRI to T_1-weighted MRI [169].

Among the various clinical intraosseous practices, transcatheter arterial chemoembolization (TACE) can be used as a minimally invasive procedure for treating advanced hepatocellular carcinoma (HCC) and is conducted using MRI guidance. Thus, ferroptosis-inducing nanomedicines combined with TACE offer great potential for cancer treatment. Drug-eluting microspheres comprise a commonly used clinical chemoembolization agent with moderate therapeutic outcomes. Recently, Chen et al. developed gelatin microspheres containing Adriamycin (ADM) and Fe_3O_4 NPs (ADM/Fe_3O_4-MS) for localized ferroptosis-induction cancer therapy (Fig. 12a) [112]. ADM/Fe_3O_4-MSs were homogeneously synthesized via a high-voltage electrospray method (Fig. 12b). With angiographic guidance, the microspheres were used to completely block the hepatic artery (Fig. 12c). Consequently, the HCC tumor cells were deprived of essential oxygen and nutrients and ADM was locally released. The Fe_3O_4 NPs provided both T_2-weighted MR contrast and ferroptosis-inducing cancer therapy in combination with microwave-induced hyperthermia (Fig. 12d). When microwaves irradiated ADM/Fe_3O_4-MS, Fe_3O_4 NPs generated enough heat to make the tumor cells sensitive to the released ADM and microspheres. Moreover, iron oxide NPs released Fe^{3+} and Fe^{2+} ions into the TME and successfully induced ferroptosis, as confirmed by significant decreases in ferroptosis markers GPX4 and ACSL4 (Fig. 12e and f). This study is an excellent demonstration of using MRI-guided ferroptosis-induction nanomedicine with clinically interventional oncology procedures.

Recently, the unique characteristics of Mn and its derivatives such as

pH-responsiveness and degradability have led to their widespread application in cancer therapy [170]. Wang et al. created Mn silicate NPs via bubble formation due to the decomposition of ethanol to CO_2 during the synthesis process [113]. The bubble structures were less stable and degraded more rapidly than their solid NP counterparts. Degradation of the nanobubbles caused the fast reduction of Mn oxides to Mn^{2+} ions by GSH, which increased the r_1 relaxivity for T_1 MRI. Hence, greater GSH depletion and subsequently enhanced ferroptosis and MRI contrast were seen with the Mn silicate nanobubbles than with solid silica NPs.

Metal-organic frameworks (MOFs) in which metal ions and organic ligands form periodic and coordinative bonds with each other have emerged as a new class of NPs. The distinct feature of MOFs is their structure; around 90% of their volume is free, into which small molecules can be loaded. Furthermore, their coordinatively bonded structure makes them sensitive to the acidic TME, thereby enabling the release of drugs and metal ions. Fe-based MOFs have attracted attention as competitive ferroptosis inducers. Meng et al. reported a novel FePt-MOF nanocomplex as a theranostic agent for cancer therapy [114]. They encapsulated FePt NPs into a hexagram-shaped MIL-101(Fe) MOF and decorated its surface with a tumor-homing peptide (tLyp-1) to enhance its tumor targetability (Fig. 13a and b). As the MOF degraded in the acidic TME, it released drugs and metal ions leading to the accumulation of LPO. Moreover, the Fe and Pt components offered dual MRI and CT capability, thereby enabling precise image-guided drug delivery (Fig. 13c and d); the released Fe ions generated highly reactive hydroxyl radicals in the TME via the Fenton reaction and consequently contributed to the inhibition of tumor growth via ferroptosis (Fig. 13e). Xu and
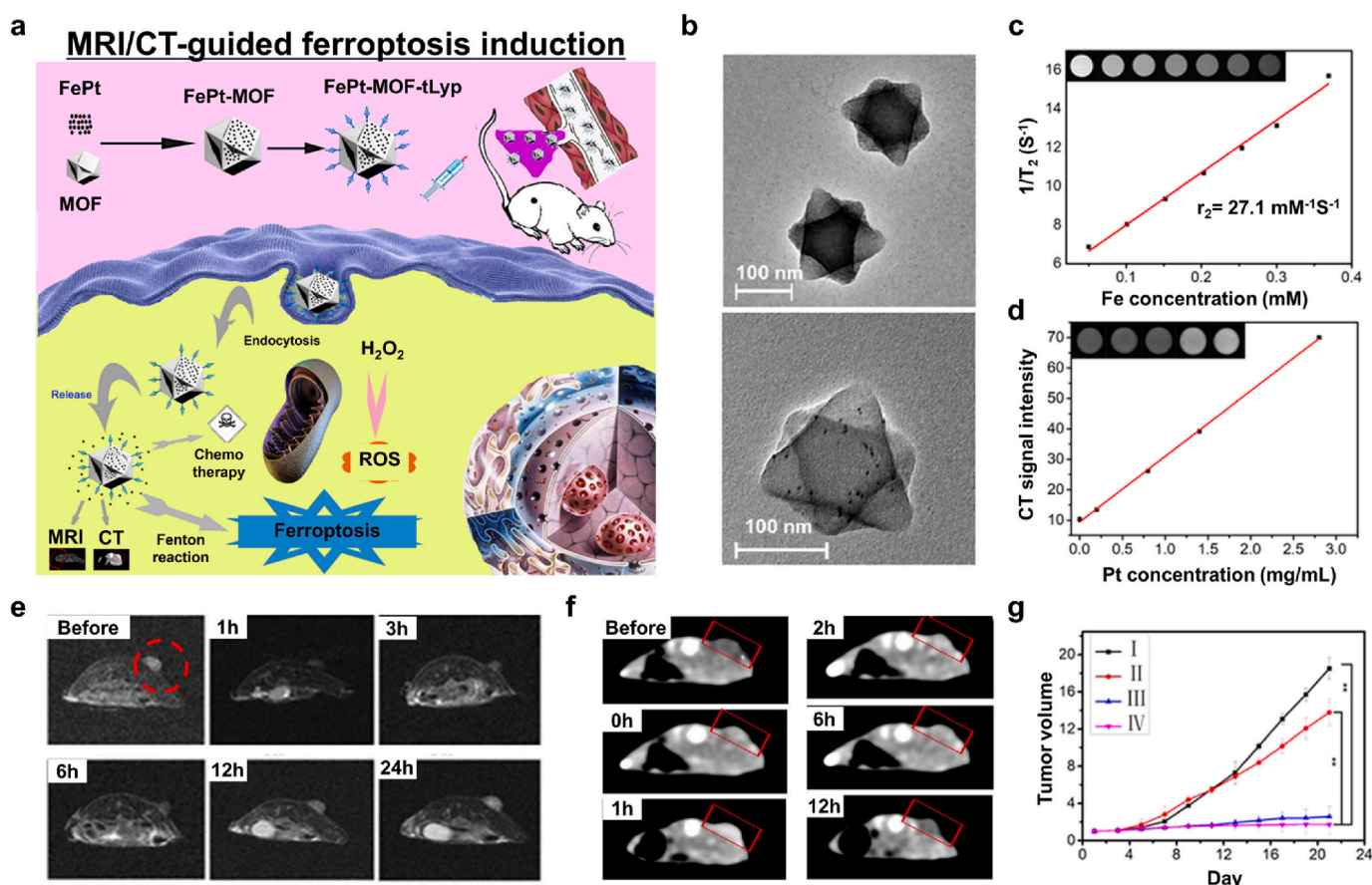

Fig. 13. MRI/CT-guided FePt MOF ferroptosis nanomedicine. (a) A schematic diagram of FePt-MOFs-tLyp-1 NCs and their mechanism of pH-responsive action for ferroptosis therapy and MRI/CT imaging. (b) TEM image of FePt-MOF NCs. (c) Iron concentration dependent T_2 relaxation times. (d) Pt concentration dependent CT intensity (Hounsfield intensity). (e) *In vivo* T_2-weighted MRI (axial plane), and (f) *in vivo* CT imaging (axial plane) of 4T1 tumor-bearing mice after intravenous injection of FePt-MOF-tLyp-1 NCs. (g) Tumor response after treatment (I, PBS; II, MOF-tLyp-1; III, FePt(R)-MOF-tLyp-1; and IV, FePt(S)-MOF-tLyp-1). Reproduced with permission [114]. Copyright 2020, American Chemical Society.

coworkers studied similar concept utilizing the localized release of iron ions [171]. They synthesized a MOF comprising Fe^{2+} and 2-aminoterephthalic acid (BCD) and coated it with hyaluronic acid (HA) to make it hydrophilic and enhance the drug retention time. The Fe^{2+}-BCD MOF maintained its structural stability under physiological conditions but degraded in the acidic TME. Besides, synergistic ferroptosis nanomedicines with diagnostic imaging utilizing fluorescent dyes, upconverting NPs, and PAI have been reported [172].

Iron oxide NPs release iron ions in the acidic TME that can provide T_2-weighted MR contrast owing to their magnetic property. Guan et al. suggested superparamagnetic iron oxide NPs and SRF-incorporated mesoporous polydopamine (MPDA) NPs (SRF@MPDA-SPIO) as a ferroptosis nanomedicine (Fig. 14a and b) [115]. MPDA NPs were formed through π−π interactions between SRF and polydopamine (PDA). Since PDA is amphiphilic, the SPIO NPs clustered on the MDPA via hydrophobic interactions could interact with their neighbors, leading to a relatively decreased T_2 relaxation time (Fig. 14c). Intravenously injected SRF@MPDA-SPIO was efficiently accumulated to the tumor. After confirming the localization of NPs by time-dependent MRI (Figs. 14d), 808 nm NIR laser irradiation was applied to boost the release of iron ions. Released SRF, Fe^{2+}, and Fe^{3+} successfully induced ferroptosis (Fig. 14e–i).

In an approach to add the MRI contrast effect to a novel ferroptosis nanoagent, Zhang and coworkers developed porous nanopeanuts composed of Gd-oxide and Fe-oxide (GINP) [116]. To synthesize the porous GINPs, they utilized a solvothermal method to first form anisotropic nanowires and the allowed the reaction to proceed for 4 days to sufficiently grow the internal lumen (Fig. 15a). The GINPs were able to store oxygen and Pt (IV) prodrug in the free space therein. Tf-labeled amino polyethylene glycol (Tf-PEG-NH$_2$) was conjugated to the GINPs to enhance their tumor-targeting ability, biocompatibility, dispersion stability under physiological conditions, and GSH responsiveness. According to inductively coupled plasma mass spectrometry (ICP-MS) results, the GINPs loaded more Pt^{4+} content than other nanozymes. They also confirmed that the GINPs were composed of superparamagnetic Fe_3O_4 and paramagnetic Gd_2O_3 by attaining magnetic hysteresis loops at 3 and 300 K. Moreover, the GINPs exhibited better T_1 MR contrast ability than other Gd-based clinical contrast agents. In a tumor-bearing mice model, the GINPs provided obvious T_1 MR contrast 30 min after injection (Fig. 15b). After the GINPs were taken up by cancer cells, they released oxygen, the Pt prodrug, as well as Fe^{2+}, and Fe^{3+} ions in acidic TME. Released Pt (IV) prodrug depleted intracellular GSH and was reduced to Pt (II). Consequently, Pt (II) contents activated members of the nitric oxide synthase family resulting in a significant increase in the intracellular H_2O_2 level by converting oxygen into superoxide anions. Here, the porous GINP-Pt nanodrug system effectively inhibited tumor growth by inducing ferroptosis and apoptosis (Fig. 15c).
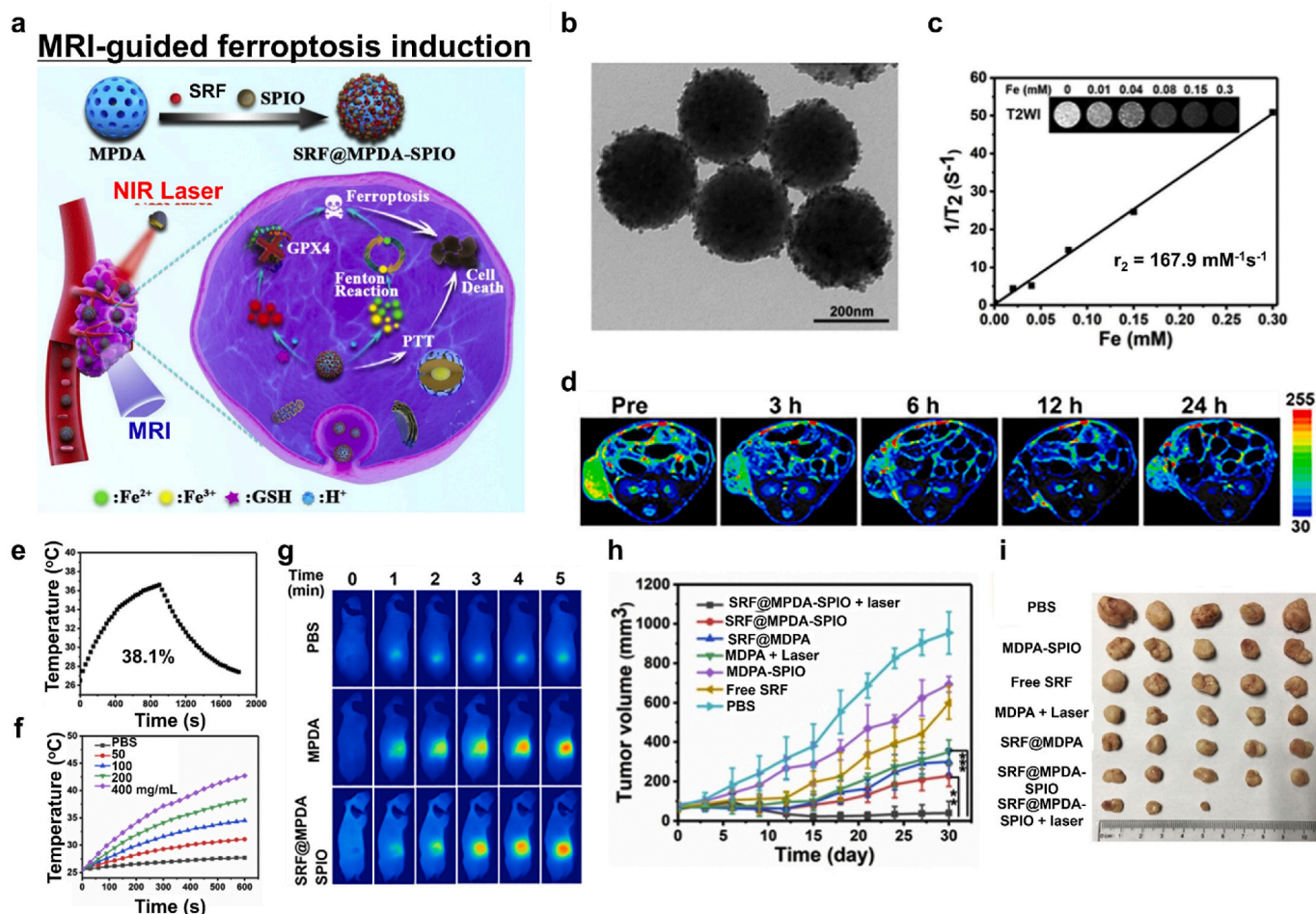

Fig. 14. MRI-guided ferroptosis induction with photothermal therapy (PTT). (a) Schematic diagram of MRI-guided ferroptosis/PTT combinational therapy using SRF@MPDA-SPIO. (b) A representative TEM image of SRF@MPDA-SPIO. (c) The T_2 relaxation rate of SRF@MPDA-SPIO. (d) *In vivo* pseudo-colored T_2-weighted MR image. (e) Photothermal conversion of SRF@MPDA-SPIO after NIR laser irradiation (808 nm, 1 W cm^{-2}). (f) Temperature elevation of SRF@MPDA-SPIO solution with various NP concentrations. (g) Infrared thermal images after laser irradiation. (h, i) The anticancer effect of SRF@MPDA-SPIO *in vivo*. Reproduced with permission [115]. Copyright 2020 Elsevier B.V.
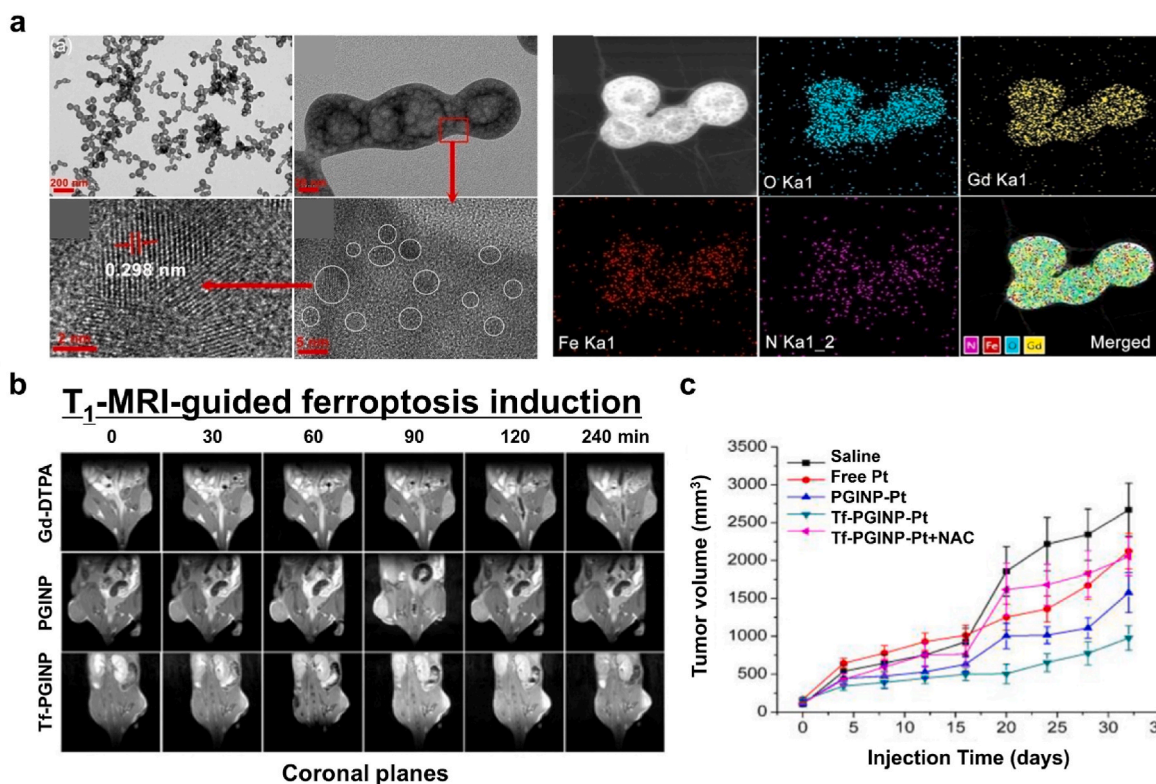
Fig. 15. T_1-weighted MRI-guided ferroptosis. (a) Representative TEM and elemental mapping images of the GINPs. (b) T_1-weighted MR images of tumor-bearing mice before and after injection of Gd-DTPA (clinical T_1 contrast agent), PGINP (porous Fe_3O_4/Gd_2O_3 nanopeanut), and Tf-GINP-Pt (Transferrin-coated PGINP loaded with Pt (IV) prodrugs). (c) The *in vivo* anticancer activity of Tf-GINP-Pt. Reproduced with permission [116]. Copyright 2020, Elsevier B.V.
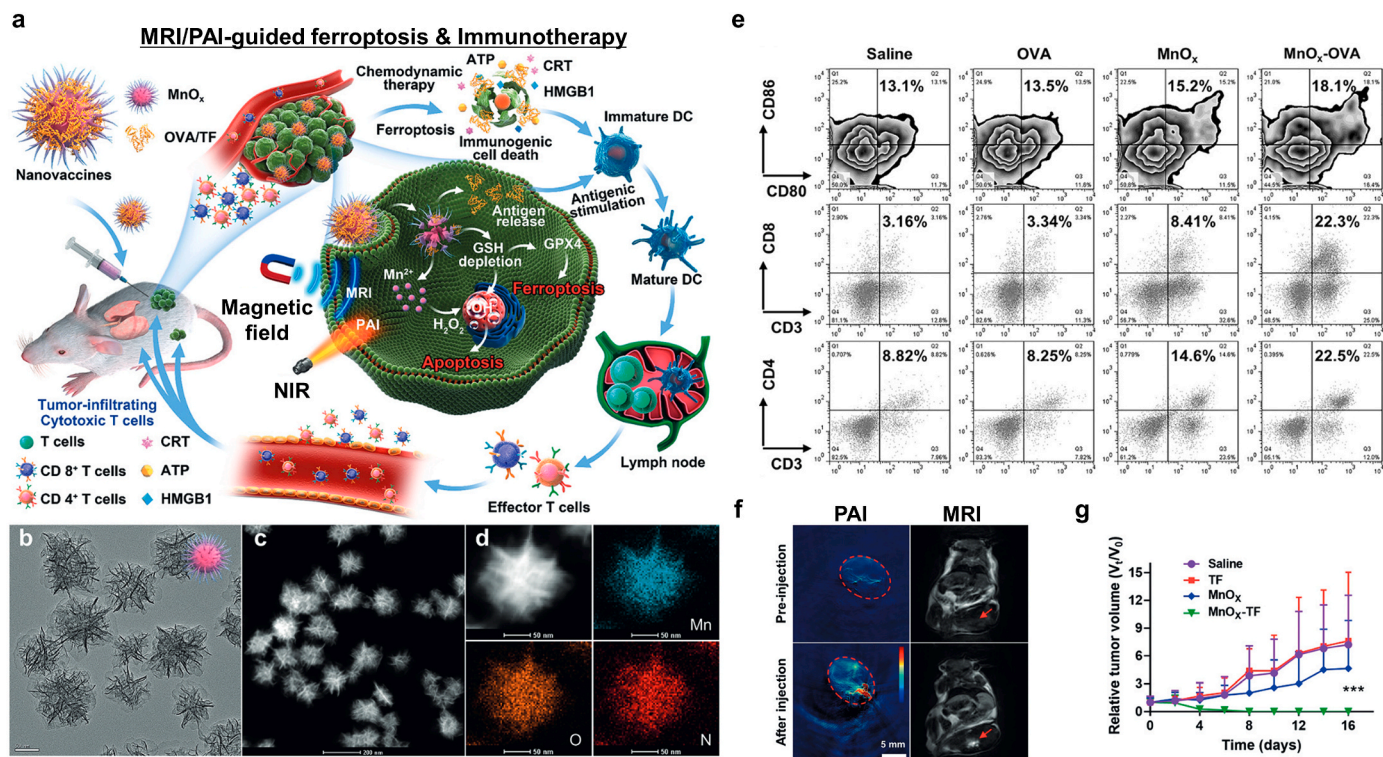
Fig. 16. Dual MRI/PAI-guided ferroptosis and cancer immunotherapy. (a) An illustration of the MnO_x-OVA/tumor cell fragment cancer immunotherapy vaccine with dual MRI/PAI. (b) TEM, (c) STEM, and (d) elemental mapping of MnO_x nanovaccines. (e) *In vivo* flow cytometry analysis of the DC, CD8 T cell, and CD4 T cell populations in tumor-bearing mice after treatment with various vaccine formulations. (f) *In vivo* MRI/PAI and (g) the relative tumor-growth curves of distant tumors. ANOVA was used to assess statistical significance: ***$p < 0.001$. Reproduced with permission [117]. Copyright 2020, John Wiley & Sons.

4.5. Magnetic ferroptosis nanomedicine with immunotherapy

Cancer immunotherapy, which activates and modulates the patients' immune system to kill cancer cells, has emerged as a powerful strategy to treat cancer [173]. Recently, it has been reported that cytotoxic T cells utilize ferroptosis for killing cancer cells. The JAK-STAT1 pathway is activated by cytotoxic T cells and leads to the downregulation of SLC7A11 and SLC3A2, which subsequently stimulates ferroptosis in cancer cells [56]. Downregulation of SLC3A2 in cancer cells is positively related to the efficacy of immune checkpoint inhibitor (ICI) immunotherapy [174]. Ferroptosis can be exploited in cancer therapy by linking it to various ligands that can activate STAT1. For example, transforming growth factor β1 (TGFβ1) can cause ferroptosis by downregulating SLC7A11 and upregulating zinc finger E-box binding homeobox1 (ZEB1) through SMAD signaling [175]. Ferroptotic cells release damage-associated molecular patterns (DAMPs), which can underlie antitumor immunity by arousing immunogenic cell death (ICD) [176]. Interplay between ferroptosis and the immune system is not always positively correlated (e.g., ferroptosis in melanoma is hindered by the increased monounsaturated fatty acid due to acyl-coenzyme A synthetase long-chain family member 3 (ACSL3). ICI immunotherapy has shown promising therapeutic outcomes in various cancers, while ferroptosis induction in combination with ICI immunotherapy is of great interest for cancer therapy since they may synergistically induce tumor growth inhibition. Recently, a combination of immunotherapy with ferroptosis using a TGF-β inhibitor and anti-PD-L1 loaded onto Fe_3O_4 NCs produced a synergistic antitumor effect in mice models for melanoma and breast cancer [106]. Ferroptosis was effectively induced via the reduction of the Fe_3O_4 NCs. The concurrent release of the immunotherapeutic resulted in an increase in the M1/M2 macrophage, $CD4^+/T_{reg}$, and $CD8^+/T_{reg}$ ratios in the TME. In other cases, co-delivery

of anti-TGF-β antibody and SRF using Fe_3O_4/Gd_2O_3 hybrid NP could induce ferroptosis as well as convert cold TME into hot TME [177]. Thus, the synergistic combination of ferroptosis and immunotherapy has been widely demonstrated. Here, recently published representative findings are discussed.

Ding et al. produced mixed MnO_x nanospikes (NSs) for cancer vaccine-based immunotherapy (Fig. 16a) [117]. They have a large lumen inside which antigens can be loaded (average pore size: 4.3 nm, total pore volume: 2.5 cm^3g^{-1}) (Fig. 16b–d). Intracellular GSH degraded the MnO_x NSs to produce Mn^{2+} ions, leading to escaping Mn^{2+} ions from the endo/lysosomes and GSH depletion. Moreover, intracellular ROS was enhanced, resulting in endosomal membrane oxidation and rupturing, as well as depletion of GPX4 and upregulation of LPO. On the other hand, high-mobility group box 1 (HMGB1) and ATP were increased after chemodynamic therapy (CDT). As a result, MnO_x NSs successfully employed mature DCs (Fig. 16e). Interestingly, MnO_x NSs had TME-sensitive imaging ability, exhibiting photoacoustic contrasting via the MnO_x phase and T_1 MR contrasting via the production of Mn^{2+} (Fig. 16f). The MnO_x cancer vaccine exhibited not only effective inhibition of tumor growth by utilizing ferroptosis and CDT via DC immunotherapy but also dual MRI/PAI for therapeutic procedure tracking.

One of the primary challenges in current immunotherapy is that immunogenicity can arouse cytokine-release syndrome and/or an abnormal inflammatory response. Jiang et al. reported SAS-loaded mesoporous Fe_3O_4 NPs and platelet (PLT) membrane (Fe_3O_4-SAS@PLT) for inducing ferroptosis and controlled immunogenicity (Fig. 17a) [118]. SAS, a commercial drug for treating rheumatoid arthritis, hinders inflammatory cell migration, blocks the IκB kinase pathway, and obstructs cysteine uptake, resulting in tumor growth inhibition and ferroptosis [178]. Fe_3O_4 NPs were synthesized via a polyol method using ammonium acetate and poly (γ-glutamic acid) and SAS
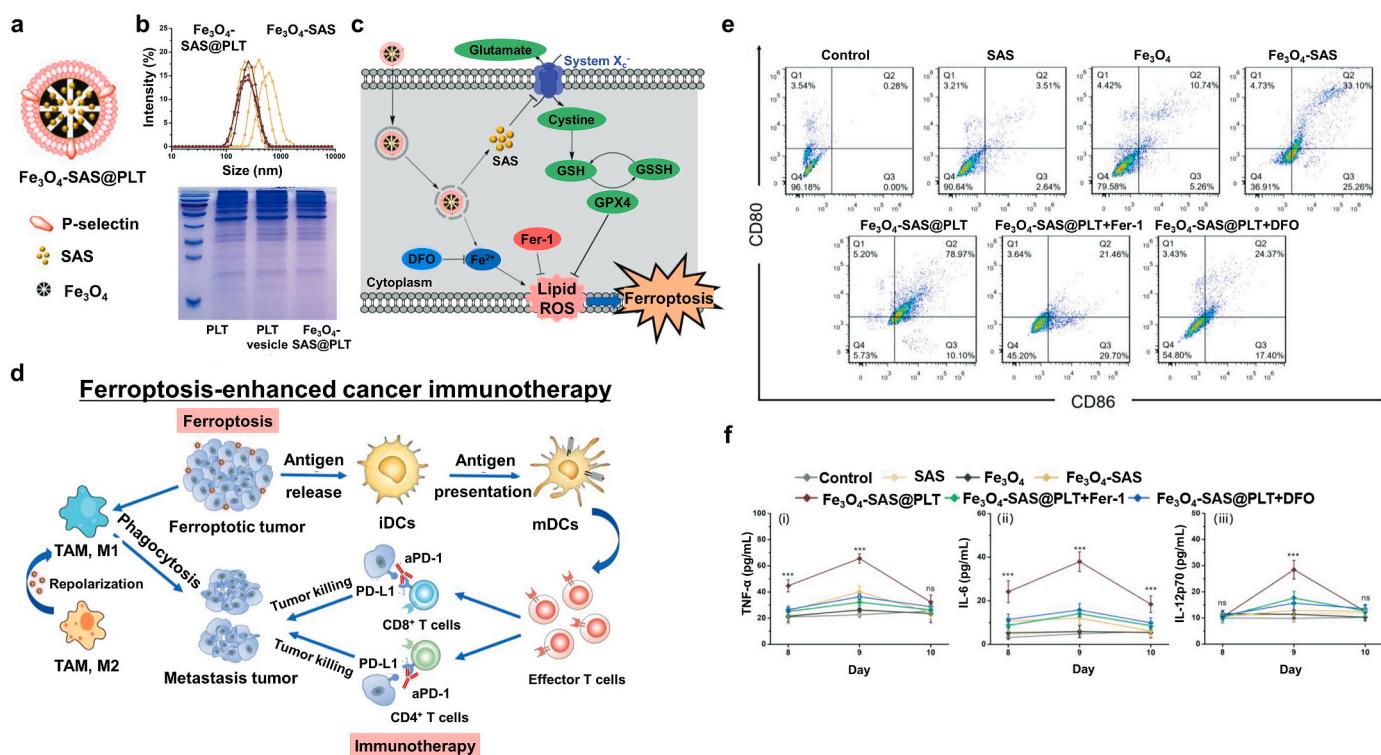

Fig. 17. Ferroptosis-enhanced cancer immunotherapy. (a) An illustration of Fe_3O_4-SAS@PLT nanoparticles. (b) Dispersion stability of Fe_3O_4-SAS@PLT in 10% fetal bovine serum (FBS)/phosphate-buffered saline (PBS) over a week and protein composition analysis of the PLT membrane. (c) A schematic diagram of Fe_3O_4-SAS@PLT-induced ferroptosis. (d) The mechanisms of Fe_3O_4-SAS@PLT-mediated ferroptosis-induced immunotherapy for metastatic tumors. (e) *In vivo* flow cytometry analysis of mature DCs in the lymph nodes of 4T1 metastatic tumor-bearing mice at 24 h after receiving various treatment regimens. (f) Secretion of TNF-α, IL-6, and IL-12p70 in the serum after treatment; n = 5; ns represented no significance, ***p < 0.001. Reproduced with permission [118]. Copyright 2020, John Wiley & Sons.

was physically incorporated into the pores of mesoporous Fe_3O_4 NPs via mechanical stirring. A PLT membrane was coated with Fe_3O_4-SAS via an extrusion method to produce an immunosurveillance-stealthy ferroptosis inducer. The PLT membrane formed a 10 nm thick shell and exhibited a higher negative surface zeta potential than Fe_3O_4-SAS (Fig. 17b). Fe_3O_4-SAS@PLT was successfully delivered to the cancer cells by evading the immunosurveillance system and mediated LPO by releasing iron ions, thereby downregulating system X_c^- and GPX4 in 4T1 cells (Fig. 17c). Consequently, the cells undergoing ferroptosis released abundant tumor antigens and stimulated DC maturation (Fig. 17d and e). Fe_3O_4-SAS@PLT could effectively target metastatic tumors and thereby produce a higher mature/immature DC ratio than other treatment groups. After treating Fe_3O_4-SAS@PLT, the significant upregulation of tumor necrosis factor-α (TNF-α), interleukin (IL)-6, and IL-12p70 was observed 48 h after intravenous injection (Fig. 17f). The authors suggested that Fe_3O_4-SAS@PLT-mediated ferroptosis could release moderate levels of tumor antigens and effectively induce activation of the immune system. Fe_3O_4-SAS@PLT also repolarized M2 macrophages to the M1 phenotype. Thus, it provides a novel approach for synergistic ferroptosis mediated immunotherapy for metastatic tumors.

Yao et al. developed FePt NPs embedded on ultrathin black phosphorous nanosheets (FePt/BP) for photothermal therapy (PTT), photodynamic therapy (PDT), CDT, ferroptosis, and immunotherapy [119]. First, they synthesized FePt NPs via thermal decomposition and then coated them with DMSA. After that, they modified the surface of BP with polyethylenimine (PEI) via electrostatic interaction. Subsequently, folic acid (FA) was conjugated with the BP to enhance tumor targetability (Fig. 18a). The FePt/BP-PEI-FA nanocomposite could be armed with versatile tumor therapeutic options: generating heat under 808 nm laser irradiation, singlet oxygen under 660 nm laser irradiation, specific cytotoxicity toward tumor cell displaying FA receptors, and lipid ROS accumulation via the Fenton reaction (Fig. 18b). In addition, the superparamagnetic properties originating from the small FePt NPs provided T_2-weighted MR contrasting. As a result of the multimodal tumor therapies, the number of mature DCs was increased and TNF-α, IFN-γ, and IL-12 were upregulated. Furthermore, they administered a cytotoxic T lymphocyte-associated protein 4 (CTLA-4) checkpoint inhibitor via the FePt/BP-PEI-FA nanocomposite that consequently inhibited both
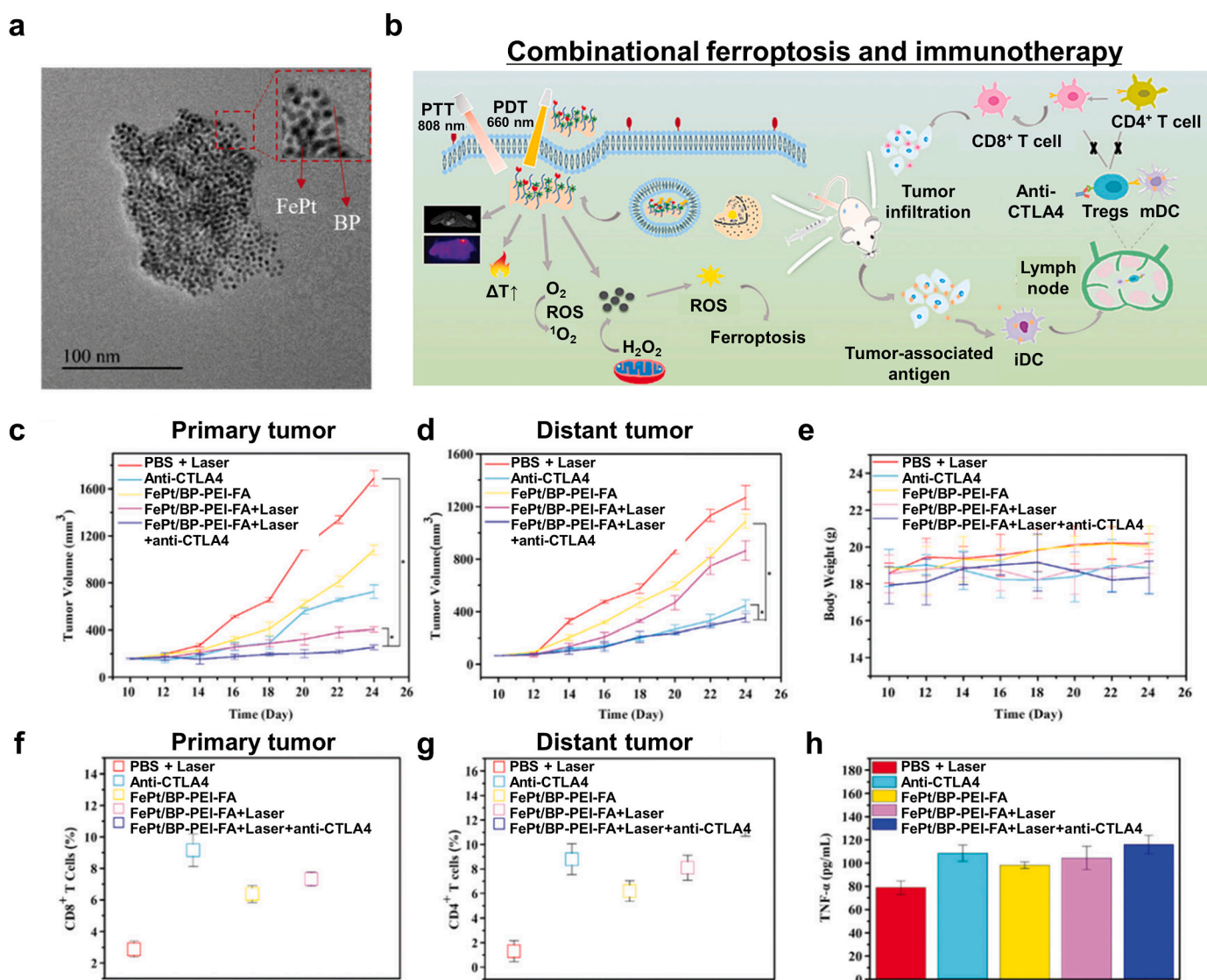

Fig. 18. Combinational PTT, PDT, CDT, and ferroptosis therapy. (a) A TEM image of the FePt/BP NCs. (b) A schematic diagram of the dual-mode imaging-guided synergistic PTT/PDT/CDT cancer therapies. (c, d) The antitumor effects toward primary (c) and distant (d) tumors under various treatment regimens: PBS, anti-CTLA4, FePt/BT-PEI-FA, FePt/BP-PEI-FA with laser irradiation (808 nm, 1.75 W cm^{-2}, 5 min), and FePt/BP-PEI-FA + anti-CTLA4 with laser irradiation (n = 3, *p < 0.05). (e) Body weight changes during the treatment. (f, g) T cells in distant tumors with the above-mentioned treatment regimens. (h) Cytokine levels for TNF-α. Reproduced with permission [119]. Copyright 2020, Royal Society of Chemistry.
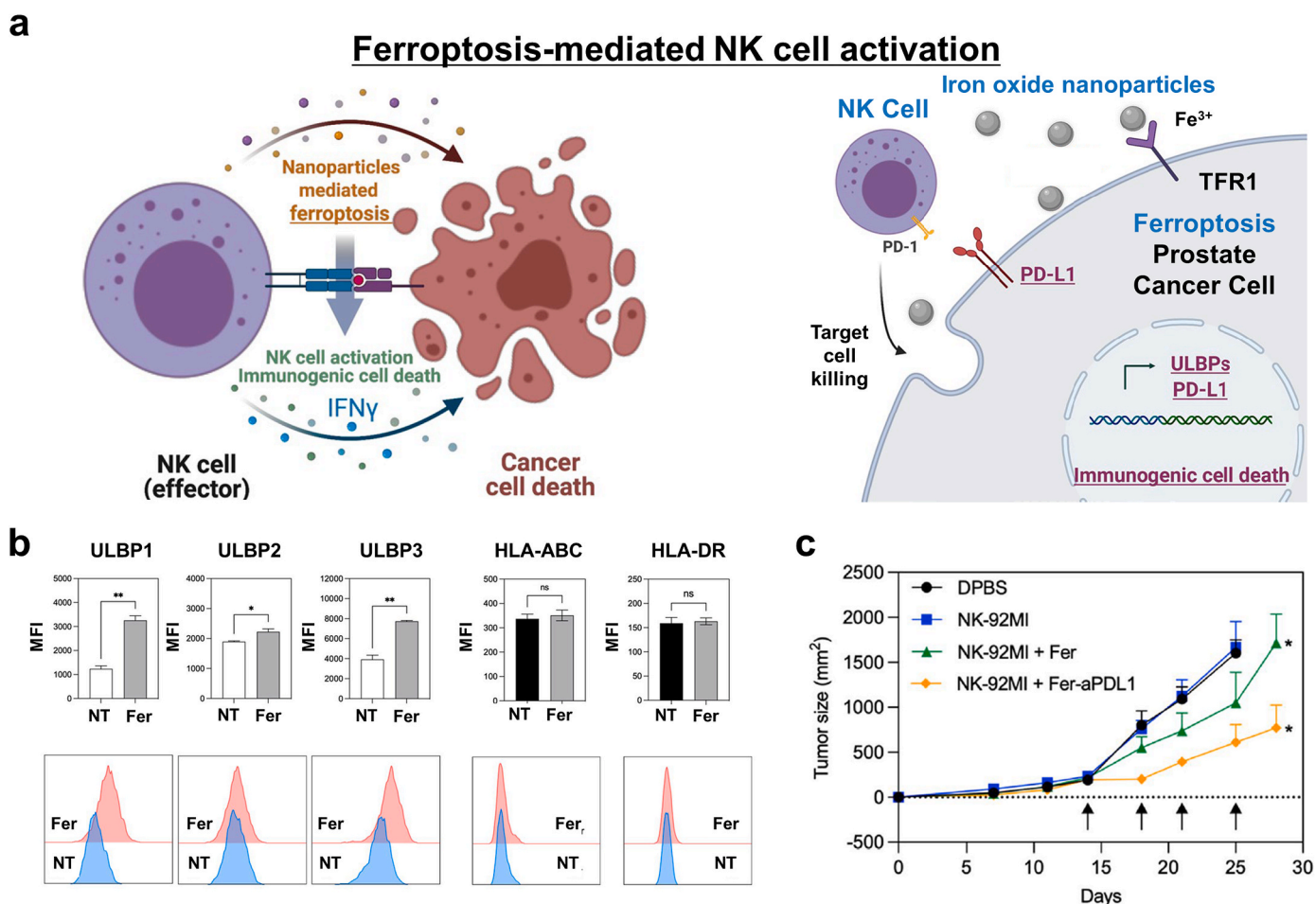
Fig. 19. Ferroptosis-mediated innate immunity. (a) A schematic diagram of combinational NK cell and iron oxide NP-mediated ferroptosis cancer therapy. (b) The expression of UL16BPs and MHC class I and II expression in PC-3 prostate cancer cells after iron oxide NP treatment. (c) Tumor-size curves for each treatment group: DPBS, NK-92MI, NK-92MI + Fer, NK-92MI + Fer-aPDL1. Reproduced with permission [120]. Copyright 2022, Springer Nature.

primary and distant tumor growth (Fig. 18c–h). The experimental results suggest that FePt/BP-PEI-FA NCs mediate ferroptosis and in combination with the ICI, is an effective approach for treating both primary and secondary tumors.

Ferroptosis can activate innate immunity as well as adaptive immunity for cancer treatment. Our group (Kim et al.) reported that iron oxide-mediated ferroptosis induction can activate natural killer (NK) cells to kill cancer cells (Fig. 19a) [120]. We focused on the immune response after ferroptosis, especially the release of NK cell-activating surface molecules, due to ferroptosis-induced ICD. The anticancer cytotoxicity of NK cells could be activated by the recognition of stress-inducible protein by activating receptors on the NK cell surface for NKG2D (natural killer group 2D). The stress-inducible molecules for NKG2D are UL16 binding proteins (ULBPs) and MHC class I chain-related protein A and B (MICA/B). Ferumoxytol (a clinical treatment for Fe-deficiency anemia using iron oxide NPs) successfully induced ferroptosis in prostate cancer PC-3 cells. Moreover, when PC-3 cells were co-treated with iron oxide NPs and NK cells, the degree of lipid ROS accumulation was significantly increased. Interestingly, the secretion of IFN-γ and the lysis of cancer cells due to the anticancer activity of the NK cells increased, and degranulation was also observed. Furthermore, UL16BP1, ULB16P2, and UL16BP3 were upregulated on the PC-3 cell surface after iron oxide NPs treatment (Fig. 19b). The UL16BPs on the cancer cells bound to the NKG2D ligand on the NK cells, which subsequently enhanced the anticancer efficacy of the latter. Since NK cells are innate immune cells, they have PD-1 receptors. Thus, adding anti-PD-L1 to the combinational NK cell and ferroptosis-inducing therapy is a novel strategy for treating cancer (Fig. 19c).

4.6. Synergistic magnetic ferroptosis combination therapy with multimodal imaging

Molecular mechanism regulating ferroptosis in cancer cells has been commonly involved with various cellular signals of cancer cells [179–181]. Combinational ferroptosis cancer therapy by finding synergistic biochemical pathways might be an effective way to maximize the anti-cancer therapeutic efficacy [182,183]. Those synergistic effects of combinational magnetic ferroptosis cancer medicine will be achieved by rational designing of MNPs or MNPs based hybrid nano-structures. MNPs based hybrid structures can possess extended options for the additional opportunity of ferroptosis based cancer therapy combined with various other cancer therapies along with additional medical imaging contrasts. In this section, we review synergistic ferroptosis combination therapy using MNPs based hybrid nanostructures.

Polypeptide-modified Fe_3O_4-containing 1H-PFP NPs (GBP@Fe_3O_4) to target prostate cancer cells were synthesized by encapsulating Fe_3O_4 NPs and 1H-PFP with PEG-PLGA. GBP@Fe_3O_4 mediated ferroptosis after light irradiation by first producing heat and then by releasing Fe_3O_4 via 808 nm laser irradiation. The release of Fe_3O_4 induced the production of ROS, leading to ferroptosis. In addition, the photothermic effect induced
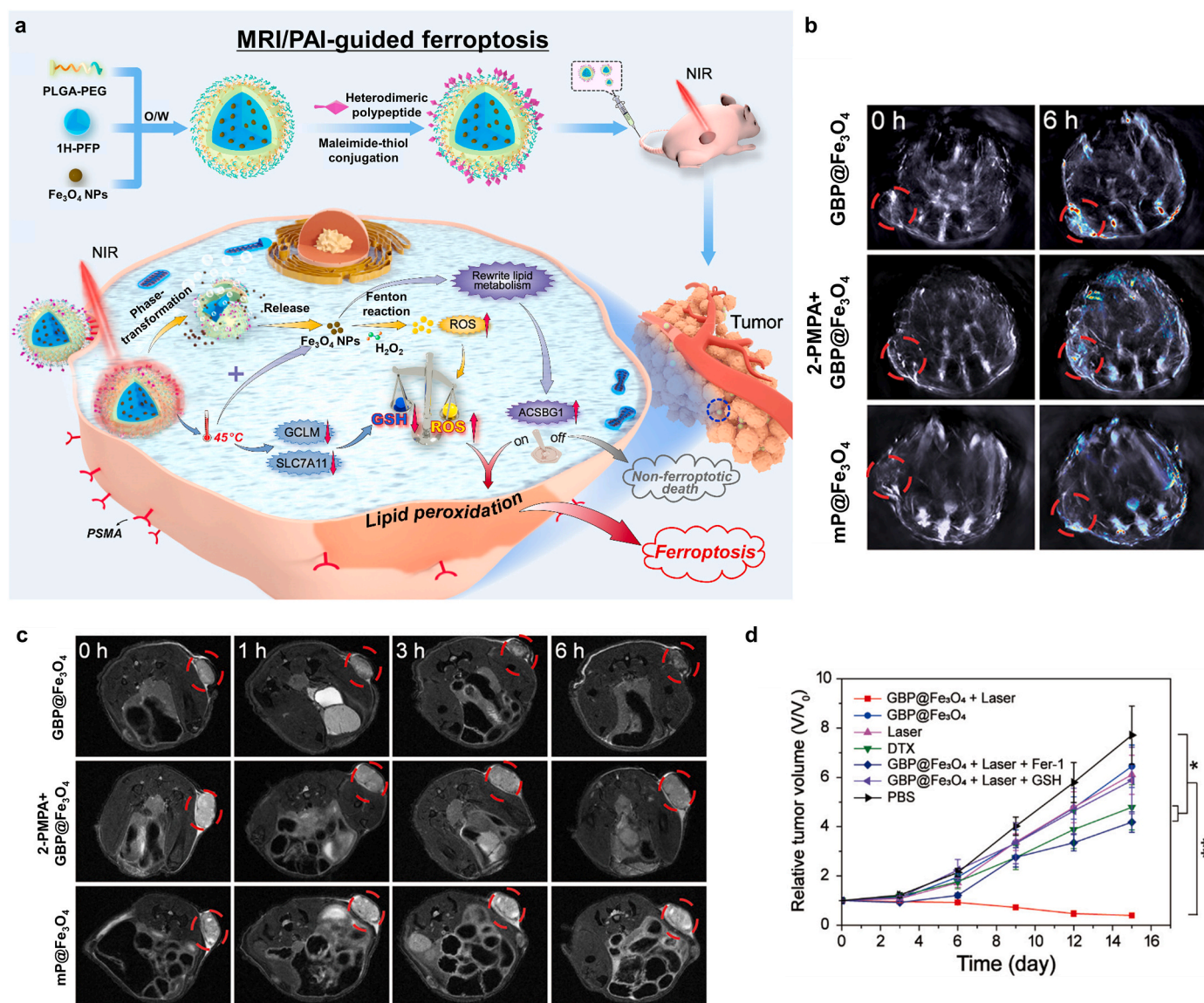
Fig. 20. Photo-triggered ferroptosis cancer nanomedicine with PAI/MRI guidance. (a) Schematic diagrams of the synthesis and therapeutic mechanism of GBP@Fe$_3$O$_4$. (b) PAI and (c) T$_2$-weighted MRI results after the injection of various nanoformulations. (d) Relative tumor volume changes after various treatment regimens (%ID/g: percentage injected dose per gram, *p $<$ 0.05, **p $<$ 0.01, ***p $<$ 0.001). Reproduced with permission [122]. Copyright 2021, American Chemical Society.

GSH depletion and limited the antioxidant response, which enhanced ROS-mediated ferroptosis [38,184–186]. The photothermal effect also enabled 1H-PFP phase transformation and Fe$_3$O$_4$ release by producing a large amount of LPO by facilitating the Fenton reaction, leading to ferroptosis [187]. The photothermal effect sustained the tumor antioxidant response through GSH depletion, leading to LPO overproduction and acetyl-CoA synthetase bubblegum family member 1 (ACSBG1)-dependent ferroptosis, which is an important component for the ferroptosis-mediated therapy in castration-resistant prostate cancer cell lines (Fig. 20a) [122]. Several imaging modalities were enabled by GBP@Fe$_3$O$_4$ and Fe release-based T$_2$-weighted MRI and photothermal effect-mediated PAI and ultrasound imaging. Accumulation of GBP@Fe$_3$O$_4$ at the tumor sites was indicated through PAI (Fig. 20b). Furthermore, T$_2$-weight MRI showed tumor site accumulation after injection of GBP@Fe$_3$O$_4$, with 2-phosphonomethylpentanedioic acid, a PSMA (prostate-specific membrane antigen) receptor antagonist, blocking its accumulation along with MP@Fe$_3$O$_4$ aggregation (Fig. 20c). To confirm the ferroptosis of tumor cells, ferroptosis inhibitor ferrostatin

1 (Fer-1) was used, which interfered with the tumor growth inhibition by GBP@Fe$_3$O$_4$ (Fig. 20d). However, GBP@Fe$_3$O$_4$ with laser irradiation provided a noticeable reduction in tumor volume without any cytotoxic effects *in vivo*. These results suggested synergistic effects of PTT and ferroptosis that moderate heat supply to local tumor successfully led to burst release of GBP@Fe$_3$O$_4$, resulting in significant LPO. Furthermore, heat stress hindered the synthesis of GSH, consequently, cancer cells became much more vulnerable to oxidative stress.

PTT can synergistically affect chemotherapy. PEGylated Fe-Cu-SS MOF (FCSP)@DOX was first synthesized by using a hydrothermal method via bridging Fe and Cu ions with disulfide bonds to form the FCSP MOF followed by the hydrophobic interaction-mediated loading of DOX. Furthermore, C18PMH-mPEG was used to enhance hydrophilicity and biocompatibility, and to support the EPR effect. FCSP@DOX induced ferroptosis based on the release of Fe and Cu ions and the downregulation of GSH [188]. The depletion of GSH provided a large amount of ROS through the Fenton reaction using Fe and Cu ions [189–192]. Furthermore, DOX released inside the NPs produced H$_2$O$_2$,
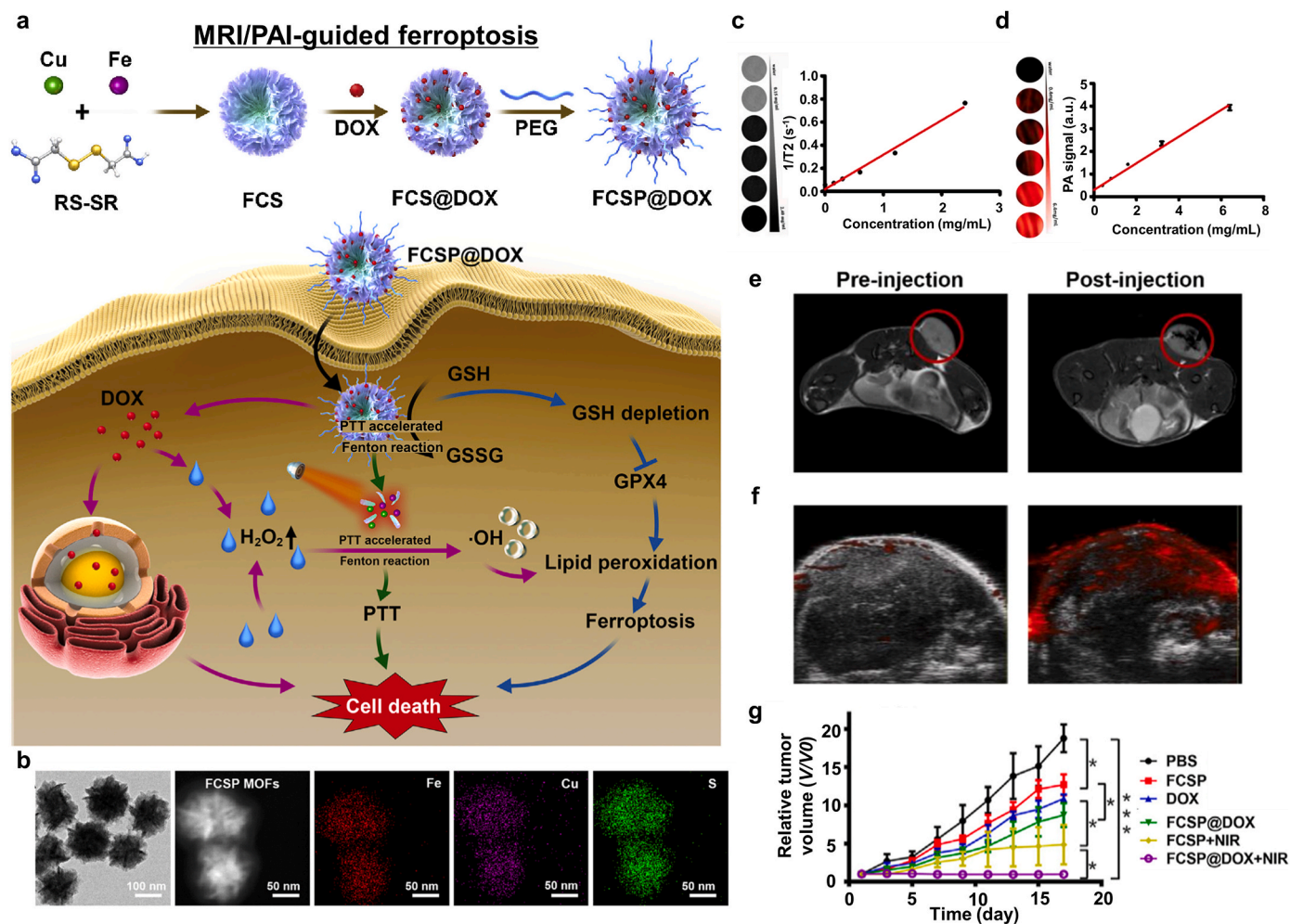
Fig. 21. MRI/PAI-guided ferroptosis cancer nanomedicine accelerated by PTT. (a) A schematic diagram of the therapeutic mechanism of FCSP@DOX. (b) A TEM image and elemental mapping of the FCSP MOF. (c) T_2-weighted MR images and the T_2 relaxivity rate according to the concentration of FCSP@DOX. (d) PAI results and intensity according to the concentration of FCSP@DOX. (e) MRI results of 4T1 tumor-bearing mice after injection of FCSP@DOX. (f) PAI results of 4T1 tumor-bearing mice after injection of FCSP@DOX into the tumor sites (n = 3). (g) Relative tumor volume changes after various treatment regimens (*p < 0.05, **p < 0.01, ***p < 0.001). Reproduced with permission [123]. Copyright 2021, Elsevier B.V.

which induced ferroptosis [193]. This mediated the chemotherapy and enhanced ferroptosis. Owing to strong NIR absorption of FCSF MOFs, it exhibited effective photothermal conversion. The photothermal effect increased ROS production and the temperature in the TME, thereby causing cancer cell death (Fig. 21a) [123,194]. They confirmed mild hyperthermia contributed to about 20% more hydroxyl radical generation compared to control group without photothermal heating. TEM analysis showed that the FCSP MOF comprised flower-like shapes around 127.53 nm in size (Fig. 21b). Both MRI and PAI were enabled by using FCSP@DOX. To be specific, T_2-weighted MRI showed increased T_2 relaxivity as the FCSP@DOX concentration was increased (Fig. 21c). *In vivo* MR images showed significant changes before and after injection of FCSP@DOXs (Fig. 21e). Likewise, PAI provided a linear relationship between FCSP@DOX concentration and the photoacoustic intensity (Fig. 21d). A significant increase in the photoacoustic signal intensity *in vivo* after FCSP@MOF injection into the tumor sites further validates the PAI modality of FCSP@DOX (Fig. 21f). As expected, significant tumor volume reduction after FCSP@DOX + NIR laser therapy was observed (Fig. 21g) with no distinct cytotoxic effects in treated mice. This paper suggested that co-delivery of DOX and FCSP induces apoptosis and ferroptosis at local tumor and furthermore provides synergistic effect by generating H_2O_2 for Fenton reaction. Additionally, moderate heating by PTT can boost the Fenton reaction efficiency.

Another combinational approach for delivering Fe^{3+} ions to enhance the Fenton reaction in cancer cells was reported by Zeng et al. After the interaction between croconaine (Cro) and Fe^{3+} to produce Cro-Fe, BSA was then added to encapsulate Cro-Fe, which enhanced the biocompatibility of the NPs named Cro-Fe@BSA [124]. When heat stress applied to cancer cells, heat shock proteins usually were upregulated as a self-defense mechanism of cancer cells. However, as Fe^{3+} ions were released in an acidic condition, ROS production was boosted and consequently hindered the production of heat shock protein, leading to ferroptosis. The photothermal effect enhanced the Fenton reaction through the production of •OH and LPO. Upon irradiation, the Fe^{2+} level also increased, which enhanced ferroptosis (Fig. 22a). PAI and T_1-weighted MRI were used to track the Cro-Fe@BSA after injection *in vivo*, the results of which show that the concentration of Cro-Fe@BSA reached its maximum 24 h post-injection (Fig. 22b and d). The results imply that the EPR effect mediated the efficient internalization of the NPs by the tumor cells. Thermal images were taken to determine the photothermal effect after irradiation. The temperature increased in mice treated with Cro-Fe@BSA and Cro@BSA to 55.2 °C and 50.1 °C, respectively (Fig. 22c). The difference is due to the lower accumulation rate of Cro@BSA at the tumor sites due to its larger size. The tumor volume and inhibition rate are measured after various treatment regimens (Fig. 22e); efficient tumor growth reduction was observed after
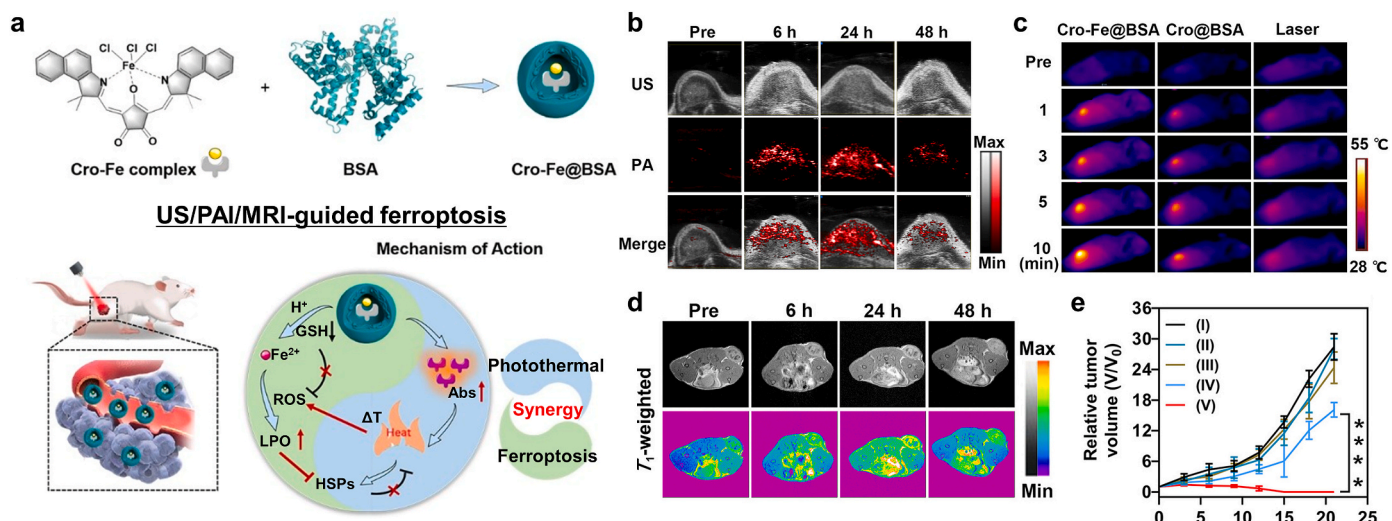
Fig. 22. Synergistic PTT and ferroptosis cancer nanomedicine with MRI/PAI/US guidance. (a) Schematic illustrations of the synthesis and therapeutic mechanism of Cro-Fe@BSA. (b) PAI/US images of tumor-bearing mice after injection of Cro-Fe@BSA. (c) Thermal images of tumor-bearing mice after 10 min of laser irradiation. (d) T_1-weighted MRI results of tumor-bearing mice after injection of Cro-Fe@BSA. (e) Tumor volume changes after various treatment regimens (Group I: Control, Group II: Cro@BSA, Group III: Cro@BSA + laser, Group IV: Cro-Fe@BSA, Group V: Cro-Fe@BSA + laser). Reproduced with permission [124]. Copyright 2021, John Wiley & Sons.

treatment with Cro-Fe@BSA and laser irradiation. The Cro-Fe@BSA NPs provided a responsive combinational ferroptosis and photothermal effect. The release of Fe^{3+} ions generated Fe^{2+} ions in the reaction with GSH for the ferroptosis induction. Additional photothermal effect enhanced the Fenton reaction rate for the formation of ROS and LPO. This study provides insight into designing Fe-based ferroptosis agents that can perform enhanced synergetic combinational cancer therapy.

The cRGD/Pt + DOX@GFNPs (RPDGs) can activate the Fenton reaction, with Pt (IV) downregulating the level of GSH and upregulating the level of ROS. After NIR irradiation, the Fenton reaction was increased via the gallic acid/Fe^{2+} NPs (GFNPs) and Pt (IV) enhanced the depletion of GSH. In addition, the GFNPs provided the photothermal effect and the release of Fe^{2+} from the NPs was accelerated (Fig. 23a) [125]. TEM analysis of RPDG showed that it is 60.4 nm in size, with DLS data showing a uniform size distribution (68.06 nm) (Fig. 23b and c). As Fe^{2+} from the GFNPs provide T_2-weighted MRI capability, MR images were taken according to the RPDG concentration (Fig. 23d). Furthermore, the r_2 value was further measured according to the Fe concentration (81.0 mM^{-1} s^{-1}) (Fig. 23e). MR images were taken after administering various treatment regimens: GFNPs, Pt (IV)@GFNPs, Pt (IV) + DOX@GFNPs, and RPDGs. Among them, the RPDGs provided an obvious signal reduction, which supports the assumption that they provide an efficient diagnostic method (Fig. 23f). To observe the tumor-specific targeting ability, fluorescent Cy7 was loaded onto the RPDGs and showed significant accumulation at the tumor sites (Fig. 23g). The photothermal effect after NIR irradiation with each treatment regimen provided a temperature increase (Fig. 23h and i), with that employing the RPGDs being the highest. Finally, bioluminescence was measured to examine the therapeutic effect of the RPDGs. It was reduced dramatically, which indicates that tumor therapy via the RPDGs is effective. This paper suggested that RPDGs provided a combinational approach to chemotherapy, ferroptosis, and PTT. Locally elevated temperature not only accelerates the Fenton reaction but also increases the local blood flow to the tumor tissue leading to enhanced drug delivery overcoming the blood-brain barrier.

Ce6, a common photosensitizer for PDT, enhances ROS production and GSH or GPX4 depletion, leading to the ferroptosis of cancer cells. NIR fluorescence imaging (FI) is commonly enabled by conjugating or encapsulating NPs with photosensitizers such as Ce6 whereas MRI is enabled by Fe-containing NPs [195–198].

Fe_3O_4-PLGA-Ce6 NPs provided ferroptosis and PDT via NIR irradiation. Fe^{2+}, Fe^{3+}, and Ce6 are released from PLGA under the acidic conditions of the TME and facilitate Fenton reaction-mediated ROS production [108,199]. Upon NIR irradiation, Ce6-mediated PDT supported both apoptosis- and ferroptosis-mediated cell death [200]. Fe_3O_4-PLGA-Ce6 NPs were synthesized by loading Ce6 and citric acid-coated Fe_3O_4 (CA-Fe_3O_4) onto PLGA NPs (Fig. 24a) [126]. Ce6-mediated FI was conducted to observe the enhanced penetration and retention in subcutaneous tumors (Fig. 24b). In addition, the major organs and tumors were harvested 72 h after injection and Fe_3O_4-PLGA-Ce6 NPs accumulation at the tumor sites was observed (Fig. 24c). T_2-weighted MRI was enabled by the loaded Fe_3O_4 [116,201]. The MRI signals could be observed up to 72 h after injection (Fig. 24d). Thus, they administrated Fe_3O_4-PLGA-Ce6 NPs every 3 days and a day after administration they conducted PDT. These therapeutic cycles were repeated total 3 times. Fe_3O_4-PLGA-Ce6+laser treatment showed the most dramatic tumor size reduction and inhibition owing to the combination of ferroptosis and PDT (Fig. 24e). They also mentioned that the synergism between ferroptosis and PDT is large amounts of oxygen as a result of the Fenton reaction relieved hypoxia in the malignant TME and supplied PDT sources simultaneously.

Liang et al. reported combinational ferroptosis and PDT approach using iron oxide MNPs loaded with porphyrin-lipids [127]. Porphyrin-grafted lipid (PGL) and DSPE-polyethylene glycols (DSPE-PEG) self-assembled on the surface of oleic acid capped Fe_3O_4 NPs (Fe_3O_4@PGL NPs) (Fig. 25a). Porphyrin photosensitizers were then covalently conjugated on the NPs to avoid their uncontrolled release. *In vitro* testing on macrophage cell line RAW 264.7 shows that the Fe_3O_4@PGL NPs could generate a large amount of ROS via the Fenton reaction, as shown in the FI (Fig. 25b). Thus, the ROS generation activated tumor associated macrophages, leading to ferroptosis-mediated cell death of human colon cancer cells (HT-29 cell line). To observe the tumor-targeting ability of the Fe_3O_4@PGL NPs, PGL-mediated FI was taken, showing that the fluorescence signals at the tumor sites reached the maximum 24 h after injection. In addition, fluorescence signals measured after harvesting the major organs and tumors clearly reveal that Fe_3O_4@PGL NPs had well accumulated at the tumor sites. T_2-weighted was also possible with the Fe_3O_4@PGL NPs; darkening according to the concentration of NPs was. The measured r_2 was 628.6 $mM^{-1}s^{-1}$ (Fig. 25c). The Fenton reaction and oxidative stress of
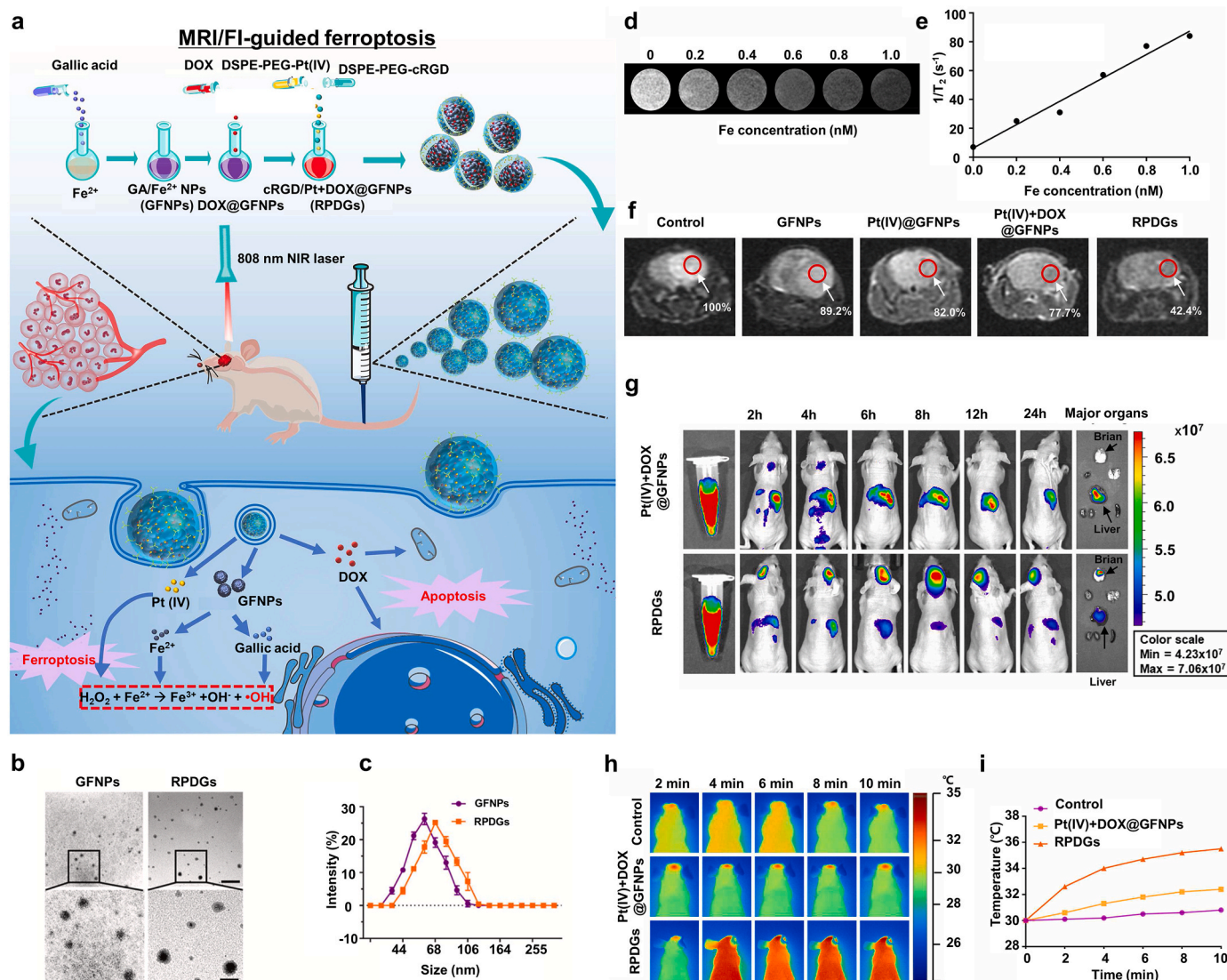
Fig. 23. MRI/FI-guided ferroptosis nanomedicine. (a) Schematic illustrations of the synthesis and therapeutic mechanism of RPDGs. (b) TEM images and (c) DLS data of the GFNPs and RPDGs. (d) T_2-weighted MRI results according to the Fe concentration in the RPDGs. (e) The transverse relaxation coefficients of the RPDGs. (f) T_2-weighted MRI results of tumor-bearing mice 24 h after injection of various components. (g) FI results of tumor-bearing mice, their major organs, and tumors after injection of Pt (IV) + DOX@GFNPs or RPDGs. (h) Thermal images of mice and (i) temperature changes 8 h post-injection of Pt (IV) + DOX@GFNPs or RPDGs. Reproduced with permission [125]. Copyright 2021, Elsevier B.V.

macrophages were effectively accelerated via PDT treatment. The relatively small-sized Fe₃O₄@ PGL NPs showed a high porphyrin photosensitizer-loading efficacy and excellent biocompatibility. Cancer cells were effectively killed by using a small amount of the Fe₃O₄@PGL NPs with PDT treatment. An *in vivo* animal study further demonstrated complete tumor growth inhibition after treatment with the Fe₃O₄@PGL NPs and PDT (Fig. 25d). This result suggested that the combination of Fenton reaction, PDT and stimulation of tumor-associated macrophage successively induce ferroptosis-mediated cell death. This work contributes to the current emerging context of combinational ferroptosis and PDT therapy where magnetic Fe-oxide NPs can be used together with conventional porphyrin photosensitizers to maximize ROS generation for cancer therapy.

5. Conclusion

Despite the remarkable strides made in the advancement of cancer therapy via a heightened comprehension of cancer biology and molecular biology, cancer is still a leading cause of mortality, largely due to

the apoptosis-based cancer therapy and subsequent therapeutic resistance of cancers. Typically, the apoptotic pathways of cancers are evaded by numerous mutations such as overexpression of antiapoptotic proteins (BCL-2, BCL-XL, BCL-W, MCL-1, BFL-1/A1) and underexpression of proapoptotic proteins (BAX, BAK, BAD, BID, etc), or tumor suppressing p53 protein [202–204]. Many of these changes associated with the apoptosis cause the therapeutic resistance to the most common anticancer therapies. Thus, there is an imminent need to explore alternative strategies that leverage non-apoptotic cancer cell death as a means of improving therapeutic outcomes. Ferroptosis-based cancer therapy can bypass the common apoptosis based therapeutic resistance mechanisms. Ferroptosis can serve as an alternative or complementary pathway to conventional apoptosis-based cancer treatment. Here beforehand introduced research on ferroptosis-mediated cancer cell death highlights the great potential for new ferroptosis based cancer therapy approaches. As demonstrated the effectiveness of ferroptosis based cancer therapies, the importance of ferroptosis in cancer treatment is rapidly growing and attracting attention as a new clinical cancer treatment approach. However, the therapeutic efficacy of conventional
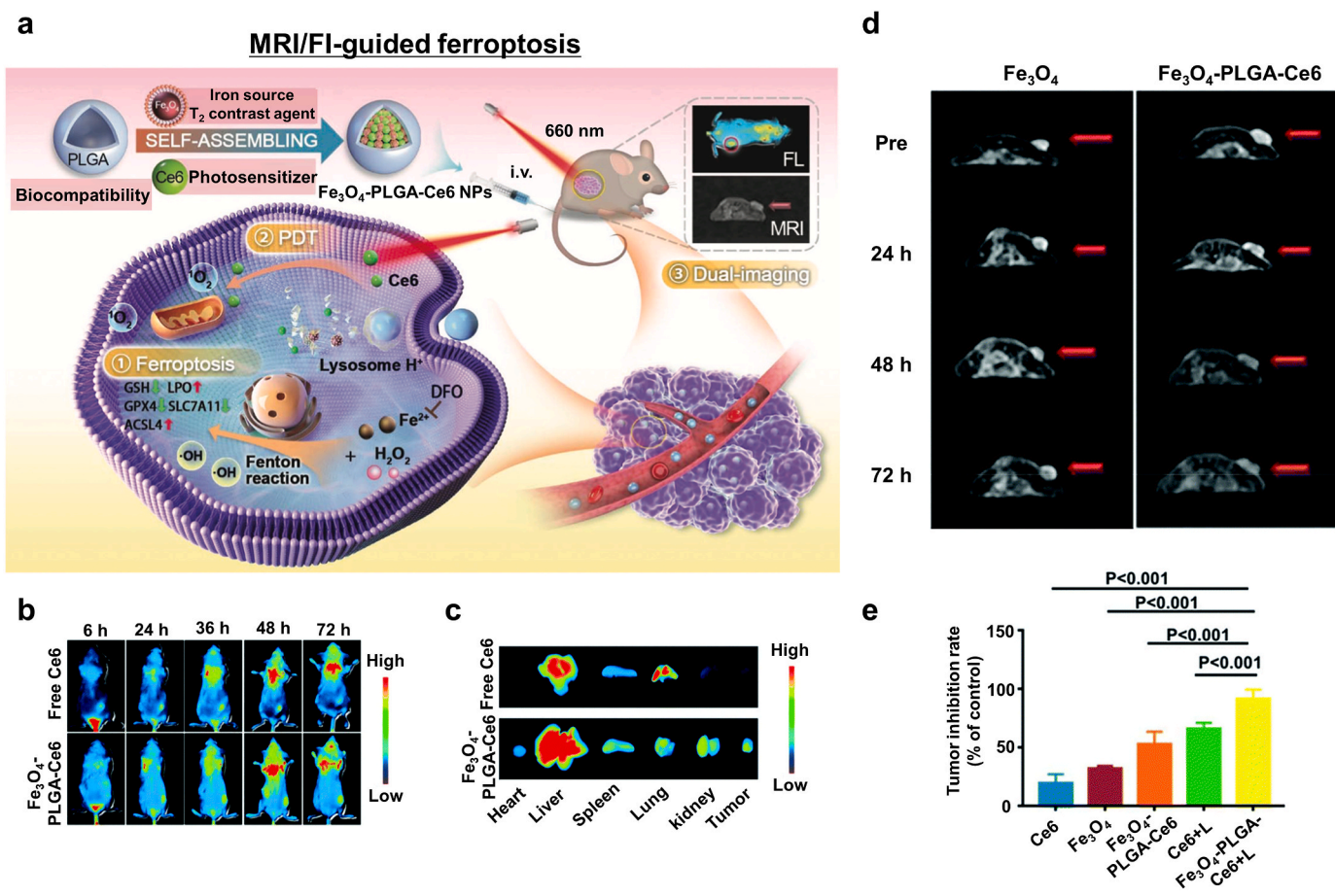
Fig. 24. MRI/FI-guided ferroptosis nanomedicine enhanced by PDT. (a) Schematic illustrations of the synthesis and therapeutic mechanism of Fe_3O_4-PLGA-Ce6 NPs. (b) FI results of tumor-bearing mice after injection of free Ce6 or Fe_3O_4-PLGA-Ce6 NPs. (c) FI results of the major organs and tumors 72 h after injection of free Ce6 or Fe_3O_4-PLGA-Ce6 NPs. (d) T_2-weighted MRI results after injection of Fe_3O_4 or Fe_3O_4-PLGA-Ce6 NPs. (e) The tumor inhibition rate after various treatment regimens. Reproduced with permission [126]. Copyright 2021, The Royal Society of Chemistry.

small-molecule ferroptosis agents in the clinical setting can be significantly limited with the lack of tumor-specificity, as witnessed by the side effects and failure of numerous chemotherapy trials. The next frontier in the advancement of ferroptosis-based cancer therapeutics lies in the effective ferroptosis induction of cancer cells with minimized side effects. An effective mean of harnessing the clinical potential of ferroptosis-mediated cancer therapy is local image guided ferroptosis- and combinational ferroptosis-cancer therapy regimen [205–208]. As considering combinational ferroptosis cancer therapy, the rational design of the combination for the synergistic anticancer effects is of significant importance [209–213]. Further, additional efforts on investigating the ferroptosis targeting mechanism, feasible clinical targeted ferroptosis approaches, and optimized synergistic combinational ferroptosis cancer therapy, and ideas for constructing ferroptosis nanocarriers are required for the successful clinical translation of this approach.

MNPs are one of the most extensively studied NPs in biomedical applications. Their innate magnetic properties of MNPs originate from unpaired spins/electrons of the atom. Advanced nanotechnology found their remote dynamic control such as remote steering, heat generation, mechanical force generation, and MRI contrast with an external magnetic field. For the biomedical applications, highly magnetic field responsive MNPs are commonly composed of iron, which is one of essential component in human body. Non-ionizing external magnetic fields can pass through the human body without harmful effects. Magnetic field response MNPs can be precisely localized to specific sites of the human or trigger the mechanical force or heat [214,215]. The

presence of MNPs in the human body is easily detected by diagnostic MRI. Indeed, magnetic field responsive MNPs are the most versatile option for the future nanomedicine. In association with ferroptosis, iron metabolism is easily affected by the iron oxide MNPs and iron oxide MNPs become one of the key targets for the ferroptosis cancer treatment. Iron oxide MNPs can be dissolved in acidic TME and release ROS-generating Fe^{2+} and Fe^{3+} ions, resulting in ferroptosis induction of cancer cells. Enhancing the ferroptosis catalytic process of iron oxide MNPs in the TME has been one of the main strategies for the ferroptosis cancer nanomedicine. Various types of iron oxide MNPs such as anisotropic, porous, or hierarchical morphologies have been studied for the multifunctional ferroptosis nanomedicine agents [103,216,217]. Forming a hybrid MNP nanostructures composed of iron oxide MNPs and other transition metal oxides also provides a strategy to sustain the multivalent metal ion redox cycle [218,219]. Further, the magnetic field responsive mechanical or thermal energy of iron oxide MNPs which are related to lipid peroxidation and ferroptosis pathways provide an opportunity for the triggered and local ferroptosis induction [220,221]. Those approaches allow precise spatial and temporal regulation of ferroptosis induction, contributing to personalized cancer treatment. Multimodal imaging characters of MNPs and hybrid MNPs also provide real-time feedback on treatment progress and tumor response. Finally, the therapeutic multifunctionality of MNPs and hybrid MNPs further allows combinational synergistic ferroptosis approaches such as ferroptosis/chemotherapy, ferroptosis/pyroptosis, ferroptosis/radiation, ferroptosis/ablations, and ferroptosis/immunotherapies [219,222]. Especially, combining MNP-mediated ferroptosis induction with
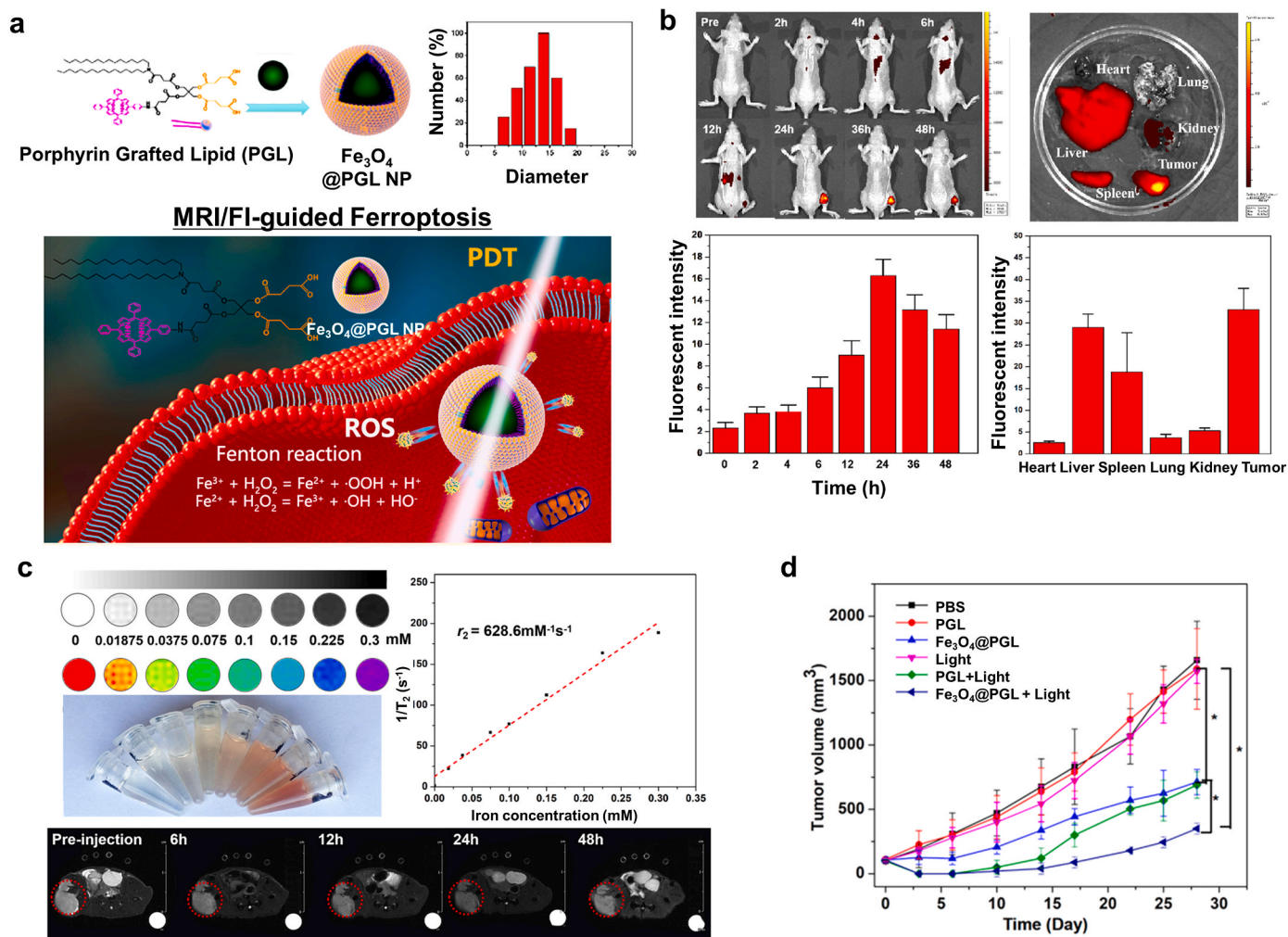
Fig. 25. PDT-mediated ferroptosis cancer nanomedicine with MRI/FI guidance. (a) Preparation and characterization of Fe$_3$O$_4$@PGL NPs. (b) Real-time FI using Fe$_3$O$_4$@PGL NPs and their biodistribution. (c) MR contrast enhancing property of Fe$_3$O$_4$@PGL NPs. (d) *In vivo* PDT of Fe$_3$O$_4$@PGL NPs. Reproduced with permission [127]. Copyright 2021, American Chemical Society.

immunotherapy has shown great promise. Ferroptosis mediated DAMP release and PD-L1 upregulation strongly suggest that combinational ferroptosis induction and immunotherapy using MNPs could be a highly efficient method of killing cancer cells and enhancing the overall therapeutic outcomes.

One challenge for ferroptosis-induction cancer nanomedicine is inconsistent therapeutic outcomes depending on the tumor type. For instance, the molecular features of prostate cancer involve Fe dysmetabolism, including Fe-ion influx, intracellular Fe-ion distribution, and Fe-ion flux. Diffuse large B cell lymphomas and renal cell carcinomas have been shown to be more susceptible to erastin-induced ferroptosis compared to other cancer cell lines from six different tissue types (breast, lung, colon, melanocytes, central nervous system, and ovary) [223]. This variability in the sensitivity of different cell lines to ferroptosis could be attributed to differences in their underlying metabolic states. Additionally, TME varies significantly across different cancer types. For example, tumor makes acidic TME via increased glycolysis, but the degree of glycolysis may vary with their type, size, and stage [224,225]. The acidity difference in TME affects to the tendency of iron ions dissolution, resulting in a difference in ferroptosis induction. Thus, a specific tumor type focused MNPs ferroptosis cancer nanomedicine should be developed. MNP that can trigger the ferroptosis cycle remotely might control the ferroptosis induction behaviors for each type of cancer along with their imaging capabilities. To advance MNPs

mediated ferroptosis cancer nanomedicine to the clinical translation, interdisciplinary cooperation between material scientists and clinicians is required to determine the suitability of MNPs for the treatment of specific cancer types.

In this review, the mechanism of ferroptosis and various ideas for the design and development of ferroptosis therapeutic nanoplatforms were examined, and innovative possibilities were proposed along with a summary of previous findings. This information should expand the horizon of MNP platforms for ferroptosis-induction cancer nanomedicine applications. Although the NP platforms are still under investigation for clinical translation, their consideration should be the top priority for the successful deployment of ferroptosis-induction cancer nanomedicine. Immunotherapy is a relatively new and emerging approach for treating cancer. Further studies on ferroptosis combined with immunotherapy involving MNPs are needed to clarify the molecular mechanisms and to provide an opportunity for designing new therapeutic interventions. Addressing these issues will deepen our understanding of ferroptosis-based cancer nanomedicine and advance its clinical applicability. Additionally, there is a gap between cutting-edge pre-clinical research of MNPs ferroptosis cancer nanomedicine and their clinical translation. Innovative MNPs ferroptosis cancer nanomedicine should be validated for superior cancer therapy based on the thorough investigation of ferroptosis regulating molecules and signaling pathways. Consistent efforts on evaluating the safety of MNPs or MNPs based hybrid nanostructures

and developing image guided localized approaches of ferroptosis nanomedicine are required for the clinical translation of MNPs mediated ferroptosis cancer nanomedicine. Multidisciplinary and interdisciplinary collaborations are critically needed. At the same time, additional attention on economic feasibility, regulatory considerations, safety assessments, relevance with clinical unmet needs, and public perspective will be essential for the successful translation of promising ferroptosis magnetic cancer nanomedicine.

Ethics approval and consent to participate

This review article does not require any ethical approval or allied consents for publication.

CRediT authorship contribution statement

Min Jun Ko: Visualization, Conceptualization, Writing-Original Draft, Investigation. **Sunhong Min:** Visualization, Investigation, Conceptualization. **Hyunsik Hong:** Validation, Conceptualization. **Woojung Yoo:** Investigation, Resources, Visualization. **Jinmyoung Joo:** Investigation, Project administration. **Yu Shrike Zhang:** Supervision, Project administration, Resources. **Heemin Kang:** Conceptualization, Funding acquisition, Project administration, Supervision, Writing-Review & Editing. **Dong-Hyun Kim:** Conceptualization, Funding acquisition, Supervision, Project administration, Writing-Original Draft, Writing-Review & Editing.

Declaration of competing interest

The authors declare that they have no known competing financial interests or personal relationships that could have appeared to influence the work reported in this paper.

Acknowledgements

References

[1] R.L. Siegel, K.D. Miller, N.S. Wagle, A. Jemal, Cancer statistics, 2023, CA: A Cancer J. Clinic. 73 (2023) 17–48. https://doi.org/10.3322/caac.21763.

[2] J. Lee, S. Mehrotra, E. Zare-Eelanjegh, R.O. Rodrigues, A. Akbarinejad, D. Ge, L. Amato, K. Kiaee, Y.C. Fang, A. Rosenkranz, W. Keung, B.B. Mandal, R.A. Li, T. Zhang, H. Lee, M.R. Dokmeci, Y.S. Zhang, A. Khademhosseini, S.R. Shin, A heart-breast cancer-on-a-chip platform for disease modeling and monitoring of cardiotoxicity induced by cancer chemotherapy, Small 17 (2021), 2004258, https://doi.org/10.1002/smll.202004258.

[3] F. Gong, J.C. Xu, B. Liu, N.L. Yang, L. Cheng, P. Huang, C.J. Wang, Q. Chen, C. F. Ni, Z. Liu, Nanoscale CaH2 materials for synergistic hydrogen-immune cancer therapy, Chem 8 (2022) 268–286, https://doi.org/10.1016/j.chempr.2021.11.020.

[4] M. Ermis, N. Falcone, N. Roberto de Barros, M. Mecwan, R. Haghniaz, A. Choroomi, M. Monirizad, Y. Lee, J. Song, H.J. Cho, Y. Zhu, H. Kang, M. R. Dokmeci, A. Khademhosseini, J. Lee, H.J. Kim, Tunable hybrid hydrogels with multicellular spheroids for modeling desmoplastic pancreatic cancer, Bioact. Mater. 25 (2023) 360–373, https://doi.org/10.1016/j.bioactmat.2023.02.005.

[5] R. Haghniaz, H.J. Kim, H. Montazerian, A. Baidya, M. Tavafoghi, Y. Chen, Y. Zhu, S. Karamikamkar, A. Sheikhi, A. Khademhosseini, Tissue adhesive hemostatic microneedle arrays for rapid hemorrhage treatment, Bioact. Mater. 23 (2023) 314–327, https://doi.org/10.1016/j.bioactmat.2022.08.017.

[6] W. Zhao, C. Hu, T. Xu, In vivo bioprinting: broadening the therapeutic horizon for tissue injuries, Bioact. Mater. 25 (2023) 201–222, https://doi.org/10.1016/j.bioactmat.2023.01.018.

[7] Z.H. Jing, R.H. Ni, J.D. Wang, X.H. Lin, D.Y. Fan, Q.G. Wei, T. Zhang, Y.F. Zheng, H. Cai, Z.J. Liu, Practical strategy to construct anti-osteosarcoma bone substitutes by loading cisplatin into 3D-printed titanium alloy implants using a thermosensitive hydrogel, Bioact. Mater. 6 (2021) 4542–4557, https://doi.org/10.1016/j.bioactmat.2021.05.007.

[8] Y.S. Lee, K. Kalimuthu, Y.S. Park, X. Luo, M.H.A. Choudry, D.L. Bartlett, Y.J. Lee, BAX-dependent mitochondrial pathway mediates the crosstalk between ferroptosis and apoptosis, Apoptosis 25 (2020) 625–631, https://doi.org/10.1007/s10495-020-01627-z.

[9] L.A. Timmerman, T. Holton, M. Yuneva, R.J. Louie, M. Padro, A. Daemen, M. Hu, D.A. Chan, S.P. Ethier, L.J. van 't Veer, K. Polyak, F. McCormick, J.W. Gray, Glutamine sensitivity analysis identifies the xCT antiporter as a common triple-negative breast tumor therapeutic target, Cancer Cell 24 (2013) 450–465, https://doi.org/10.1016/j.ccr.2013.08.020.

[10] W.C. Qi, Z.H. Li, L.J. Xia, J.S. Dai, Q. Zhang, C.F. Wu, S. Xu, LncRNA GABPB1-AS1 and GABPB1 regulate oxidative stress during erastin-induced ferroptosis in HepG2 hepatocellular carcinoma cells, Sci. Rep. 9 (2019), https://doi.org/10.1038/s41598-019-52837-8.

[11] E.H. Kim, D. Shin, J. Lee, A.R. Jung, J.L. Roh, CISD2 inhibition overcomes resistance to sulfasalazine-induced ferroptotic cell death in head and neck cancer, Cancer Lett. 432 (2018) 180–190, https://doi.org/10.1016/j.canlet.2018.06.018.

[12] C. Louandre, Z. Ezzoukhry, C. Godin, J.C. Barbare, J.C. Maziere, B. Chauffert, A. Galmiche, Iron-dependent cell death of hepatocellular carcinoma cells exposed to sorafenib, Int. J. Cancer 133 (2013) 1732–1742, https://doi.org/10.1002/ijc.28159.

[13] C. Mao, X.G. Liu, Y.L. Zhang, G. Lei, Y.L. Yan, H. Lee, P. Koppula, S.Q. Wu, L. Zhuang, B.L. Fang, M.V. Poyurovsky, K. Olszewski, B.Y. Gan, DHODH-mediated ferroptosis defence is a targetable vulnerability in cancer, Nature 593 (2021) 586–590, https://doi.org/10.1038/s41586-021-03539-7.

[14] S. Briganti, M. Picardo, Antioxidant activity, lipid peroxidation and skin diseases. What's new, J. Eur. Acad. Dermatol. Venereol. 17 (2003) 663–669, https://doi.org/10.1046/j.1468-3083.2003.00751.x.

[15] M.P. Mattson, Modif ication of ion homeostasis by lipid peroxidation: roles in neuronal degeneration and adaptive plasticity, Trends Neurosci. 21 (1998) 53–57, https://doi.org/10.1016/S0166-2236(97)01188-0.

[16] Q. Sun, Y. Hou, Z. Chu, Q. Wei, Soft overcomes the hard: flexible materials adapt to cell adhesion to promote cell mechanotransduction, Bioact. Mater. 10 (2022) 397–404, https://doi.org/10.1016/j.bioactmat.2021.08.026.

[17] S. Min, M.J. Ko, H.J. Jung, W. Kim, S.-B. Han, Y. Kim, G. Bae, S. Lee, R. Thangam, H. Choi, N. Li, J.E. Shin, Y.S. Jeon, H.S. Park, Y.J. Kim, U.K. Sukumar, J.-J. Song, S.-K. Park, S.-H. Yu, Y.C. Kang, K.-B. Lee, Q. Wei, D.-H. Kim, S.M. Han, R. Paulmurugan, Y.K. Kim, H. Kang, Remote control of time-regulated stretching of ligand-presenting nanocoils in situ regulates the cyclic adhesion and differentiation of stem cells, Adv. Mater. 33 (2021), 2008353, https://doi.org/10.1002/adma.202008353.

[18] X.Y. Kong, Y.H. Qi, X.Y. Wang, R. Jiang, J. Wang, Y. Fang, J.D. Gao, K.C. Hwang, Nanoparticle drug delivery systems and their applications as targeted therapies for triple negative breast cancer, Prog. Mater. Sci. 134 (2023), 101070, https://doi.org/10.1016/j.pmatsci.2023.101070.

[19] J. Tang, Y.F. Wu, X. Li, L.H. Bu, B.S. Chang, Single-atom iron catalysts for biomedical applications, Prog. Mater. Sci. 128 (2022), 100959, https://doi.org/10.1016/j.pmatsci.2022.100959.

[20] X. Li, W. Li, M. Wang, Z. Liao, Magnetic nanoparticles for cancer theranostics: advances and prospects, J. Contr. Release 335 (2021) 437–448, https://doi.org/10.1016/j.jconrel.2021.05.042.

[21] V. Agrahari, V. Agrahari, M.-L. Chou, C.H. Chew, J. Noll, T. Burnouf, Intelligent micro-/nanorobots as drug and cell carrier devices for biomedical therapeutic advancement: promising development opportunities and translational challenges, Biomaterials 260 (2020), 120163, https://doi.org/10.1016/j.biomaterials.2020.120163.

[22] J. Nam, S. Son, K.S. Park, W. Zou, L.D. Shea, J.J. Moon, Cancer nanomedicine for combination cancer immunotherapy, Nat. Rev. Mater. 4 (2019) 398–414, https://doi.org/10.1038/s41578-019-0108-1.

[23] K. Gwon, H.J. Hong, A.M. Gonzalez-Suarez, M.Q. Slama, D. Choi, J. Hong, H. Baskaran, G. Stybayeva, Q.P. Peterson, A. Revzin, Bioactive hydrogel microcapsules for guiding stem cell fate decisions by release and reloading of growth factors, Bioact. Mater. 15 (2022) 1–14, https://doi.org/10.1016/j.bioactmat.2021.12.008.

[24] L. Ren, Y. Gao, Y. Cheng, A manganese (II)-based coordinative dendrimer with robust efficiency in intracellular peptide delivery, Bioact, Materials 9 (2022) 44–53, https://doi.org/10.1016/j.bioactmat.2021.08.006.

[25] M. Yu, D. Luo, J. Qiao, J. Guo, D. He, S. Jin, L. Tang, Y. Wang, X. Shi, J. Mao, S. Cui, Y. Fu, Z. Li, D. Liu, T. Zhang, C. Zhang, Z. Li, Y. Zhou, Y. Liu, A hierarchical bilayer architecture for complex tissue regeneration, Bioact. Mater. 10 (2022) 93–106, https://doi.org/10.1016/j.bioactmat.2021.08.024.

[26] R. Thangam, M.S. Kim, G. Bae, Y. Kim, N. Kang, S. Lee, H.J. Jung, J. Jang, H. Choi, N. Li, M. Kim, S. Park, S.Y. Kim, T.M. Koo, H.E. Fu, Y.S. Jeon, A. Ambriović-Ristov, J.-J. Song, S.Y. Kim, S. Park, Q. Wei, C. Ko, K.-B. Lee, R. Paulmurugan, Y.K. Kim, H. Kang, Remote switching of elastic movement of decorated ligand nanostructures controls the adhesion-regulated polarization of host macrophages, Adv. Funct. Mater. 31 (2021), 2008698, https://doi.org/10.1002/adfm.202008698.

[27] Z. Shen, J. Song, B.C. Yung, Z. Zhou, A. Wu, X. Chen, Emerging strategies of cancer therapy based on ferroptosis, Adv. Mater. 30 (2018), 1704007, https://doi.org/10.1002/adma.201704007.

[28] X. Jiang, B.R. Stockwell, M. Conrad, Ferroptosis: mechanisms, biology and role in disease, Nat. Rev. Mol. Cell Biol. 22 (2021) 266–282, https://doi.org/10.1038/s41580-020-00324-8.

[29] G. Lei, L. Zhuang, B. Gan, Targeting ferroptosis as a vulnerability in cancer, Nat. Rev. Cancer 22 (2022) 381–396, https://doi.org/10.1038/s41568-022-00459-0.

[30] J. Zheng, M. Conrad, The metabolic underpinnings of ferroptosis, Cell Metabol. 32 (2020) 920–937, https://doi.org/10.1016/j.cmet.2020.10.011.

[31] X. Hong, W. Roh, R.J. Sullivan, K.H.K. Wong, B.S. Wittner, H. Guo, T.D. Dubash, M. Sade-Feldman, B. Wesley, E. Horwitz, G.M. Boland, D.L. Marvin, T. Bonesteel, C. Lu, F. Aguet, R. Burr, S.S. Freeman, L. Parida, K. Calhoun, M.K. Jewett, L. T. Nieman, N. Hacohen, A.M. Naar, D.T. Ting, M. Toner, S.L. Stott, G. Getz, S. Maheswaran, D.A. Haber, The lipogenic regulator SREBP2 induces transferrin in circulating melanoma cells and suppresses ferroptosis, Cancer Discov. 11 (2021) 678–695, https://doi.org/10.1158/2159-8290.CD-19-1500.

[32] T.R. Daniels, E. Bernabeu, J.A. Rodríguez, S. Patel, M. Kozman, D.A. Chiappetta, E. Holler, J.Y. Ljubimova, G. Helguera, M.L. Penichet, The transferrin receptor and the targeted delivery of therapeutic agents against cancer, Biochim. Biophys. Acta Gen. Subj. 1820 (2012) 291–317, https://doi.org/10.1016/j.bbagen.2011.07.016.

[33] W.S. Yang, B.R. Stockwell, Synthetic lethal screening identifies compounds activating iron-dependent, nonapoptotic cell death in oncogenic-RAS-harboring cancer cells, Chem. Biol. 15 (2008) 234–245, https://doi.org/10.1016/j.chembiol.2008.02.010.

[34] J. Wang, S. Tian, R.A. Petros, M.E. Napier, J.M. DeSimone, The complex role of multivalency in nanoparticles targeting the transferrin receptor for cancer therapies, J. Am. Chem. Soc. 132 (2010) 11306–11313, https://doi.org/10.1021/ja1043177.

[35] Z.J. Lin, D.N. Shen, W.X. Zhou, Y.F. Zheng, T.T. Kong, X.Y. Liu, S.L. Wu, P.K. Chu, Y. Zhao, J. Wu, K.M.C. Cheung, K.W.K. Yeung, Regulation of extracellular bioactive cations in bone tissue microenvironment induces favorable osteoimmune conditions to accelerate in situ bone regeneration, Bioact. Mater. 6 (2021) 2315–2330, https://doi.org/10.1016/j.bioactmat.2021.01.018.

[36] J.Y. Cao, S.J. Dixon, Mechanisms of ferroptosis, Cell. Mol. Life Sci. 73 (2016) 2195–2209, https://doi.org/10.1007/s00018-016-2194-1.

[37] H.J. Forman, H. Zhang, A. Rinna, Glutathione: overview of its protective roles, measurement, and biosynthesis, Mol. Aspect. Med. 30 (2009) 1–12, https://doi.org/10.1016/j.mam.2008.08.006.

[38] W.S. Yang, R. SriRamaratnam, M.E. Welsch, K. Shimada, R. Skouta, V. S. Viswanathan, J.H. Cheah, P.A. Clemons, A.F. Shamji, C.B. Clish, L.M. Brown, A. W. Girotti, V.W. Cornish, S.L. Schreiber, B.R. Stockwell, Regulation of ferroptotic cancer cell death by GPX4, Cell 156 (2014) 317–331, https://doi.org/10.1016/j.cell.2013.12.010.

[39] T.M. Seibt, B. Proneth, M. Conrad, Role of GPX4 in ferroptosis and its pharmacological implication, Free Radic. Biol. Med. 133 (2019) 144–152, https://doi.org/10.1016/j.freeradbiomed.2018.09.014.

[40] M. Valko, C. Rhodes, J. Moncol, M. Izakovic, M. Mazur, Free radicals, metals and antioxidants in oxidative stress-induced cancer, Chem. Biol. Interact. 160 (2006) 1–40, https://doi.org/10.1016/j.cbi.2005.12.009.

[41] M. Ott, V. Gogvadze, S. Orrenius, B. Zhivotovsky, Mitochondria, oxidative stress and cell death, Apoptosis 12 (2007) 913–922, https://doi.org/10.1007/s10495-007-0756-2.

[42] M.L. Circu, T.Y. Aw, Reactive oxygen species, cellular redox systems, and apoptosis, Free Radic. Biol. Med. 48 (2010) 749–762, https://doi.org/10.1016/j.freeradbiomed.2009.12.022.

[43] K. D'Herde, D.V. Krysko, Oxidized PEs trigger death, Nat. Chem. Biol. 13 (2017) 4–5, https://doi.org/10.1038/nchembio.2261.

[44] M.E. Begin, G. Ells, D.F. Horrobin, Polyunsaturated fatty acid-induced cytotoxicity against tumor cells and its relationship to lipid peroxidation, J. Natl. Cancer Inst. 80 (1988) 188–194, https://doi.org/10.1093/jnci/80.3.188.

[45] W.S. Yang, K.J. Kim, M.M. Gaschler, M. Patel, M.S. Shchepinov, B.R. Stockwell, Peroxidation of polyunsaturated fatty acids by lipoxygenases drives ferroptosis, Proc. Natl. Acad. Sci. U.S.A. 113 (2016) E4966–E4975, https://doi.org/10.1073/pnas.1603244113.

[46] H. Yuan, X. Li, X. Zhang, R. Kang, D. Tang, Identification of ACSL4 as a biomarker and contributor of ferroptosis, Biochem. Biophys. Res. Commun. 478 (2016) 1338–1343, https://doi.org/10.1016/j.bbrc.2016.08.124.

[47] S. Doll, B. Proneth, Y.Y. Tyurina, E. Panzilius, S. Kobayashi, I. Ingold, M. Irmler, J. Beckers, M. Aichler, A. Walch, H. Prokisch, D. Trümbach, G. Mao, F. Qu, H. Bayir, J. Füllekrug, C.H. Scheel, W. Wurst, J.A. Schick, V.E. Kagan, J. P. Friedmann Angeli, M. Conrad, ACSL4 dictates ferroptosis sensitivity by shaping cellular lipid composition, Nat. Chem. Biol. 13 (2017) 91–98, https://doi.org/10.1038/nchembio.2239.

[48] V.E. Kagan, G. Mao, F. Qu, J.P.F. Angeli, S. Doll, C.S. Croix, H.H. Dar, B. Liu, V. A. Tyurin, V.B. Ritov, A.A. Kapralov, A.A. Amoscato, J. Jiang, T. Anthonymuthu, D. Mohammadyani, Q. Yang, B. Proneth, J. Klein-Seetharaman, S. Watkins, I. Bahar, J. Greenberger, R.K. Mallampalli, B.R. Stockwell, Y.Y. Tyurina, M. Conrad, H. Bayır, Oxidized arachidonic and adrenic PEs navigate cells to ferroptosis, Nat. Chem. Biol. 13 (2017) 81–90, https://doi.org/10.1038/nchembio.2238.

[49] E. Agmon, J. Solon, P. Bassereau, B.R. Stockwell, Modeling the effects of lipid peroxidation during ferroptosis on membrane properties, Sci. Rep. 8 (2018) 1–11, https://doi.org/10.1038/s41598-018-23408-0.

[50] T. Li, N. Kon, L. Jiang, M. Tan, T. Ludwig, Y. Zhao, R. Baer, W. Gu, Tumor suppression in the absence of p53-mediated cell-cycle arrest, apoptosis, and senescence, Cell 149 (2012) 1269–1283, https://doi.org/10.1016/j.cell.2012.04.026.

[51] L. Jiang, N. Kon, T. Li, S.-J. Wang, T. Su, H. Hibshoosh, R. Baer, W. Gu, Ferroptosis as a p53-mediated activity during tumour suppression, Nature 520 (2015) 57–62, https://doi.org/10.1038/nature14344.

[52] Y. Xie, S. Zhu, X. Song, X. Sun, Y. Fan, J. Liu, M. Zhong, H. Yuan, L. Zhang, T. R. Billiar, M.T. Lotze, H.J. Zeh III, R. Kang, G. Kroemer, D. Tang, The tumor suppressor p53 limits ferroptosis by blocking DPP4 activity, Cell Rep. 20 (2017) 1692–1704, https://doi.org/10.1016/j.celrep.2017.07.055.

[53] B. Chu, N. Kon, D. Chen, T. Li, T. Liu, L. Jiang, S. Song, O. Tavana, W. Gu, ALOX12 is required for p53-mediated tumour suppression through a distinct ferroptosis pathway, Nat. Cell Biol. 21 (2019) 579–591, https://doi.org/10.1038/s41556-019-0305-6.

[54] L. Jiang, J.H. Hickman, S.-J. Wang, W. Gu, Dynamic roles of p53-mediated metabolic activities in ROS-induced stress responses, Cell Cycle 14 (2015) 2881–2885, https://doi.org/10.1080/15384101.2015.1068479.

[55] S.-J. Wang, D. Li, Y. Ou, L. Jiang, Y. Chen, Y. Zhao, W. Gu, Acetylation is crucial for p53-mediated ferroptosis and tumor suppression, Cell Rep. 17 (2016) 366–373, https://doi.org/10.1016/j.celrep.2016.09.022.

[56] W. Wang, M. Green, J.E. Choi, M. Gijón, P.D. Kennedy, J.K. Johnson, P. Liao, X. Lang, I. Kryczek, A. Sell, H. Xia, J. Zhou, G. Li, J. Li, W. Li, S. Wei, L. Vatan, H. Zhang, W. Szeliga, W. Gu, R. Liu, T.S. Lawrence, C. Lamb, Y. Tanno, M. Cieslik, E. Stone, G. Georgiou, T.A. Chan, A. Chinnaiyan, W. Zou, CD8+ T cells regulate tumour ferroptosis during cancer immunotherapy, Nature 569 (2019) 270–274, https://doi.org/10.1038/s41586-019-1170-y.

[57] Y. Zhang, J. Shi, X. Liu, L. Feng, Z. Gong, P. Koppula, K. Sirohi, X. Li, Y. Wei, H. Lee, L. Zhuang, G. Chen, Z.-D. Xiao, M.-C. Hung, J. Chen, P. Huang, W. Li, B. Gan, BAP1 links metabolic regulation of ferroptosis to tumour suppression, Nat. Cell Biol. 20 (2018) 1181–1192, https://doi.org/10.1038/s41556-018-0178-0.

[58] Y. Zhang, P. Koppula, B. Gan, Regulation of H2A ubiquitination and SLC7A11 expression by BAP1 and PRC1, Cell Cycle 18 (2019) 773–783, https://doi.org/10.1080/15384101.2019.1597506.

[59] Y.S. Lee, D.H. Lee, S.Y. Jeong, S.H. Park, S.C. Oh, Y.S. Park, J. Yu, H.A. Choudry, D.L. Bartlett, Y.J. Lee, Ferroptosis-inducing agents enhance TRAIL-induced apoptosis through upregulation of death receptor 5, J. Cell. Biochem. 120 (2019) 928–939, https://doi.org/10.1002/jcb.27456.

[60] G. Bae, M.S. Kim, R. Thangam, T.M. Koo, W.Y. Jang, J. Yoon, S.B. Han, L. Yang, S. Y. Kim, N. Kang, S. Min, H. Hong, H.E. Fu, M.J. Ko, D.-H. Kim, W.K. Jeong, D. H. Kim, T.-H. Kim, J.-W. Choi, K.-B. Lee, R. Paulmurugan, Y. Zhu, H.-J. Kim, J. Lee, J.S. Kim, A. Khademhosseini, Y.K. Kim, H. Kang, Receptor-level proximity and fastening of ligands modulates stem cell differentiation, Adv. Funct. Mater. 32 (2022), 2200828, https://doi.org/10.1002/adfm.202200828.

[61] Y. Zhang, H. Tan, J.D. Daniels, F. Zandkarimi, H. Liu, L.M. Brown, K. Uchida, O. A. O'Connor, B.R. Stockwell, Imidazole ketone erastin induces ferroptosis and slows tumor growth in a mouse lymphoma model, Cell Chem. Biol. 26 (2019) 623–633, https://doi.org/10.1016/j.chembiol.2019.01.008.

[62] C. Louandre, I. Marcq, H. Bouhlal, E. Lachaier, C. Godin, Z. Saidak, C. François, D. Chatelain, V. Debuysscher, J.-C. Barbare, The retinoblastoma (Rb) protein regulates ferroptosis induced by sorafenib in human hepatocellular carcinoma cells, Cancer Lett. 356 (2015) 971–977, https://doi.org/10.1016/j.canlet.2014.11.014.

[63] P. Gout, A. Buckley, C. Simms, N. Bruchovsky, Sulfasalazine, a potent suppressor of lymphoma growth by inhibition of the xc− cystine transporter: a new action for an old drug, Leukemia 15 (2001) 1633–1640, https://doi.org/10.1038/sj.leu.2402238.

[64] J.K. Eaton, L. Furst, R.A. Ruberto, D. Moosmayer, A. Hilpmann, M.J. Ryan, K. Zimmermann, L.L. Cai, M. Niehues, V. Badock, A. Kramm, S. Chen, R.C. Hillig, P.A. Clemons, S. Gradl, C. Montagnon, K.E. Lazarski, S. Christian, B. Bajrami, R. Neuhaus, A.L. Eheim, V.S. Viswanathan, S.L. Schreiber, Selective covalent targeting of GPX4 using masked nitrile-oxide electrophiles, Nat. Chem. Biol. 16 (2020) 497–506, https://doi.org/10.1038/s41589-020-0501-5.

[65] J.K. Eaton, R.A. Ruberto, A. Kramm, V.S. Viswanathan, S.L. Schreiber, Diacylfuroxans are masked nitrile oxides that inhibit GPX4 covalently, J. Am. Chem. Soc. 141 (2019) 20407–20415, https://doi.org/10.1021/jacs.9b10769.

[66] M.M. Gaschler, A.A. Andia, H. Liu, J.M. Csuka, B. Hurlocker, C.A. Vaiana, D. W. Heindel, D.S. Zuckerman, P.H. Bos, E. Reznik, L.F. Ye, Y.Y. Tyurina, A.J. Lin, M.S. Shchepinov, A.Y. Chan, E. Peguero-Pereira, M.A. Fomich, J.D. Daniels, A. V. Bekish, V.V. Shmanai, V.E. Kagan, L.K. Mahal, K.A. Woerpel, B.R. Stockwell, FINO2 initiates ferroptosis through GPX4 inactivation and iron oxidation, Nat. Chem. Biol. 14 (2018) 507–515, https://doi.org/10.1038/s41589-018-0031-6.

[67] K. Shimada, R. Skouta, A. Kaplan, W.S. Yang, M. Hayano, S.J. Dixon, L.M. Brown, C.A. Valenzuela, A.J. Wolpaw, B.R. Stockwell, Global survey of cell death mechanisms reveals metabolic regulation of ferroptosis, Nat. Chem. Biol. 12 (2016) 497–503, https://doi.org/10.1038/nchembio.2079.

[68] J. Tsoi, L. Robert, K. Paraiso, C. Galvan, K.M. Sheu, J. Lay, D.J.L. Wong, M. Atefi, R. Shirazi, X. Wang, D. Braas, C.S. Grasso, N. Palaskas, A. Ribas, T.G. Graeber, Multi-stage differentiation defines melanoma subtypes with differential vulnerability to drug-induced iron-dependent oxidative stress, Cancer Cell 33 (2018) 890–904, https://doi.org/10.1016/j.ccell.2018.03.017.

[69] M.J. Hangauer, V.S. Viswanathan, M.J. Ryan, D. Bole, J.K. Eaton, A. Matov, J. Galeas, H.D. Dhruv, M.E. Berens, S.L. Schreiber, F. McCormick, M.T. McManus, Drug-tolerant persister cancer cells are vulnerable to GPX4 inhibition, Nature 551 (2017) 247–250, https://doi.org/10.1038/nature24297.

[70] Y. Li, D. Feng, Z. Wang, Y. Zhao, R. Sun, D. Tian, D. Liu, F. Zhang, S. Ning, J. Yao, Ischemia-induced ACSL4 activation contributes to ferroptosis-mediated tissue injury in intestinal ischemia/reperfusion, Cell Death Differ. 26 (2019) 2284–2299, https://doi.org/10.1038/s41418-019-0299-4.

[71] M. Xu, J. Tao, Y. Yang, S. Tan, H. Liu, J. Jiang, F. Zheng, B. Wu, Ferroptosis involves in intestinal epithelial cell death in ulcerative colitis, Cell Death Dis. 11 (2020) 1–13, https://doi.org/10.1038/s41419-020-2299-1.

[72] F. Simões, J. Ousingsawat, P. Wanitchakool, A. Fonseca, I. Cabrita, R. Benedetto, R. Schreiber, K. Kunzelmann, CFTR supports cell death through ROS-dependent activation of TMEM16F (anoctamin 6), Pflueg. Arch. Eur. J. Physiol. 470 (2018) 305–314, https://doi.org/10.1007/s00424-017-2065-0.

[73] D. Schnabel, E. Salas-Vidal, V. Narváez, M. del Rayo Sánchez-Carbente, D. Hernández-García, R. Cuervo, L. Covarrubias, Expression and regulation of antioxidant enzymes in the developing limb support a function of ROS in interdigital cell death, Dev. Biol. 291 (2006) 291–299, https://doi.org/10.1016/j.ydbio.2005.12.023.

[74] J. Zhao, B. Xu, Q. Xiong, Y. Feng, H. Du, Erastin-induced ferroptosis causes physiological and pathological changes in healthy tissues of mice, Mol. Med. Rep. 24 (2021) 713, https://doi.org/10.3892/mmr.2021.12352.

[75] Y. Zhu, W.Y. Wang, P. Gong, Y.F. Zhao, Y.B. Pan, J.H. Zou, R.J. Ao, J. Wang, H. L. Cai, H.W. Huang, M.L. Yu, H.J. Wang, L.S. Lin, X.Y. Chen, Y. Wu, Enhancing catalytic activity of a nickel single atom enzyme by polynary heteroatom doping for ferroptosis-based tumor therapy, ACS Nano 17 (2023) 3064–3076, https://doi.org/10.1021/acsnano.2c11923.

[76] H. Hong, S. Min, S. Koo, Y. Lee, J. Yoon, W.Y. Jang, N. Kang, R. Thangam, H. Choi, H.J. Jung, S.-B. Han, Q. Wei, S.-H. Yu, D.-H. Kim, R. Paulmurugan, W. K. Jeong, K.-B. Lee, T. Hyeon, D. Kim, H. Kang, Dynamic ligand screening by magnetic nanoassembly modulates stem cell differentiation, Adv. Mater. 34 (2022) 2105460, https://doi.org/10.1002/adma.202105460.

[77] S. Min, Y.S. Jeon, H.J. Jung, C. Khatua, N. Li, G. Bae, H. Choi, H. Hong, J.E. Shin, M.J. Ko, H.S. Ko, I. Jun, H.E. Fu, S.H. Kim, R. Thangam, J.-J. Song, V.P. Dravid, Y. K. Kim, H. Kang, Independent tuning of nano-ligand frequency and sequences regulates the adhesion and differentiation of stem cells, Adv. Mater. 32 (2020), 2004300, https://doi.org/10.1002/adma.202004300.

[78] Z. Zhou, J. Song, R. Tian, Z. Yang, G. Yu, L. Lin, G. Zhang, W. Fan, F. Zhang, G. Niu, L. Nie, X. Chen, Activatable singlet oxygen generation from lipid hydroperoxide nanoparticles for cancer therapy, Angew. Chem. 129 (2017) 6592–6596, https://doi.org/10.1002/ange.201701181.

[79] W.-P. Li, C.-H. Su, Y.-C. Chang, Y.-J. Lin, C.-S. Yeh, Ultrasound-induced reactive oxygen species mediated therapy and imaging using a fenton reaction activable polymersome, ACS Nano 10 (2016) 2017–2027, https://doi.org/10.1021/acsnano.5b06175.

[80] Y. Qiu, Y. Cao, W. Cao, Y. Jia, N. Lu, The application of ferroptosis in diseases, Pharmacol. Res. 159 (2020), 104919, https://doi.org/10.1016/j.phrs.2020.104919.

[81] H.F. Yan, T. Zou, Q.Z. Tuo, S. Xu, H. Li, A.A. Belaidi, P. Lei, Ferroptosis: mechanisms and links with diseases, Signal Transduct. Targeted Ther. 6 (2021) 49, https://doi.org/10.1038/s41392-020-00428-9.

[82] S.H. Lee, S. An, Y.C. Ryu, S.H. Seo, S. Park, M.J. Lee, S.W. Cho, K.Y. Choi, Adhesive hydrogel patch-mediated combination drug therapy induces regenerative wound healing through reconstruction of regenerative microenvironment, Adv. Healthcare Mater. (2023) 2203094, https://doi.org/10.1002/adhm.202203094.

[83] A.N. Cho, Y. Jin, Y. An, J. Kim, Y.S. Choi, J.S. Lee, J. Kim, W.Y. Choi, D.J. Koo, W. Yu, G.E. Chang, D.Y. Kim, S.H. Jo, J. Kim, S.Y. Kim, Y.G. Kim, J.Y. Kim, N. Choi, E. Cheong, Y.J. Kim, H.S. Je, H.C. Kang, S.W. Cho, Microfluidic device with brain extracellular matrix promotes structural and functional maturation of human brain organoids, Nat. Commun. 12 (2021) 4730, https://doi.org/10.1038/s41467-021-24775-5.

[84] C. Chen, Y. Wang, H. Zhang, H. Zhang, W. Dong, W. Sun, Y. Zhao, Responsive and self-healing structural color supramolecular hydrogel patch for diabetic wound treatment, Bioact. Mater. 15 (2022) 194–202, https://doi.org/10.1016/j.bioactmat.2021.11.037.

[85] H. Wu, Y. Shang, W. Sun, X. Ouyang, W. Zhou, J. Lu, S. Yang, W. Wei, X. Yao, X. Wang, X. Zhang, Y. Chen, Q. He, Z. Yang, H. Ouyang, Seamless and early gap healing of osteochondral defects by autologous mosaicplasty combined with bioactive supramolecular nanofiber-enabled gelatin methacryloyl (BSN-GelMA) hydrogel, Bioact. Mater. 19 (2023) 88–102, https://doi.org/10.1016/j.bioactmat.2022.03.038.

[86] Z. Yang, B. Wang, W. Liu, X. Li, K. Liang, Z. Fan, J.J. Li, Y. Niu, Z. He, H. Li, D. Wang, J. Lin, Y. Du, J. Lin, D. Xing, In situ self-assembled organoid for osteochondral tissue regeneration with dual functional units, Bioact. Mater. 27 (2023) 200–215, https://doi.org/10.1016/j.bioactmat.2023.04.002.

[87] Y. Kim, H. Choi, J.E. Shin, G. Bae, R. Thangam, H. Kang, Remote active control of nanoengineered materials for dynamic nanobiomedical engineering, View 1 (2020), 20200029, https://doi.org/10.1002/VIW.20200029.

[88] T. Kang, G.D. Cha, O.K. Park, H.R. Cho, M. Kim, J. Lee, D. Kim, B. Lee, J. Chu, S. Koo, T. Hyeon, D.H. Kim, S.H. Choi, Penetrative and sustained drug delivery using injectable hydrogel nanocomposites for postsurgical brain tumor treatment, ACS Nano 17 (2023) 5435–5447, https://doi.org/10.1021/acsnano.2c10094.

[89] Y. Lim, S.H. Noh, T.H. Shin, J.U. Lee, D. Lungerich, J.H. Lee, J. Cheon, Magnetothermally activated nanometer-level modular functional group grafting of nanoparticles, Nano Lett. 21 (2021) 3649–3656, https://doi.org/10.1021/acs.nanolett.1c00770.

[90] S.H.D. Wong, X. Xu, X. Chen, Y. Xin, L.M. Xu, C.H.N. Lai, J. Oh, W.K.R. Wong, X. M. Wang, S.S. Han, W.X. You, X.T. Shuai, N. Wong, Y.H. Tan, L. Duan, L. Bian, Manipulation of the nanoscale presentation of integrin ligand produces cancer cells with enhanced stemness and robust tumorigenicity, Nano Lett. 21 (2021) 3225–3236, https://doi.org/10.1021/acs.nanolett.1c00501.

[91] M. Jung, H. Kim, J.W. Hwang, Y. Choi, M. Kang, C. Kim, J. Hong, N.K. Lee, S. Moon, J.W. Chang, S.J. Choi, S.Y. Oh, H. Jang, D.L. Na, B.S. Kim, Iron oxide nanoparticle-incorporated mesenchymal stem cells for alzheimer's disease

[92] J. Lee, Y.G. Wang, C.B. Xue, Y. Chen, M.Y. Qu, J. Thakor, X.W. Zhou, N.R. Barros, N. Falcone, P. Young, F.W. van den Dolder, K. Lee, Y.Z. Zhu, H.J. Cho, W.J. Sun, B. Zhao, S. Ahadian, V. Jucaud, M.R. Dokmeci, A. Khademhosseini, H.J. Kim, pH-Responsive doxorubicin delivery using shear-thinning biomaterials for localized melanoma treatment, Nanoscale 14 (2022) 350–360, https://doi.org/10.1039/d1nr05738c.

[93] C. Gao, Z. Zeng, S. Peng, C. Shuai, Magnetostrictive alloys: promising materials for biomedical applications, Bioact. Mater. 8 (2022) 177–195, https://doi.org/10.1016/j.bioactmat.2021.06.025.

[94] E. Georgas, M. Yuan, J. Chen, Y. Wang, Y.X. Qin, Bioactive superparamagnetic iron oxide-gold nanoparticles regulated by a dynamic magnetic field induce neuronal Ca(2+) influx and differentiation, Bioact. Mater. 26 (2023) 478–489, https://doi.org/10.1016/j.bioactmat.2023.01.007.

[95] Y. Shou, L. Liu, Q. Liu, Z. Le, K.L. Lee, H. Li, X. Li, D.Z. Koh, Y. Wang, T.M. Liu, Z. Yang, C.T. Lim, C. Cheung, A. Tay, Mechano-responsive hydrogel for direct stem cell manufacturing to therapy, Bioact. Mater. 24 (2023) 387–400, https://doi.org/10.1016/j.bioactmat.2022.12.019.

[96] Y. Zhang, J. Li, P. Habibovic, Magnetically responsive nanofibrous ceramic scaffolds for on-demand motion and drug delivery, Bioact. Mater. 15 (2022) 372–381, https://doi.org/10.1016/j.bioactmat.2022.02.028.

[97] C. Zhang, W. Bu, D. Ni, S. Zhang, Q. Li, Z. Yao, J. Zhang, H. Yao, Z. Wang, J. Shi, Synthesis of iron nanometallic glasses and their application in cancer therapy by a localized Fenton reaction, Angew. Chem. 128 (2016) 2141–2146, https://doi.org/10.1002/anie.201510031.

[98] M. Huo, L. Wang, Y. Chen, J. Shi, Tumor-selective catalytic nanomedicine by nanocatalyst delivery, Nat. Commun. 8 (2017) 1–12, https://doi.org/10.1038/s41467-017-00424-8.

[99] R. Shintoku, Y. Takigawa, K. Yamada, C. Kubota, Y. Yoshimoto, T. Takeuchi, I. Koshiishi, S. Torii, Lipoxygenase-mediated generation of lipid peroxides enhances ferroptosis induced by erastin and RSL3, Cancer Sci. 108 (2017) 2187–2194, https://doi.org/10.1111/cas.13380.

[100] Y. Luo, B. Li, X. Liu, Y. Zheng, E. Wang, Z. Li, Z. Cui, Y. Liang, S. Zhu, S. Wu, Simultaneously enhancing the photocatalytic and photothermal effect of NH(2)-MIL-125-GO-Pt ternary heterojunction for rapid therapy of bacteria-infected wounds, Bioact, Materials 18 (2022) 421–432, https://doi.org/10.1016/j.bioactmat.2022.03.035.

[101] G. Bae, Y.S. Jeon, M.J. Ko, Y. Kim, S.-B. Han, R. Thangam, W. Kim, H.J. Jung, S. Lee, H. Choi, S. Min, H. Hong, S. Park, S.Y. Kim, K.D. Patel, N. Li, J.E. Shin, B. C. Park, H.S. Park, J.H. Moon, Y.J. Kim, U.K. Sukumar, J.-J. Song, S.Y. Kim, S.-H. Yu, Y.C. Kang, S. Park, S.M. Han, D.-H. Kim, K.-B. Lee, Q. Wei, L. Bian, R. Paulmurugan, Y.K. Kim, H. Kang, Immunoregulation of macrophages by controlling winding and unwinding of nanohelical ligands, Adv. Funct. Mater. 31 (2021), 2103409, https://doi.org/10.1002/adfm.202103409.

[102] J.U. Lee, W. Shin, Y. Lim, J. Kim, W.R. Kim, H. Kim, J.H. Lee, J. Cheon, Non-contact long-range magnetic stimulation of mechanosensitive ion channels in freely moving animals, Nat. Mater. 20 (2021) 1029–1036, https://doi.org/10.1038/s41563-020-00896-y.

[103] J. Shin, N. Kang, B. Kim, H. Hong, L. Ye, J. Kim, H. Kang, J.S. Kim, One-dimensional nanomaterials for cancer therapy and diagnosis, Chem. Soc. Rev. 52 (2023) 4488–4514, https://doi.org/10.1039/D2CS00840H.

[104] B. Li, X. Chen, W. Qiu, R. Zhao, J. Duan, S. Zhang, Z. Pan, S. Zhao, Q. Guo, Y. Qi, W. Wang, L. Deng, S. Ni, Y. Sang, H. Xue, H. Liu, G. Li, Synchronous disintegration of ferroptosis defense Axis via engineered exosome-conjugated magnetic nanoparticles for glioblastoma therapy, Adv. Sci. 9 (2022), 2105451, https://doi.org/10.1002/advs.202105451.

[105] B. Yu, B. Choi, W. Li, D.-H. Kim, Magnetic field boosted ferroptosis-like cell death and responsive MRI using hybrid vesicles for cancer immunotherapy, Nat. Commun. 11 (2020) 3637, https://doi.org/10.1038/s41467-020-17380-5.

[106] F. Zhang, F. Li, G.H. Lu, W. Nie, L. Zhang, Y. Lv, W. Bao, S. Gao, W. Wei, K. Pu, H. Y. Xie, Engineering magnetosomes for ferroptosis/immunomodulation synergism in cancer, ACS Nano 13 (2019) 5662–5673, https://doi.org/10.1021/acsnano.9b00892.

[107] S. Luo, D. Ma, R. Wei, W. Yao, X. Pang, Y. Wang, X. Xu, X. Wei, Y. Guo, X. Jiang, Y. Yuan, R. Yang, A tumor microenvironment responsive nanoplatform with oxidative stress amplification for effective MRI-based visual tumor ferroptosis, Acta Biomater 138 (2022) 518–527, https://doi.org/10.1016/j.actbio.2021.11.007.

[108] Z. Shen, T. Liu, Y. Li, J. Lau, Z. Yang, W. Fan, Z. Zhou, C. Shi, C. Ke, V.I. Bregadze, S.K. Mandal, Y. Liu, Z. Li, T. Xue, G. Zhu, J. Munasinghe, G. Niu, A. Wu, X. Chen, Fenton-reaction-acceleratable magnetic nanoparticles for ferroptosis therapy of orthotopic brain tumors, ACS Nano 12 (2018) 11355–11365, https://doi.org/10.1021/acsnano.8b06201.

[109] Y. Xu, Y. Guo, C. Zhang, M. Zhan, L. Jia, S. Song, C. Jiang, M. Shen, X. Shi, Fibronectin-coated metal–phenolic networks for cooperative tumor chemo-/chemodynamic/immune therapy via enhanced ferroptosis-mediated immunogenic cell death, ACS Nano 16 (2022) 984–996, https://doi.org/10.1021/acsnano.1c08585.

[110] L. Zhu, J. Wang, X. Tang, C. Zhang, P. Wang, L. Wu, W. Gao, W. Ding, G. Zhang, X. Tao, Efficient magnetic nanocatalyst-induced chemo-and ferroptosis synergistic cancer therapy in combination with T1–T2 dual-mode magnetic resonance imaging through doxorubicin delivery, ACS Appl. Mater. Interfaces 14 (2022) 3621–3632, https://doi.org/10.1021/acsami.1c17507.

[111] G. Zhang, N. Li, Y. Qi, Q. Zhao, J. Zhan, D. Yu, Synergistic ferroptosis-gemcitabine chemotherapy of the gemcitabine loaded carbonaceous nanozymes to enhance

the treatment and magnetic resonance imaging monitoring of pancreatic cancer, Acta Biomater. 142 (2022) 284–297, https://doi.org/10.1016/j.actbio.2022.02.006.

[112] M. Chen, J. Li, G. Shu, L. Shen, E. Qiao, N. Zhang, S. Fang, X. Chen, Z. Zhao, J. Tu, J. Song, Y. Du, J. Ji, Homogenous multifunctional microspheres induce ferroptosis to promote the anti-hepatocarcinoma effect of chemoembolization, J. Nanobiotechnol. 20 (2022) 179, https://doi.org/10.1186/s12951-022-01385-x.

[113] S. Wang, F. Li, R. Qiao, X. Hu, H. Liao, L. Chen, J. Wu, H. Wu, M. Zhao, J. Liu, R. Chen, X. Ma, D. Kim, J. Sun, T.P. Davis, C. Chen, J. Tian, T. Hyeon, D. Ling, Arginine-rich manganese silicate nanobubbles as a ferroptosis-inducing agent for tumor-targeted theranostics, ACS Nano 12 (2018) 12380–12392, https://doi.org/10.1021/acsnano.8b06399.

[114] Y. Meng, D. Zhang, X. Chen, Z. Dai, X. Yao, P. Cui, D. Yu, G. Zhang, X. Zheng, FePt nanoparticles embedded in metal–organic framework nanoparticles for tumor imaging and eradication, ACS Appl. Nano Mater. 3 (2020) 4494–4503, https://doi.org/10.1021/acsanm.0c00581.

[115] Q. Guan, R. Guo, S. Huang, F. Zhang, J. Liu, Z. Wang, X. Yang, X. Shuai, Z. Cao, Mesoporous polydopamine carrying sorafenib and SPIO nanoparticles for MRI-guided ferroptosis cancer therapy, J. Contr. Release 320 (2020) 392–403, https://doi.org/10.1016/j.jconrel.2020.01.048.

[116] G. Zhang, L. Zhang, Y. Si, Q. Li, J. Xiao, B. Wang, C. Liang, Z. Wu, G. Tian, Oxygen-enriched Fe3O4/Gd2O3 nanopeanuts for tumor-targeting MRI and ROS-triggered dual-modal cancer therapy through platinum (IV) prodrugs delivery, Chem. Eng. J. 388 (2020), 124269, https://doi.org/10.1016/j.cej.2020.124269.

[117] B. Ding, P. Zheng, F. Jiang, Y. Zhao, M. Wang, M. Chang, P.a. Ma, J. Lin, MnOx nanospikes as nanoadjuvants and immunogenic cell death drugs with enhanced antitumor immunity and antimetastatic effect, Angew. Chem. Int. Ed. 59 (2020) 16381–16384, https://doi.org/10.1002/anie.202005111.

[118] Q. Jiang, K. Wang, X. Zhang, B. Ouyang, H. Liu, Z. Pang, W. Yang, Platelet membrane-camouflaged magnetic nanoparticles for ferroptosis-enhanced cancer immunotherapy, Small 16 (2020), 2001704, https://doi.org/10.1002/smll.202001704.

[119] X. Yao, B. Yang, S. Wang, Z. Dai, D. Zhang, X. Zheng, Q. Liu, A novel multifunctional FePt/BP nanoplatform for synergistic photothermal/photodynamic/chemodynamic cancer therapies and photothermally-enhanced immunotherapy, J. Mater. Chem. B 8 (2020) 8010–8021, https://doi.org/10.1039/D0TB00411A.

[120] K.-S. Kim, B. Choi, H. Choi, M.J. Ko, D.-H. Kim, D.-H. Kim, Enhanced natural killer cell anti-tumor activity with nanoparticles mediated ferroptosis and potential therapeutic application in prostate cancer, J. Nanobiotechnol. 20 (2022) 428, https://doi.org/10.1186/s12951-022-01635-y.

[121] W. Qin, J. Huang, C. Yang, Q. Yue, S. Chen, M. Wang, S. Gao, X. Zhou, X. Yang, Y. Zhang, Protease-Activatable nanozyme with photoacoustic and tumor-enhanced magnetic resonance imaging for photothermal ferroptosis cancer therapy, Adv. Funct. Mater. 33 (2023), 2209748, https://doi.org/10.1002/adfm.202209748.

[122] S.W. Xie, W.S. Sun, C.F. Zhang, B.J. Dong, J.X. Yang, M.F. Hou, L.Q. Xiong, B.A. Cai, X.S. Liu, W. Xue, Metabolic control by heat stress determining cell fate to ferroptosis for effective cancer therapy, ACS Nano 15 (2021) 7179–7194, https://doi.org/10.1021/acsnano.1c00380.

[123] Y. Liang, L. Zhang, C. Peng, S.Y. Zhang, S.W. Chen, X. Qian, W.X. Luo, Q. Dan, Y.Y. Ren, Y.J. Li, B.X. Zhao, Tumor microenvironments self-activated nanoscale metal-organic frameworks for ferroptosis based cancer chemodynamic/photothermal/chemo therapy, Acta Pharm. Sin. B 11 (2021) 3231–3243, https://doi.org/10.1016/j.apsb.2021.01.016.

[124] F. Zeng, L. Tang, Q. Zhang, C. Shi, Z. Huang, S. Nijiati, X. Chen, Z. Zhou, Coordinating the mechanisms of action of ferroptosis and the photothermal effect for cancer theranostics, Angew. Chem., Int. Ed. Engl. 61 (2022), e202112925, https://doi.org/10.1002/anie.202112925.

[125] Y.L. Zhang, K.Y. Xi, X. Fu, H.F. Sun, H. Wang, D.X. Yu, Z.W. Li, Y. Ma, X.J. Liu, B. Huang, J. Wang, G. Li, J.W. Cui, X.G. Li, S.L. Ni, Versatile metal-phenolic network nanoparticles for multitargeted combination therapy and magnetic resonance tracing in glioblastoma, Biomaterials 278 (2021) 121163, https://doi.org/10.1016/j.biomaterials.2021.121163.

[126] Q. Chen, X. Ma, L. Xie, W. Chen, Z. Xu, E. Song, X. Zhu, Y. Song, Iron-based nanoparticles for MR imaging-guided ferroptosis in combination with photodynamic therapy to enhance cancer treatment, Nanoscale 13 (2021) 4855–4870, https://doi.org/10.1039/D0NR08757B.

[127] X.L. Liang, M. Chen, P. Bhattarai, S. Hameed, Y.D. Tang, Z.F. Dal, Complementing cancer photodynamic therapy with ferroptosis through iron oxide loaded porphyrin-grafted lipid nanoparticles, ACS Nano 15 (2021) 20164–20180, https://doi.org/10.1021/acsnano.1c08108.

[128] S. Son, J. Kim, J. Kim, B. Kim, J. Lee, Y. Kim, M. Li, H. Kang, J.S. Kim, Cancer therapeutics based on diverse energy sources, Chem. Soc. Rev. 51 (2022) 8201–8215, https://doi.org/10.1039/D2CS00102K.

[129] S. Yan, K. Hu, M. Zhang, J. Sheng, X. Xu, S. Tang, Y. Li, S. Yang, G. Si, Y. Mao, Y. Zhang, F. Zhang, N. Gu, Extracellular magnetic labeling of biomimetic hydrogel-induced human mesenchymal stem cell spheroids with ferumoxytol for MRI tracking, Bioact. Mater. 19 (2023) 418–428, https://doi.org/10.1016/j.bioactmat.2022.04.024.

[130] S.Y. Kim, R. Thangam, N. Kang, H. Hong, C. Kim, S. Lee, S. Son, H.-J. Lee, K.-R. Tag, S. Min, D. Jeong, J. Hwang, K. Kim, D. Kim, Y. Kim, J. Joo, B.H. Kim, Y. Zhu, S.-G. Park, H.-C. Song, W. Sun, J.-P. Ahn, W.Y. Jang, R. Paulmurugan, H.-K. Kim, J.S. Kim, H. Kang, Modulation of macrophages by in situ ligand bridging,

[131] Y. Kim, H.J. Jung, Y. Lee, S. Koo, R. Thangam, W.Y. Jang, S.Y. Kim, S. Park, S. Lee, G. Bae, K.D. Patel, Q. Wei, K.-B. Lee, R. Paulmurugan, W.K. Jeong, T. Hyeon, D. Kim, H. Kang, Manipulating nanoparticle aggregates regulates receptor-ligand binding in macrophages, J. Am. Chem. Soc. 144 (2022) 5769–5783, https://doi.org/10.1021/jacs.1c08861.

[132] B.C. Park, M.J. Ko, Y.K. Kim, G.W. Kim, M.S. Kim, T.M. Koo, H.E. Fu, Y.K. Kim, Surface-ligand-induced crystallographic disorder–order transition in oriented attachment for the tuneable assembly of mesocrystals, Nat. Commun. 13 (2022) 1–11, https://doi.org/10.1038/s41467-022-28830-7.

[133] C. Zhou, C. Wang, K. Xu, Z. Niu, S. Zou, D. Zhang, Z. Qian, J. Liao, J. Xie, Hydrogel platform with tunable stiffness based on magnetic nanoparticles cross-linked GelMA for cartilage regeneration and its intrinsic biomechanism, Bioact. Mater. 25 (2023) 615–628, https://doi.org/10.1016/j.bioactmat.2022.07.013.

[134] J. Zhu, J. Zhou, E.M. Gerhard, S. Zhang, F.I. Parra Rodriguez, T. Pan, H. Yang, Y. Lin, J. Yang, H. Cheng, Smart bioadhesives for wound healing and closure, Bioact. Mater. 19 (2023) 360–375, https://doi.org/10.1016/j.bioactmat.2022.04.020.

[135] Z. Zhao, M. Li, J. Zeng, L. Huo, K. Liu, R. Wei, K. Ni, J. Gao, Recent advances in engineering iron oxide nanoparticles for effective magnetic resonance imaging, Bioact. Mater. 12 (2022) 214–245, https://doi.org/10.1016/j.bioactmat.2021.10.014.

[136] D.D. Stark, R. Weissleder, G. Elizondo, P. Hahn, S. Saini, L. Todd, J. Wittenberg, J. Ferrucci, Superparamagnetic iron oxide: clinical application as a contrast agent for MR imaging of the liver, Radiology 168 (1988) 297–301, https://doi.org/10.1148/radiology.168.2.3393649.

[137] B.J. McCullough, O. Kolokythas, J.H. Maki, D.E. Green, Ferumoxytol in clinical practice: implications for MRI, J. Magn. Reson. Imag. 37 (2013) 1476–1479, https://doi.org/10.1002/jmri.23879.

[138] S.E. Kim, L. Zhang, K. Ma, M. Riegman, F. Chen, I. Ingold, M. Conrad, M.Z. Turker, M. Gao, X. Jiang, S. Monette, M. Pauliah, M. Gonen, P. Zanzonico, T. Quinn, U. Wiesner, M.S. Bradbury, M. Overholtzer, Ultrasmall nanoparticles induce ferroptosis in nutrient-deprived cancer cells and suppress tumour growth, Nat. Nanotechnol. 11 (2016) 977–985, https://doi.org/10.1038/nnano.2016.164.

[139] S.Y. Shen, R. Singhania, G. Fehringer, A. Chakravarthy, M.H. Roehrl, D. Chadwick, P.C. Zuzarte, A. Borgida, T.T. Wang, T. Li, Sensitive tumour detection and classification using plasma cell-free DNA methylomes, Nature 563 (2018) 579–583, https://doi.org/10.1038/s41586-018-0703-0.

[140] L. Gao, J. Zhuang, L. Nie, J. Zhang, Y. Zhang, N. Gu, T. Wang, J. Feng, D. Yang, S. Perrett, X. Yan, Intrinsic peroxidase-like activity of ferromagnetic nanoparticles, Nat. Nanotechnol. 2 (2007) 577–583, https://doi.org/10.1038/nnano.2007.260.

[141] X. Shan, S. Li, B. Sun, Q. Chen, J. Sun, Z. He, C. Luo, Ferroptosis-driven nanotherapeutics for cancer treatment, J. Contr. Release 319 (2020) 322–332, https://doi.org/10.1016/j.jconrel.2020.01.008.

[142] S. Lee, M.S. Kim, K.D. Patel, H. Choi, R. Thangam, J. Yoon, T.M. Koo, H.J. Jung, S. Min, G. Bae, Y. Kim, S.-B. Han, N. Kang, M. Kim, N. Li, H.E. Fu, Y.S. Jeon, J.-J. Song, D.-H. Kim, S. Park, J.-W. Choi, R. Paulmurugan, Y.C. Kang, H. Lee, Q. Wei, V.P. Dravid, K.-B. Lee, Y.K. Kim, H. Kang, Magnetic control and real-time monitoring of stem cell differentiation by the ligand nanoassembly, Small 17 (2021), 2102892, https://doi.org/10.1002/smll.202102892.

[143] M. Riegman, M.S. Bradbury, M. Overholtzer, Population dynamics in cell death: mechanisms of propagation, Trends Cancer 5 (2019) 558–568, https://doi.org/10.1016/j.trecan.2019.07.008.

[144] F. Petrat, H. de Groot, U. Rauen, Subcellular distribution of chelatable iron: a laser scanning microscopic study in isolated hepatocytes and liver endothelial cells, Biochem. J. 356 (2001) 61–69, https://doi.org/10.1042/bj3560061.

[145] G. Gao, J. Li, Y. Zhang, Y.-Z. Chang, Cellular Iron Metabolism and Regulation, Brain Iron Metabolism and CNS Diseases, 2019, pp. 21–32, https://doi.org/10.1007/978-981-13-9589-5_2.

[146] V. Trujillo-Alonso, E.C. Pratt, H. Zong, A. Lara-Martinez, C. Kaittanis, M.O. Rabie, V. Longo, M.W. Becker, G.J. Roboz, J. Grimm, M.L. Guzman, FDA-approved ferumoxytol displays anti-leukaemia efficacy against cells with low ferroportin levels, Nat. Nanotechnol. 14 (2019) 616–622, https://doi.org/10.1038/s41565-019-0406-1.

[147] C. Zhang, F. Zhang, Iron homeostasis and tumorigenesis: molecular mechanisms and therapeutic opportunities, Protein Cell 6 (2015) 88–100, https://doi.org/10.1007/s13238-014-0119-z.

[148] D.H. Manz, N.L. Blanchette, B.T. Paul, F.M. Torti, S.V. Torti, Iron and cancer: recent insights, Ann. N. Y. Acad. Sci. 1368 (2016) 149–161, https://doi.org/10.1111/nyas.13008.

[149] Y. Liu, J. Wang, Effects of DMSA-coated Fe3O4 nanoparticles on the transcription of genes related to iron and osmosis homeostasis, Toxicol. Sci. 131 (2013) 521–536, https://doi.org/10.1093/toxsci/kfs300.

[150] H. Liang, X. Wu, G. Zhao, K. Feng, K. Ni, X. Sun, Renal clearable ultrasmall single-crystal Fe nanoparticles for highly selective and effective ferroptosis therapy and immunotherapy, J. Am. Chem. Soc. 143 (2021) 15812–15823, https://doi.org/10.1021/jacs.1c07471.

[151] J. Gao, T. Luo, J. Wang, Gene interfered-ferroptosis therapy for cancers, Nat. Commun. 12 (2021) 5311, https://doi.org/10.1038/s41467-021-25632-1.

[152] C.-C. Xue, M.-H. Li, Y. Zhao, J. Zhou, Y. Hu, K.-Y. Cai, Y. Zhao, S.-H. Yu, Z. Luo, Tumor microenvironment-activatable Fe-doxorubicin preloaded amorphous CaCO3 nanoformulation triggers ferroptosis in target tumor cells, Sci. Adv. 6 (2020), https://doi.org/10.1126/sciadv.aax1346 eaax1346.

[153] P. Li, M. Gao, Z. Hu, T. Xu, J. Chen, Y. Ma, S. Li, Y. Gu, Synergistic ferroptosis and macrophage re-polarization using engineering exosome-mimic M1 nanovesicles for cancer metastasis suppression, Chem. Eng. J. 409 (2021) 128217, https://doi.org/10.1016/j.cej.2020.128217.

[154] L. Zhou, C. Dong, L. Ding, W. Feng, L. Yu, X. Cui, Y. Chen, Targeting ferroptosis synergistically sensitizes apoptotic sonodynamic anti-tumor nanotherapy, Nano Today 39 (2021), 101212, https://doi.org/10.1016/j.nantod.2021.101212.

[155] X. Zhang, S. Lin, F. Zhao, J. Zhang, S. Lei, F. Bai, Q. Liu, J. Wu, T. He, P. Huang, J. Lin, Programmably controllable delivery of metastable ferrous ions for multiscale dynamic imaging guided photothermal primed chemodynamic therapy, Adv. Mater. (2023), 2210876, https://doi.org/10.1002/adma.202210876.

[156] R. Thangam, S.Y. Kim, N. Kang, H. Hong, H.-J. Lee, S. Lee, D. Jeong, K.-R. Tag, K. Kim, Y. Zhu, W. Sun, H.-J. Kim, S.-W. Cho, J.-P. Ahn, W.Y. Jang, J.S. Kim, R. Paulmurugan, A. Khademhosseini, H.-K. Kim, H. Kang, Ligand coupling and decoupling modulates stem cell fate, Adv. Funct. Mater. 33 (2023), 2206673, https://doi.org/10.1002/adfm.202206673.

[157] J. An, H. Hong, M. Won, H. Rha, Q. Ding, N. Kang, H. Kang, J.S. Kim, Mechanical stimuli-driven cancer therapeutics, Chem. Soc. Rev. 52 (2023) 30–46, https://doi.org/10.1039/D2CS00546H.

[158] H. Wang, Y. Guan, C. Li, J. Chen, S. Yue, J. Qian, B. Dai, C. Jiang, C. Wen, L. Wen, PEGylated manganese–zinc ferrite nanocrystals combined with intratumoral implantation of micromagnets enabled synergetic prostate cancer therapy via ferroptotic and immunogenic cell death, Small 19 (2023), 2207077, https://doi.org/10.1002/smll.202207077.

[159] M.J. Ko, B.C. Park, T.M. Koo, Y.S. Jeon, M.S. Kim, Y.K. Kim, Multi-component mesocrystalline nanoparticles with enhanced photocatalytic activity, Small 16 (2020), 2004696, https://doi.org/10.1002/smll.202004696.

[160] R. Thangam, R. Paulmurugan, H. Kang, Functionalized nanomaterials as tailored theranostic agents in brain imaging, Nanomaterials 12 (2022) 18, https://doi.org/10.3390/nano12010018.

[161] T.H. Shin, P.K. Kim, S. Kang, J. Cheong, S. Kim, Y. Lim, W. Shin, J.Y. Jung, J.D. Lah, B.W. Choi, J. Cheon, High-resolution T-1 MRI via renally clearable dextran nanoparticles with an iron oxide shell, Nat. Biomed. Eng. 5 (2021) 252–263, https://doi.org/10.1038/s41551-021-00687-z.

[162] Y. Shu, M. Ma, X. Pan, M. Shafiq, H. Yu, H. Chen, Cobalt protoporphyrin-induced nano-self-assembly for CT imaging, magnetic-guidance, and antioxidative protection of stem cells in pulmonary fibrosis treatment, Bioact. Mater. 21 (2023) 129–141, https://doi.org/10.1016/j.bioactmat.2022.08.008.

[163] Y. Zhang, S. He, C. Xu, Y. Jiang, Q. Miao, K. Pu, An activatable polymeric nanoprobe for fluorescence and photoacoustic imaging of tumor-associated neutrophils in cancer immunotherapy, Angew. Chem. Int. Ed. 61 (2022), e202203184, https://doi.org/10.1002/anie.202203184.

[164] J. Jeon, B. Yoon, S.H. Hong, W. Um, Y. Song, J. Lee, D.G. You, J.Y. An, J.H. Park, Chemiluminescence resonance energy transfer-based immunostimulatory nanoparticles for sonoimmunotherapy, Biomaterials 283 (2022) 121466, https://doi.org/10.1016/j.biomaterials.2022.121466.

[165] Y. He, F. Li, P. Jiang, F. Cai, Q. Lin, M. Zhou, H. Liu, F. Yan, Remote control of the recruitment and capture of endogenous stem cells by ultrasound for in situ repair of bone defects, Bioact. Mater. 21 (2022) 223–238, https://doi.org/10.1016/j.bioactmat.2022.08.012.

[166] N.K. Pandey, W. Xiong, L. Wang, W. Chen, B. Bui, J. Yang, E. Amador, M. Chen, C. Xing, A.A. Athavale, Y. Hao, W. Feizi, L. Lumata, Aggregation-induced emission luminogens for highly effective microwave dynamic therapy, Bioact. Mater. 7 (2022) 112–125, https://doi.org/10.1016/j.bioactmat.2021.05.031.

[167] M. Wen, N. Yu, S. Wu, M. Huang, P. Qiu, Q. Ren, M. Zhu, Z. Chen, On-demand assembly of polymeric nanoparticles for longer-blood-circulation and disassembly in tumor for boosting sonodynamic therapy, Bioact. Mater. 18 (2022) 242–253, https://doi.org/10.1016/j.bioactmat.2022.03.009.

[168] S. Koo, O.K. Park, J. Kim, S.I. Han, T.Y. Yoo, N. Lee, Y.G. Kim, H. Kim, C. Lim, J.-S. Bae, J. Yoo, D. Kim, S.H. Choi, T. Hyeon, Enhanced chemodynamic therapy by Cu–Fe peroxide nanoparticles: tumor microenvironment-mediated synergistic fenton reaction, ACS Nano 16 (2022) 2535–2545, https://doi.org/10.1021/acsnano.1c09171.

[169] B. Yang, Y. Zhang, L. Sun, J. Wang, Z. Zhao, Z. Huang, W. Mao, R. Xue, R. Chen, J. Luo, Modulated ultrasmall γ-Fe2O3 nanocrystal assemblies for switchable magnetic resonance imaging and photothermal-ferroptotic-chemical synergistic cancer therapy, Adv. Funct. Mater. 33 (2023), 2211251, https://doi.org/10.1002/adfm.202211251.

[170] Y. Sun, X. Li, M. Zhao, Y. Chen, Y. Xu, K. Wang, S. Bian, Q. Jiang, Y. Fan, X. Zhang, Bioinspired supramolecular nanofiber hydrogel through self-assembly of biphenyl-tripeptide for tissue engineering, Bioact. Mater. 8 (2022) 396–408, https://doi.org/10.1016/j.bioactmat.2021.05.054.

[171] X. Xu, Y. Chen, Y. Zhang, Y. Yao, P. Ji, Highly stable and biocompatible hyaluronic acid-rehabilitated nanoscale MOF-Fe 2+ induced ferroptosis in breast cancer cells, J. Mater. Chem. B 8 (2020) 9129–9138, https://doi.org/10.1039/D0TB01616K.

[172] D. Li, J. Ren, J. Li, Y. Zhang, Y. Lou, J. Zhu, P. Liu, Y. Chen, Z. Yu, L. Zhao, L. Zhang, X. Chen, J. Zhu, J. Tao, Ferroptosis-apoptosis combined anti-melanoma immunotherapy with a NIR-responsive upconverting mSiO(2) photodynamic platform, Chem. Eng. J. 419 (2021) 129557, https://doi.org/10.1016/j.cej.2021.129557.

[173] R. Thangam, K.D. Patel, H. Kang, R. Paulmurugan, Advances in engineered polymer nanoparticle tracking platforms towards cancer immunotherapy—current status and future perspectives, Vaccines 9 (2021) 935, https://doi.org/10.3390/vaccines9080935.

[174] L. Liu, Y. Pan, C. Zhao, P. Huang, X. Chen, L. Rao, Boosting checkpoint immunotherapy with biomaterials, ACS Nano 17 (2023) 3225–3258, https://doi.org/10.1021/acsnano.2c11691.

[175] D.H. Kim, W.D. Kim, S.K. Kim, D.H. Moon, S.J. Lee, TGF-β1-mediated repression of SLC7A11 drives vulnerability to GPX4 inhibition in hepatocellular carcinoma cells, Cell Death Dis. 11 (2020) 1–13, https://doi.org/10.1038/s41419-020-2618-6.

[176] L. Galluzzi, A. Buqué, O. Kepp, L. Zitvogel, G. Kroemer, Immunogenic cell death in cancer and infectious disease, Nat. Rev. Immunol. 17 (2017) 97–111, https://doi.org/10.1038/nri.2016.107.

[177] R. Zhou, Y. Liu, Z. Wang, J. Lv, W. Liao, Z. Shen, X. Rong, Nanoparticle-based MRI-guided tumor microenvironment heating via the synergistic effect of ferroptosis and inhibition of TGF-β signaling, Adv. Healthcare Mater. (2023), 2300176, https://doi.org/10.1002/adhm.202300176.

[178] J.-L. Roh, E.H. Kim, H.J. Jang, J.Y. Park, D. Shin, Induction of ferroptotic cell death for overcoming cisplatin resistance of head and neck cancer, Cancer Lett. 381 (2016) 96–103, https://doi.org/10.1016/j.canlet.2016.07.035.

[179] T. Xu, W. Ding, X. Ji, X. Ao, Y. Liu, W. Yu, J. Wang, Molecular mechanisms of ferroptosis and its role in cancer therapy, J. Cell Mol. Med. 23 (2019) 4900–4912, https://doi.org/10.1111/jcmm.14511.

[180] G. Xu, H. Wang, X. Li, R. Huang, L. Luo, Recent progress on targeting ferroptosis for cancer therapy, Biochem. Pharmacol. 190 (2021), 114584, https://doi.org/10.1016/j.bcp.2021.114584.

[181] A. Balihodzic, F. Prinz, M.A. Dengler, G.A. Calin, P.J. Jost, M. Pichler, Non-coding RNAs and ferroptosis: potential implications for cancer therapy, Cell Death Differ. 29 (2022) 1094–1106, https://doi.org/10.1038/s41418-022-00998-x.

[182] H. Yu, H. Zhao, Y. Zhang, Y. Hou, R. Li, T. Liang, Y. Zhang, C. Li, J. Zhao, M. Zhang, R. An, A biomimetic nanoreactor for combinational chemo/chemodynamic therapy of choriocarcinoma through synergistic apoptosis and ferroptosis strategy, Chem. Eng. J. 472 (2023), 144690, https://doi.org/10.1016/j.cej.2023.144690.

[183] G. Lei, C. Mao, Y. Yan, L. Zhuang, B. Gan, Ferroptosis, radiotherapy, and combination therapeutic strategies, Protein Cell 12 (2021) 836–857, https://doi.org/10.1007/s13238-021-00841-y.

[184] B. Hassannia, P. Vandenabeele, T. Vanden Berghe, Targeting ferroptosis to iron out cancer, Cancer Cell 35 (2019) 830–849, https://doi.org/10.1016/j.ccell.2019.04.002.

[185] B.R. Stockwell, J.P. Friedmann Angeli, H. Bayir, A.I. Bush, M. Conrad, S.J. Dixon, S. Fulda, S. Gascon, S.K. Hatzios, V.E. Kagan, K. Noel, X. Jiang, A. Linkermann, M.E. Murphy, M. Overholtzer, A. Oyagi, G.C. Pagnussat, J. Park, Q. Ran, C.S. Rosenfeld, K. Salnikow, D. Tang, F.M. Torti, S.V. Torti, S. Toyokuni, K.A. Woerpel, D.D. Zhang, Ferroptosis: a regulated cell death nexus linking metabolism, Redox Biol. Dis. Cell 171 (2017) 273–285, https://doi.org/10.1016/j.cell.2017.09.021.

[186] Z. Chu, T. Tian, Z. Tao, J. Yang, B. Chen, H. Chen, W. Wang, P. Yin, X. Xia, H. Wang, H. Qian, Upconversion nanoparticles@AgBiS(2) core-shell nanoparticles with cancer-cell-specific cytotoxicity for combined photothermal and photodynamic therapy of cancers, Bioact. Mater. 17 (2022) 71–80, https://doi.org/10.1016/j.bioactmat.2022.01.010.

[187] X. Qian, J. Zhang, Z. Gu, Y. Chen, Nanocatalysts-augmented Fenton chemical reaction for nanocatalytic tumor therapy, Biomaterials 211 (2019) 1–13, https://doi.org/10.1016/j.biomaterials.2019.04.023.

[188] S.L. Cramer, A. Saha, J. Liu, S. Tadi, S. Tiziani, W. Yan, K. Triplett, C. Lamb, S.E. Alters, S. Rowlinson, Y.J. Zhang, M.J. Keating, P. Huang, J. DiGiovanni, G. Georgiou, E. Stone, Systemic depletion of L-cyst(e)ine with cyst(e)inase increases reactive oxygen species and suppresses tumor growth, Nat. Med. 23 (2017) 120–127, https://doi.org/10.1038/nm.4232.

[189] P. Hu, T. Wu, W. Fan, L. Chen, Y. Liu, D. Ni, W. Bu, J. Shi, Near infrared-assisted Fenton reaction for tumor-specific and mitochondrial DNA-targeted photochemotherapy, Biomaterials 141 (2017) 86–95, https://doi.org/10.1016/j.biomaterials.2017.06.035.

[190] R. Hu, Y. Fang, M. Huo, H. Yao, C. Wang, Y. Chen, R. Wu, Ultrasmall Cu2-xS nanodots as photothermal-enhanced Fenton nanocatalysts for synergistic tumor therapy at NIR-II biowindow, Biomaterials 206 (2019) 101–114, https://doi.org/10.1016/j.biomaterials.2019.03.014.

[191] X. Nie, L. Xia, H.L. Wang, G. Chen, B. Wu, T.Y. Zeng, C.Y. Hong, L.H. Wang, Y.Z. You, Photothermal therapy nanomaterials boosting transformation of Fe(III) into Fe(II) in tumor cells for highly improving chemodynamic therapy, ACS Appl. Mater. Interfaces 11 (2019) 31735–31742, https://doi.org/10.1021/acsami.9b11291.

[192] A. Shahzeydi, M. Ghiaci, H. Farrokhpour, A. Shahvar, M. Sun, M. Saraji, Facile and green synthesis of copper nanoparticles loaded on the amorphous carbon nitride for the oxidation of cyclohexane, Chem. Eng. J. 370 (2019) 1310–1321, https://doi.org/10.1016/j.cej.2019.03.227.

[193] S. Wang, L. Yang, H.Y. Cho, S.T. Dean Chueng, H. Zhang, Q. Zhang, K.B. Lee, Programmed degradation of a hierarchical nanoparticle with redox and light responsivity for self-activated photo-chemical enhanced chemodynamic therapy, Biomaterials 224 (2019) 119498, https://doi.org/10.1016/j.biomaterials.2019.119498.

[194] Y. Qu, K. Lu, Y. Zheng, C. Huang, G. Wang, Y. Zhang, Q. Yu, Photothermal scaffolds/surfaces for regulation of cell behaviors, Bioact. Mater. 8 (2022) 449–477, https://doi.org/10.1016/j.bioactmat.2021.05.052.

[195] J. Huang, C. Zhang, X. Wang, X. Wei, K. Pu, Near-infrared photodynamic chemiluminescent probes for cancer therapy and metastasis detection, Angew. Chem. Int. Ed. (2023), e202303982, https://doi.org/10.1002/anie.202303982.

[196] X. Wei, J. Huang, C. Zhang, C. Xu, K. Pu, Y. Zhang, Highly bright near-infrared chemiluminescent probes for cancer imaging and laparotomy, Angew. Chem. Int. Ed. 62 (2023), e202213791, https://doi.org/10.1002/anie.202213791.

[197] L. He, N. Zheng, Q. Wang, J. Du, S. Wang, Z. Cao, Z. Wang, G. Chen, J. Mu, S. Liu, X. Chen, Responsive accumulation of nanohybrids to boost NIR-phototheranostics for specific tumor imaging and glutathione depletion-enhanced synergistic therapy, Adv. Sci. 10 (2023), 2205208, https://doi.org/10.1002/advs.202205208.

[198] G. Wen, X. Li, Y. Zhang, X. Han, X. Xu, C. Liu, K.W.Y. Chan, C.S. Lee, C. Yin, L. Bian, L. Wang, Effective phototheranostics of brain tumor assisted by near-infrared-II light-responsive semiconducting polymer nanoparticles, ACS Appl. Mater. Interfaces 12 (2020) 33492–33499, https://doi.org/10.1021/acsami.0c08562.

[199] Y. Zou, S.L. Schreiber, Progress in understanding ferroptosis and challenges in its targeting for therapeutic benefit, Cell Chem. Biol. 27 (2020) 463–471, https://doi.org/10.1016/j.chembiol.2020.03.015.

[200] J. Wei, J. Li, D. Sun, Q. Li, J. Ma, X. Chen, X. Zhu, N. Zheng, A novel theranostic nanoplatform based on Pd@Pt-PEG-Ce6 for enhanced photodynamic therapy by modulating tumor hypoxia microenvironment, Adv. Funct. Mater. 28 (2018), 1706310, https://doi.org/10.1002/adfm.201706310.

[201] P. Shou, Z. Yu, Y. Wu, Q. Feng, B. Zhou, J. Xing, C. Liu, J. Tu, O.U. Akakuru, Z. Ye, X. Zhang, Z. Lu, L. Zhang, A. Wu, Zn2+ doped ultrasmall prussian blue nanotheranostic agent for breast cancer photothermal therapy under MR imaging guidance, Adv. Healthcare Mater. 9 (2020), 1900948, https://doi.org/10.1002/adhm.201900948.

[202] C.M. Pfeffer, A.T.K. Singh, Apoptosis: a target for anticancer therapy, Int. J. Mol. Sci. 19 (2018) 448, https://doi.org/10.3390/ijms19020448.

[203] J. Kale, E.J. Osterlund, D.W. Andrews, BCL-2 family proteins: changing partners in the dance towards death, Cell Death Differ. 25 (2018) 65–80, https://doi.org/10.1038/cdd.2017.186.

[204] X. Zhou, Q. Hao, H. Lu, Mutant p53 in cancer therapy-the barrier or the path, J. Mol. Cell Biol. 11 (2019) 293–305, https://doi.org/10.1093/jmcb/mjy072.

[205] J.M. Shin, C.H. Lee, S. Son, C.H. Kim, J.A. Lee, H. Ko, S. Shin, S.H. Song, S.S. Park, J.H. Bae, J.M. Park, E.J. Choe, M.C. Baek, J.H. Park, Sulfisoxazole elicits robust antitumour immune response along with immune checkpoint therapy by inhibiting exosomal PD-L1, Adv. Sci. 9 (2022), 2103245, https://doi.org/10.1002/advs.202103245.

[206] M. Pei, Y.A. Pei, S. Zhou, E. Mikaeiliagah, C. Erickson, B. Giertych, H. Akhter, L. Wang, A. Stewart, J. Parenti, B. Wang, S. Wen, S. Sim, E. Quenneville, K. C. Hansen, S. Frisch, G. Hu, Matrix from urine stem cells boosts tissue-specific stem cell mediated functional cartilage reconstruction, Bioact. Mater. 23 (2023) 353–367, https://doi.org/10.1016/j.bioactmat.2022.11.012.

[207] L. Zhou, J. Xu, A. Schwab, W. Tong, J. Xu, L. Zheng, Y. Li, Z. Li, S. Xu, Z. Chen, L. Zou, X. Zhao, G.J.V.M.v. Osch, C. Wen, L. Qin, Engineered biochemical cues of regenerative biomaterials to enhance endogenous stem/progenitor cells (ESPCs)-mediated articular cartilage repair, Bioact. Mater. 26 (2023) 490–512, https://doi.org/10.1016/j.bioactmat.2023.03.008.

[208] Y. Kim, T.M. Koo, R. Thangam, M.S. Kim, W.Y. Jang, N. Kang, S. Min, S.Y. Kim, L. Yang, H. Hong, H.J. Jung, E.K. Koh, K.D. Patel, S. Lee, H.E. Fu, Y.S. Jeon, B. C. Park, S.Y. Kim, S. Park, J. Lee, L. Gu, D.-H. Kim, T.-H. Kim, K.-B. Lee, W. K. Jeong, R. Paulmurugan, Y.K. Kim, H. Kang, Submolecular ligand size and spacing for cell adhesion, Adv. Mater. 34 (2022), 2110340, https://doi.org/10.1002/adma.202110340.

[209] W.L. Pan, Y. Tan, W. Meng, N.H. Huang, Y.B. Zhao, Z.Q. Yu, Z. Huang, W. H. Zhang, B. Sun, J.X. Chen, Microenvironment-driven sequential ferroptosis, photodynamic therapy, and chemotherapy for targeted breast cancer therapy by a cancer-cell-membrane-coated nanoscale metal-organic framework, Biomaterials 283 (2022), 121449, https://doi.org/10.1016/j.biomaterials.2022.121449.

[210] L. Su, Y. Chen, H. Huo, N. Liao, Y. Wu, X. Ge, Z. Guo, Z. Chen, X. Zhang, J. Song, NIR-II ratiometric chemiluminescent/fluorescent reporters for real-time monitoring and evaluating cancer photodynamic therapy efficacy, Small 18 (2022), e2202551, https://doi.org/10.1002/smll.202202551.

[211] J. Jiang, W. Wang, H. Zheng, X. Chen, X. Liu, Q. Xie, X. Cai, Z. Zhang, R. Li, Nano-enabled photosynthesis in tumours to activate lipid peroxidation for overcoming cancer resistances, Biomaterials 285 (2022), 121561, https://doi.org/10.1016/j.biomaterials.2022.121561.

[212] C. Wang, Y. Zeng, K.F. Chen, J. Lin, Q. Yuan, X. Jiang, G. Wu, F. Wang, Y. Jia, W. Li, A self-monitoring microneedle patch for light-controlled synergistic treatment of melanoma, Bioact. Mater. 27 (2023) 58–71, https://doi.org/10.1016/j.bioactmat.2023.03.016.

[213] Y. Kim, R. Thangam, J. Yoo, J. Heo, J.Y. Park, N. Kang, S. Lee, J. Yoon, K.R. Mun, M. Kang, S. Min, S.Y. Kim, S. Son, J. Kim, H. Hong, G. Bae, K. Kim, S. Lee, L. Yang, J.Y. Lee, J. Kim, S. Park, D.-H. Kim, K.-B. Lee, W.Y. Jang, B.H. Kim, R. Paulmurugan, S.-W. Cho, H.-C. Song, S.J. Kang, W. Sun, Y. Zhu, J. Lee, H.-J. Kim, H.S. Jang, J.S. Kim, A. Khademhosseini, Y. Kim, S. Kim, H. Kang, Photoswitchable microgels for dynamic macrophage modulation, Adv. Mater. 34 (2022), 2205498, https://doi.org/10.1002/adma.202205498.

[214] D.-H. Kim, E.A. Rozhkova, I.V. Ulasov, S.D. Bader, T. Rajh, M.S. Lesniak, V. Novosad, Biofunctionalized magnetic-vortex microdiscs for targeted cancer-cell destruction, Nat. Mater. 9 (2010) 165–171, https://doi.org/10.1038/nmat2591.

[215] D.-H. Kim, D.E. Nikles, D.T. Johnson, C.S. Brazel, Heat generation of aqueously dispersed CoFe2O4 nanoparticles as heating agents for magnetically activated drug delivery and hyperthermia, J. Magn. Magn Mater. 320 (2008) 2390–2396, https://doi.org/10.1016/j.jmmm.2008.05.023.

[216] M. Feng, S. Xiao, Z. Liu, M. Li, X. Zhang, X. Chen, Y. Zhang, B. Chen, J. Liu, Multifunctional platinum-doped porous FeS2 nanoparticles for photothermal-enhanced photodynamic ferroptosis combination therapy, Mater, Today Nano 23 (2023), 100371, https://doi.org/10.1016/j.mtnano.2023.100371.

[217] Q. Lou, F. Feng, J. Hui, P. Zhang, S. Qin, X. Ouyang, D. Wu, X. Wang, Polytonic drug release via multi-hierarchical microstructures enabled by nano-metamaterials, Adv. Healthcare Mater. 12 (2023), 2202826, https://doi.org/10.1002/adhm.202202826.

[218] Z. Yang, C. Yang, D. Yang, Y. Zhang, Q. Yang, F. Qu, W. Guo, l-Arginine-Modified CoWO4/FeWO4 S-scheme heterojunction enhances ferroptosis against solid tumor, Adv. Healthcare Mater. 12 (2023), 2203092, https://doi.org/10.1002/adhm.202203092.

[219] S. Xu, S. Zhou, L. Xie, W. Dou, R. Zhang, B. Zhao, Y. Xu, X. Fu, M. Yuan, A versatile NiS2/FeS2 hybrid nanocrystal for synergistic cancer therapy by inducing ferroptosis and pyroptosis, Chem. Eng. J. 460 (2023), 141639, https://doi.org/10.1016/j.cej.2023.141639.

[220] X. Chen, H. Wang, J. Shi, Z. Chen, Y. Wang, S. Gu, Y. Fu, J. Huang, J. Ding, L. Yu, An injectable and active hydrogel induces mutually enhanced mild magnetic hyperthermia and ferroptosis, Biomaterials 298 (2023), 122139, https://doi.org/10.1016/j.biomaterials.2023.122139.

[221] Y. Zhang, L. Peng, K. Hu, N. Gu, Stress relaxation-induced colon tumor multicellular spheroid culture based on biomimetic hydrogel for nanoenzyme ferroptosis sensitization evaluation, Adv. Healthcare Mater. 12 (2023), 2202009, https://doi.org/10.1002/adhm.202202009.

[222] X. Zeng, Y. Ruan, Q. Chen, S.Q. Yan, W. Huang, Biocatalytic cascade in tumor microenvironment with a Fe2O3/Au hybrid nanozyme for synergistic treatment of triple negative breast cancer, Chem. Eng. J. 452 (2023), 138422, https://doi.org/10.1016/j.cej.2022.138422.

[223] Y. Mou, J. Wang, J. Wu, D. He, C. Zhang, C. Duan, B. Li, Ferroptosis, a new form of cell death: opportunities and challenges in cancer, J. Hematol. Oncol. 12 (2019) 34, https://doi.org/10.1186/s13045-019-0720-y.

[224] P.P. Hsu, D.M. Sabatini, Cancer cell metabolism: warburg and beyond, Cell 134 (2008) 703–707, https://doi.org/10.1016/j.cell.2008.08.021.

[225] G. Hao, Z.P. Xu, L. Li, Manipulating extracellular tumour pH: an effective target for cancer therapy, RSC Adv. 8 (2018) 22182–22192, https://doi.org/10.1039/C8RA02095G.